

Fall 2015

# NUMERICAL UPDATING ON COLLAPSE SIMULATION OF MULTI-STORY BUILDINGS THROUGH HYBRID TESTING

Miguel Negrete-Padilla  
*University of New Hampshire, Durham*

Follow this and additional works at: <https://scholars.unh.edu/dissertation>

---

## Recommended Citation

Negrete-Padilla, Miguel, "NUMERICAL UPDATING ON COLLAPSE SIMULATION OF MULTI-STORY BUILDINGS THROUGH HYBRID TESTING" (2015). *Doctoral Dissertations*. 2228.  
<https://scholars.unh.edu/dissertation/2228>

This Dissertation is brought to you for free and open access by the Student Scholarship at University of New Hampshire Scholars' Repository. It has been accepted for inclusion in Doctoral Dissertations by an authorized administrator of University of New Hampshire Scholars' Repository. For more information, please contact [nicole.hentz@unh.edu](mailto:nicole.hentz@unh.edu).

NUMERICAL UPDATING ON COLLAPSE SIMULATION OF MULTI-STORY BUILDINGS  
THROUGH HYBRID TESTING

BY

MIGUEL NEGRETE PADILLA  
BS, Universidad Don Vasco, A.C. / UNAM, 2000  
MS, Universidad Michoacana de San Nicolás de Hidalgo, 2007

DISSERTATION

Submitted to the University of New Hampshire  
in Partial Fulfillment of  
the Requirements for the Degree of

Doctor of Philosophy  
in  
Civil Engineering

September, 2015

This dissertation has been examined and approved in partial fulfillment of the requirements for the degree of Doctor of Philosophy in Civil Engineering by:

Dissertation Director, Dr. Ricardo A. Medina  
Associate Professor of Civil and Environmental Engineering

Dr. Erin S. Bell  
Associate Professor of Civil and Environmental Engineering

Dr. Raymond A. Cook  
Associate Professor of Civil and Environmental Engineering

Dr. Yannis Korkolis  
Associate Professor of Mechanical Engineering

Dr. Luis F. Ibarra  
Assistant Professor of Civil Engineering  
University of Utah

On August 17th, 2015.

Original approval signatures are on file with the University of New Hampshire Graduate School.

## ACKNOWLEDGEMENTS

This work was partially supported by Network for Earthquake Engineering Simulation (NEES) and the National Science Foundation with grant number CCMMI-0936633, the National Council of Science and Technology (CONACYT), Mexico and the University of New Hampshire Civil and Environmental Engineering Department. This financial support is greatly appreciated.

The author would like to express his immense gratitude to his advisor Dr. Ricardo A. Medina for his valuable guidance and support in technical as well as personal topics all along these years. High quality comments and suggestions of Dr. Eduardo Miranda during the development of this research are deeply appreciated. Several graduate and undergraduate fellows that were standing there when difficult times (and many good times too) were facing in the horizon, interchanging assistance, long interesting discussions, rain of thoughts, encouragement and overall their friendship would never be forgotten: Shokouhfeh Zargar, Antonio Garcia-Palencia, Georgian Tutuianu, Rui Zhang, Annika Mathiasson, Shahriar Beigi; the NH gang: Jeewoo Park, Philip Nuss, Onur Baycan, Zeljko Medenica. And especially the support, patience and unconditional love of my little army: Natalia Tsintsuni, Alondra Tsanda, Emma Tsitsiki and my administrator, counselor, teacher, psychologist, nurse, girlfriend, lover, and director of the orchestra, Mayis. Also at the end of this journey, a very special guy in my life did not make it to the end, wherever you are, *gracias viejo por todos esos años!*, we will always remember you. And lastly but not least, the support expressed by my family and friends back home, *gracias a todos!*

The time and effort invested on the examination of this document by the Committee Members is remarkably appreciated, thanks to Dr. Erin S. Bell, Dr. Raymond A. Cook, Dr. Yannis Korkolis and to Dr. Luis F. Ibarra.

## **ABSTRACT**

### **NUMERICAL UPDATING ON COLLAPSE SIMULATION OF MULTI-STORY BUILDINGS THROUGH HYBRID TESTING**

by

Miguel Negrete Padilla  
University of New Hampshire, September 2015.

The present dissertation introduces an innovative numerical updating approach within fully simulated hybrid testing with substructuring techniques through collapse. The proposed approach is based on utilizing the measured response from the experimental substructure to update during the test the parameters of the components of the numerical substructure. The main research objective is to improve the ability to predict and simulate collapse through hybrid testing with substructuring techniques. The proposed numerical updating approach demonstrates to be capable of reliably reduce the epistemic uncertainty existent on the calibration of initial component parameters of the numerical substructure, especially when the system is near the limit state of collapse.

# TABLE OF CONTENTS

<b>ACKNOWLEDGEMENTS</b> .....	iii
<b>ABSTRACT</b> .....	iv
<b>LIST OF FIGURES</b> .....	viii
<b>1. INTRODUCTION</b> .....	1
1.1. Experimental methods for structural evaluation .....	1
1.2. Motivation.....	8
1.3. Literature review .....	13
1.4. Problem definition .....	16
1.5. Research objectives and scope.....	17
1.6. Dissertation outline .....	18
<b>2. VALIDATION OF NUMERICAL MODELS EMPLOYED ON THE IMPLEMENTATION OF THE NUMERICAL UPDATING APPROACH</b> .....	21
2.1. Introduction.....	21
2.2. Previous shake table studies.....	22
2.3. OpenSees full frame model results vs. shake table results .....	26
2.4. General description of substructuring technique .....	31
2.5. Numerical substructuring technique vs. full numerical model .....	34
2.6. Summary and Conclusions .....	39
<b>3. NUMERICAL UPDATING APPROACH - A GENERAL OVERVIEW</b> .....	41
3.1. Introduction.....	41
3.2. Implementation of fully numerical hybrid simulation.....	41
3.3. Update parameter commands in OpenSees.....	49

3.4. Experimental errors and epistemic uncertainty in hybrid simulations.....	53
3.5. Numerical updating approach - general scope.....	56
3.6. Summary and conclusions .....	62
<b>4. NUMERICAL UPDATING APPROACH: PHASE I.....</b>	<b>64</b>
4.1. Introduction, definition, and scope .....	64
4.10. Summary and conclusions .....	92
4.2. Hysteretic model selection.....	66
4.3. Ibarra-Medina-Krawinkler Hysteretic Model.....	69
4.4. Modifications to <i>IMK</i> model.....	75
4.5. Proposed rules for <i>DIMK</i> numerical fit. ....	76
4.6. Modifications to the elastic stiffness $K_{en}$ .....	80
4.7. Modifications to yield strength demand $M_{yn}$ .....	82
4.8. Modifications to plastic deformation capacity $\delta_{pn}$ .....	86
4.9. Modifications to strain-hardening ( $\alpha_{sn}$ ) and post-capping ( $\alpha_{cn}$ ) slopes.....	88
<b>5. NUMERICAL UPDATING APPROACH: PHASE II.....</b>	<b>94</b>
5.1. Introduction.....	94
5.2. Identification of main parameters to update .....	95
5.3. Distribution of damage identified in global domain to local domain .....	99
5.3.1. Distribution of damage in the numerical substructure.....	102
5.4 Implementation of numerical updating to collapse using shake table ground motions..	109
5.5 Summary and conclusions .....	127
<b>6. EPISTEMIC UNCERTAINTY REDUCTION IN HYBRID SIMULATION THROUGH ON-LINE UPDATING.....</b>	<b>129</b>

6.1. Objectives and goals .....	129
6.2. Epistemic uncertainty reduction for different limit states.....	129
6.3. Final remarks on the applicability of the NUA.....	146
6.4. Summary and conclusions .....	146
<b>7. SUMMARY AND CONCLUSIONS .....</b>	<b>149</b>
7.1. Summary .....	149
7.2. Conclusions.....	150
7.3. Limitations .....	153
7.4. Future work.....	154
LIST OF REFERENCES .....	156



## LIST OF FIGURES

Figure 1.1. Hybrid simulation conceptualization, a) full structural model, b) numerical model and, c) physical model. ....	7
Figure 1.2. Reduced beam section connection (AISC, 2010).....	10
Figure 2.1. Prototype office building, (a) Plan view of a typical story, (b) Plan view of roof, penthouse highlighted in gray, (c) Elevation of EW SMRF (Lignos, 2008). ....	23
Figure 2.2. Four-story shake table test, (a) experimental setup, (b) natural aluminum hinges, (c) dog-bone steel hinge plates, after Lignos (2008), (d) 1:8 scaled frame assembly dimensions (in). ....	26
Figure 2.3. Numerical model of the scaled structure. ....	28
Figure 2.4. Hybrid simulation substructures, four-story SMRF model. ....	29
Figure 2.5. Comparisons of inter-story drifts of numerical model vs. shake table test, after (Hashemi, 2013).....	31
Figure 2.6. Experimental and numerical substructures and their overlapping interface, after (Hashemi, 2013).....	33
Figure 2.7. Substructuring options: (a) full SMRF experimental w-o/overlapping, (b) 3.5 stories SMRF experimental w/overlapping, (c) 2.5 stories SMRF experimental w/overlapping, (d) 1.5 stories SMRF experimental w/overlapping. ....	36
Figure 2.8. Collapse mechanism of the four-story SMRF after a shake table test, after Lignos (2008).....	37
Figure 2.9. Comparison of inter-story drifts for suggested substructures, after (Hashemi, 2013). ....	38
Figure 3.1. NEES@Buffalo hybrid testing setup; a) panoramic view of 1.5 story substructure, b)	

measuring devices (load cells and strain gauges) on columns (Hashemi, 2013).....	43
Figure 3.2. Hybrid simulation architecture. ....	44
Figure 3.3. Fully numerical hybrid simulation architecture. ....	45
Figure 3.4. Degrees of freedom utilized on the generic super-element initial stiffness matrix calculations. ....	46
Figure 3.5. Hybrid simulation information flow loop, adapted from Schellenberg et al., (2010).49	
Figure 3.6. Modified Ibarra-Medina-Krawinkler deterioration model, implemented in OpenSees, after (Lignos & Krawinkler, 2011). ....	52
Figure 3.7. Flowchart for implementation of conventional hybrid simulation with substructuring. ....	57
Figure 3.8. Flowchart for implementation of numerical updating approach. ....	58
Figure 3.9. First-story drift for a hybrid simulation case study with initial calibration errors through collapse. ....	61
Figure 4.1. Flowchart of proposed numerical updating approach. ....	65
Figure 4.2. Deviation in strength due to analysis step increment size: (a) large $\Delta t$ analysis, (b) small $\Delta t$ analysis. ....	69
Figure 4.3. Backbone curve, <i>IMK</i> model (Ibarra, et al., 2005). ....	70
Figure 4.4. Individual deterioration modes, illustrated on a peak-oriented model (Ibarra, et al., 2005): (a) basic strength deterioration; (b) post-capping strength deterioration; (c) unloading stiffness degradation; and (d) accelerated reloading stiffness degradation. ....	74
Figure 4.5. Specimen LS-1: (a) test set-up full-scale steel specimen, (b) moment vs. rotation, after Uang et. al., (2000). ....	80
Figure 4.6. Elastic stiffness modification rule: (a) no correction, (b) corrected. ....	82

Figure 4.7. Basic strength <i>DIMK</i> rule model yield strength larger than experimental: (a) positive loading, (b) negative loading. ....	83
Figure 4.8. Basic strength increment <i>DIMK</i> rule, model yield strength lower than experimental: (a) numerical fit overtaking experimental response, (b) loading reversal and, (c) end of limit of proportionality.....	86
Figure 4.9. Plastic rotation capacity ( $\theta_{pn}$ ) <i>DIMK</i> rule. ....	88
Figure 4.10. Updated available information for calculation of $\alpha_{sn}$ : (a) capping strength ( $M_c$ ) detected, (b) loading reversal detected, no $M_c$ found.....	89
Figure 4.11. Updated available information for $\alpha_{cn}$ calculations.....	90
Figure 4.12. Effect of the application of strain-hardening and post-capping stiffness <i>DIMK</i> rules: (a) base case, no correction, (b) corrected. ....	92
Figure 5.1. Flowchart of proposed numerical updating approach. ....	95
Figure 5.2. Four-story structure model (4PO) to perform pushover analyses. ....	97
Figure 5.3. Capacity curve-IMK model backbone analogy, (a) IMK model, (b) capacity curve vs. IMK model backbone. ....	98
Figure 5.4. Example of parameter selection, (a) <i>DIMK</i> selected backbone fit, (b) $K_{en}$ , (c) $F_{yn}$ , (d) $\alpha_{sn}$ , (e) $\delta_{pn}$ , (f) $\alpha_{cn}$ selection, and (g) final calibrated backbone-capacity curve.....	101
Figure 5.5. Numerical sub-domain model. ....	106
Figure 5.6. Correlation between dynamic (hybrid) and static (4PO-model pushover) stiffnesses. ....	108
Figure 5.7. First-story drift of a four-story structure hybrid simulation through collapse.....	110
Figure 5.8. Base shear/seismic weight of a four-story structure hybrid simulation through collapse, (a) <i>SLE</i> , <i>DBE</i> and <i>MCE</i> , (b) <i>CLE</i> and <i>CLEF</i> limit states. ....	112

Figure 5.9. Moment-Rotation time history of springs contained on the numerical subdomain of a four-story structure, (a) springs 1-6, (b) springs 7-12, (c) springs 13-18, (d) springs 19-24, (e) springs 25-30 and, (f) springs 31-34. ....	119
Figure 5.10. Base shear/seismic weight, four-story structure hybrid simulation through collapse study case 2. ....	121
Figure 5.11. Base shear/seismic weight of a four-story structure hybrid simulation through collapse, (a) <i>SLE</i> , <i>DBE</i> and <i>MCE</i> , (b) <i>CLE</i> and <i>CLEF</i> limit states (study case 2). ....	123
Figure 5.12. Temporal evolution of updated parameters of the numerical subdomain of a four-story structure hybrid simulation through collapse (study case 2). ....	127
Figure 6.1. Randomly generated error factors considering a COV of 10% over the mean. ....	131
Figure 6.2. First-story drift for 20 cases, (a) with induced initial parameter component errors (ICCE), (b) with the application of the proposed NUA. ....	134
Figure 6.3. First-story drift for case 5, with ICCE and with the application of the proposed NUA. ....	135
Figure 6.4. First-story drift for case 11, with ICCE and with the application of the proposed NUA. ....	136
Figure 6.5. First-story drift for case 6, with ICCE and with the application of the proposed NUA. ....	137
Figure 6.6. First-story drift for case 7, with ICCE and with the application of the proposed NUA. ....	138
Figure 6.7. Identification of second mode effect for case 7 with NUA, (a) first-story drift - base shear/seismic weight hysteresis diagram, (b) first-story drift ratio, (c) base shear / seismic weight. ....	140

Figure 6.8. Normalized base shear for 20 cases, (a) with ICCE, (b) with NUA. ....	142
Figure 6.9. Normalized base shear for case 5, with ICCE and with NUA. ....	143
Figure 6.10. Normalized base shear for case 11, with ICCE and with NUA. ....	143
Figure 6.11. Normalized base shear for case 6, with ICCE and with NUA. ....	144
Figure 6.12. Normalized base shear for case 7, with ICCE and with NUA. ....	144
Figure 6.13. First floor acceleration for 20 cases, (a) with ICCE and, (b) with NUA.....	145

## LIST OF TABLES

Table 1.1 Comparison of advantages among main experimental testing methods.....	2
Table 1.2. Statistics of ratios of effective-to-predicted component yield strength and capping strength to effective yield strength, after Lignos (2011).....	12
Table 1.3. Statistics of pre-capping rotation ( $\theta_p$ ), post-capping rotation ( $\theta_{pc}$ ) and cumulative rotation capacity ( $A$ ) of steel components with RBS connections ( $d \geq 21''$ ), after Lignos (2011).	13
Table 2.1. Analysis step size information, recalibrated model. ....	30
Table 2.2. Absolute error ratios from substructured hybrid models to base case. ....	39
Table 3.1. Interval of analysis steps for evaluator stage. ....	59
Table 4.1. Capabilities of hysteretic models, modified from Lignos (2008).....	68
Table 4.2. Test results of beams RBS, modified from Lignos (2008). ....	72
Table 5.1. IMK parameters to update and ranges of search.....	103
Table 6.1. Random generated error factors applied to the numerical component parameters of non-collapsing cases.....	132
Table 6.2. First-story temporary drift residuals for 20 cases. ....	135

# CHAPTER 1


## INTRODUCTION

### 1.1. Experimental methods for structural evaluation

Several experimental testing methods have been historically employed to evaluate the performance of components and structural systems under accidental loads induced by natural events (e.g., earthquakes, strong winds, tides). These performance evaluations were aimed to understand and improve the dynamic behavior of infrastructure civil works. Among the most important practices are the quasi-static, shake table, and pseudo-dynamic or online tests. Pseudo-dynamic tests with substructuring are also referred as to hybrid tests. Table 1.1 presents a general overview of advantages and limitations of quasi-static, shake table, and conventional hybrid simulation tests.

In quasi-static tests, the specimen (e.g., structural system, component or subassembly) is subjected to load histories and/or predefined displacements consistent with low strain rates, advantageously providing information of its nonlinear behavior. Conversely, this testing technique is not capable of considering acceleration-dependent effects such as inertial forces, velocities, as well as damping forces. Quasi-static testing cannot represent the dynamic effects of the equivalent external forces induced during a seismic event. Hence, its contribution is primarily reduced to determining the capacity of elements or structural systems with different detailing, and the mechanisms that affect their inelastic behavior. These tests are also useful to determine results that allow calibrating numerical models.

Table 1.1 Comparison of advantages among main experimental testing methods.



	QUASI-STATIC	SHAKING TABLE	HYBRID SIMULATION
PREDEFINED LOAD AND DISPLACEMENT HISTORIES	YES	YES	YES
ACCELERATION EFFECTS, INERTIAL FORCES, VELOCITIES AND DAMPING	NO	YES	YES (NUM. PORTION)
REAL SEISMIC RECORD INPUT	NO	YES	YES
TEST CONDUCTED ON REAL VELOCITY AS IN SEISMIC RECORD	NO	YES	NO
DYNAMIC EFFECT AND ALEATORITY OF EXTERNAL (SEISMIC) FORCES	NO	YES	YES
DAMPING FORCES AND ENERGY DISIPATION MECHANISMS ON SYSTEM COMPONENTS	NO	YES	NO
DETERMINE ELEMENTS/SYSTEMS CAPACITIES	YES	YES	YES
RESULTS TO CALIBRATE BEHAVIOR OF NUMERICAL MODELS	YES	YES	YES
LIMITATION ON SIZE, WEIGHT AND RESISTANCE OF SPECIMENS	MED	HIGH	LOW
LIMITATION ON FORCES AND DISPLACEMENTS DUE TO ACTUATORS	HIGH	HIGH	LOW
COST OF SPECIMENS	LOW/MODERATE	HIGH	MODERATE
COST OF TESTING EQUIPMENT	LOW	HIGH	MODERATE
GENERAL SIZE OF FACILITIES	LOW	HIGH	MODERATE
RECALIBRATION (UPDATING) DURING THE ANALYSIS	NO	NO	NO

Shaking table tests are capable of inducing the most realistic seismic loading conditions at the base of the structural specimens. The structure is placed on a vibrating table whose accelerations (e.g., ground motion records) are applied via dynamic actuators and control systems. The most significant advantage of this technique is that the base excitation is introduced in real time, equally as in an actual earthquake. The structure is deformed by the distributed inertial forces according to the mass of the structure and by the presence of damping forces and energy dissipation mechanisms of the system. The main drawbacks of shaking table testing are the limitations of the maximum applicable displacements and forces, circumscribed by the characteristics of the available actuators together with the high cost of the testing equipment itself. Additionally, limitations on the capabilities to apply vertical acceleration on most shake table facilities are present. Another disadvantage is the construction costs of multiple-degree-of-freedom (MDOF) structures on real scale and their inherent limitations in weight, size and resistance of the specimens that can be tested. Furthermore, when collapse assessment studies are conducted, given the heavy masses involved in shaking table tests (Lignos, et al., 2008), expenses on the construction of the



specimens and secondary supporting structures to assure the protection of the equipment are significant. At the same time, the safety of the testing personnel can be compromised due to collapsing structures. Given these conditions, it is imperative in many instances to utilize reduced scale models with the approximations that scaling techniques implies (e.g., similitude laws of materials, (Moncarz, 1981)).

Hybrid testing (HT) or hybrid simulation (HS) merges features of quasi-static and shake table testing along with numerical time history analysis. It combines the experimental advantages of shaking table tests and the economy of quasi-static tests, offering a safe, efficient and cost-effective alternative for testing large-scale structural models through collapse, compared to historically used procedures. The concept of HS was firstly introduced in the 1960's by Japanese researchers (Hakuno, et al., 1969) utilizing a single-degree-of-freedom cantilever beam excited by an actuator with a seismic record, combined with a vibration response calculation conducted simultaneously through an analog computer. A dynamic response was obtained for the first time without the use of a shaking table. Later on the mid 1970's was further developed by Takanashi, et al., (1975) establishing the method on its actual form through the introduction of discrete time systems and digital controllers. In this sense, a digital controller is used to solve the equations of motion whereas the loading equipment (i.e., actuator) can be relaxed to a ramp and hold procedure over an extended time scale. This improvement allowed researchers to use typical quasi-static testing equipment while the numerical integration was performed at a slower rate appropriate for the computers available at the time (Phillips & Spencer, 2012).

Subsequently, intensive research has been carried out to expand and validate hybrid simulation mainly in the United States of America and Japan. These efforts are documented in Takanashi and Nakashima (1987), Mahin, et al. (1989), Shing, et al. (1996), Magonette (2001) and

Mosqueda, et al. (2005).

HT consists on dividing the structural system in experimental and numerical portions, which interact along the entire simulation to obtain the dynamic response of a structure. The experimental component involves one or more test specimens subjected to deformation histories through the use of hydraulic actuators. On the other side, the numerical component is defined as an analytical substructure that models the rest of the structural system. Besides, substructuring techniques allow separating the complete system into several parts, leading to the possibility of performing a test in several different geographical located facilities (Mosqueda, et al., 2005). In this sense, the portions of the structure that exhibit a more complex behavior, are critical or collapse-sensitive, and consequently are more difficult to model with a high degree of precision, can be physically tested. Those sections with a consistent and well-defined behavior can be numerically analyzed facilitating the simulation and study of collapse of structures (Saouma & Sivaselvan, 2008).

Hence, the hybrid testing method overcomes some of the limitations of shaking tables, for instance:

- HT is capable of testing of large or full-scale structural models.
- HT is safe and economic with versatile configurations adding ease of accommodation in testing facilities.
- Specimens may be tested with required equipment not much different than necessary for quasi-static testing.
- Gravity loads need not be accurately reproduced in the laboratory as they are modeled numerically, leading to safer tests without large masses physically assigned to the specimens.

- Substructures are tested while the remainder of the system is modeled numerically within the time integration loop (Jeyasehar, et al., 2009).

On the other hand, challenges on the implementation of HT are present:

- Advanced HT methods are needed that can adequately simulate seismic response to collapse.
- It is necessary to reduce the epistemic uncertainty (i.e., uncertainty due to limited data and knowledge) on the calibration of numerical components.
- Substructuring techniques and effects on boundary condition assumptions must be considered.
- Validation of HT capability to trace failure to collapse is required.
- The propagation of experimental errors must be mitigated.
- Stiff systems and higher mode effects can introduce errors.

In this dissertation, a numerical updating approach aimed to recalibrate the properties of numerical components during the analysis is proposed to be included as an add-on module to the established HT methodology. Additionally, among the variety of existent lateral-load resisting systems, this study is focused on moment resisting frames tested up to collapse. In this sense, the implementation of this approach, as described in this dissertation, takes advantage of valuable information previously obtained on a scaled 1:8 four-story special moment resisting frame (SMRF), detailed on section 2.2.

The most salient impact of the present research is the development and implementation of an on-line recalibration procedure of the numerical subdomain of HT. This procedure is based on the acquired information of the experimental portion of the HT *during the analysis*. This

contribution to the hybrid testing method is aimed at improving the ability to simulate and predict collapse minimizing the epistemic uncertainty present on the initial calibration of numerical components. This uncertainty is inherent to the lack of knowledge of procedures and limited data of existing component testing. Additionally, the numerical approach can be readily incorporated as an add-on module to the well-established HT architecture.

The model structure utilized to implement the proposed numerical updating approach is presented in Figure 1.1, together with a substructuring approach to exemplify the conventional HT conceptualization.

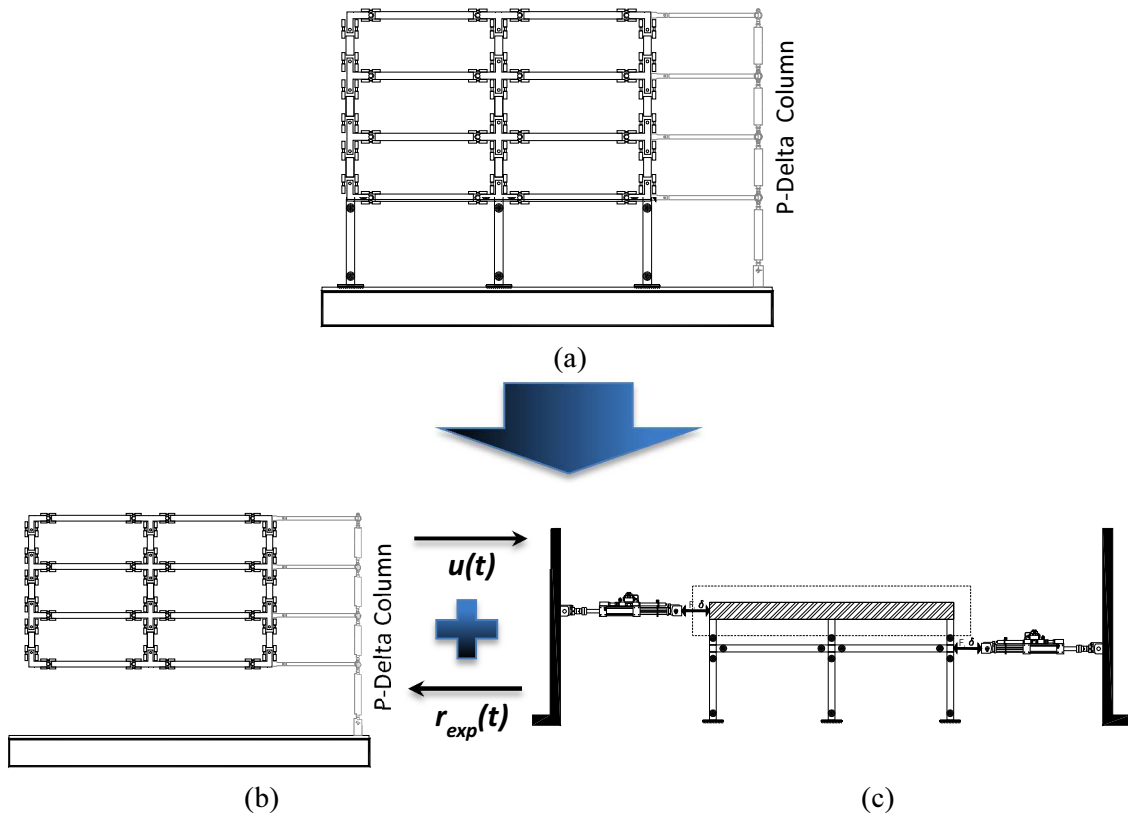


Figure 1.1. Hybrid simulation conceptualization, a) full structural model, b) numerical model and, c) physical model.

The physical subdomain of the model (Figure 1.1c)) is able to test material- and cross-section-level response of parts of the system with high nonlinear behavior that is difficult to model numerically. On its analytical counterpart (Figure 1.1b)), gravity and prestress loads (if present) are applied, accounting for second-order effects due to axial loads. It is assumed that the numerical portion is well known and can be confidently modelled.

The equation of motion for the prototype structure (Equation 1.1) relates the restoring forces ( $r_{exp}(t)$ ) obtained from physical (and numerical) models of structural resistance with the information from computer models on damping and inertia forces.

$$[m]\{a\}(t) + [c]\{v\}(t) + [r]_{num}(t) + [r]_{exp}(t) = \{p\}(t) \quad (1.1)$$

Where:

$[m]\{a\}$  = mass component,

$[c]\{v\}$  = damping component,

$[r]_{num}$  = structural restoring forces of the numerical substructure,

$[r]_{exp}$  = structural restoring forces of the experimental substructure,

$\{p\}$  = external excitation.

In HT, the restoring force is measured at each step from the experimental substructure, whereas  $m$ ,  $c$  and  $p$  are specified and  $a$ ,  $v$  and  $d$  are computed at each step. The pseudo-dynamic procedure (Mosqueda, et al., 2005) considering the general operations at step  $i$  of a test is:

1. Calculate the displacements at the next step  $d_{i+1}$ , using an appropriate numerical integration method.
2. Command the actuator to impose the displacements on the specimen using a suitable controller.
3. Measure the new restoring forces  $r_{i+1}$ .
4. Compute  $a_{i+1}$ ,  $v_{i+1}$  and other response quantities.
5. Repeat.

## 1.2. Motivation

Modern seismic design of buildings assumes that structures are intended to resist strong earthquake motions through inelastic response of their structural components (PEER, 2010). In this process, reliable collapse prediction of structures is needed. Hence, this study focuses on

developing and implementing an adaptive analytical updating scheme capable of recalibrating the initial parameters of the numerical models in HT through collapse. In this study, a model of a steel-moment-resisting-frame structure is used for this purpose. A concentrated plasticity approach is utilized to locate the nonlinear behavior on zero-length elements, focusing the adaptive updating process on the parameters related to those plastic hinges.

The general objective of model updating techniques is to correct the inaccurate parameters in the model; thus, improving the agreement between analytical predictions and test results. Specifically in the field of HS the need for updating methods is motivated by:

- Advantages of parametrization error minimization that add-on updating modules can provide to the established HS methodology,
- Uncertainties inherent to materials and geometric properties of components,
- Limitations on the size of the experimental portions that can be tested on the facilities, forcing the exclusion of parts of the system that may experience high levels of nonlinearity in complex MDOF structures.

Furthermore, when structural systems are exposed to significant cyclic lateral loads, members tend to plastify along the length of members due to plastification of successive cross sections (Deierlein, et al., 2001). For steel SMRF and according to prequalified steel beam-column connections (AISC, 2010), several configurations are recommended (reduced beam section (RBS), among others) to adequately develop localized spread of plastification (hinges) on specific positions on beams, far from the column faces. A significant portion of the inelastic behavior of the structural system is developed by these plastic hinges. Figure 1.2 exemplifies a prequalified steel beam-column connection (RBS), its designated geometry and protected zones based upon

experimental testing observations.

Numerical approaches like the concentrated plasticity method (CPM) are widely used to simulate structures subjected to inelastic demands and capture their behavior up to and through collapse. CPM allows inelastic behavior of structural systems to be modeled via plastic hinges (i.e., zero-length hinges) and elastic members, to estimate their global response under seismic loads.

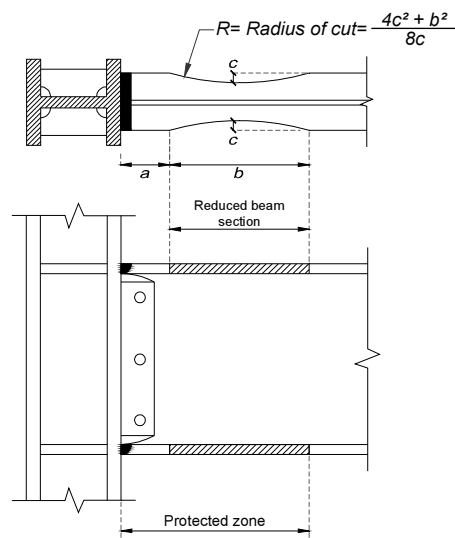


Figure 1.2. Reduced beam section connection (AISC, 2010).

Zero-length hinges allows models to locally induce relationships that associate parameters of available deterioration models with geometric properties and detailing criteria that control deterioration in actual structural systems (Lignos, 2008). The use of plastic hinges is numerically efficient. Additionally, different hysteretic models can be implemented to govern the inelastic behavior of these elements. Hysteretic models capable of controlling the main factors that affect cyclic deterioration are available, making its usage suitable for collapse studies. However, there are a few disadvantages of using concentrated plasticity approaches; they can ignore the spread of



inelasticity, and in many cases, axial deformations, the interaction between bending moments and axial forces, as well as the interaction between bending moments and shear forces. Spread of plasticity models can also be implemented to provide a more realistic modelling of progressive yielding in the cross section and along the element. These models allow the interaction between the bending moment and axial force. Their main disadvantages are the relatively high computational resources required, the need for calibration of the utilized number of fibers and segments, and the large amounts of data results to interpret (Stratan, 2014). In the particular case of this study, a concentrated plasticity approach offers the opportunity of controlling the inelastic behavior of the system via localized plastic hinges. At the same time the prototype SMRF structure, serving as benchmark case, is physically built considering elastic members acting as beam and columns and hinges designed to develop the inelastic behavior of the frame (see section 2.3), thus analytical and physical specimens follow the same idealization approach.

Hence, starting from the premise that a concentrated plasticity approach is to be employed on this research, an appropriate hysteretic model that is consistent with the behavior of the prototype structure, loading protocols, and objectives of the particular research must be adopted. Aimed at conducting an evaluation of structural systems and demand prediction at different hazard levels, hysteretic models capable of incorporate all important modes of deterioration observed in experimental studies (Ibarra, et al., 2005) are required. This need comes along with a concern that when structures are far into the inelastic range, components deteriorate in strength and stiffness.

The parameters defining the backbone curve and deterioration factors associated with the selected hysteretic model are calibrated based upon experimental testing. Nevertheless, dispersion in the results of experimental testing exists leading to uncertainty on the estimation of the parameters associated with the deterioration models. For instance, (Lignos & Krawinkler, 2011)

presented a report with a compilation of the available cyclic steel component tests conducted prior to 2008. Lignos and Krawinkler’s statistical regression analyses show mean values and dispersions for the parameters associated to a hysteretic model with strength and stiffness deterioration (Ibarra, et al., 2005).

In this dissertation, as detailed in section 2.2, wide flange sections equal to and deeper than 21” are used on the SMRF prototype model, utilizing RBS beam-column connections. Table 1.2 shows the mean values and dispersion of capping strength (i.e., peak strength of the load-deformation curve) to effective yield strength ( $M_c/M_y$ ) as well as effective to predicted component yield strength ( $M_y/M_{y,p}$ ) estimated for the beams (W-sections) of the full database utilizing RBS connections (i.e., , depth,  $d \geq 21$ ” classification). As can be seen, the dispersion of the effective-to-predicted yield strength is approximately 12% of its mean value and 3% for the capping to effective yield strength.

Table 1.2. Statistics of ratios of effective-to-predicted component yield strength and capping strength to effective yield strength, after Lignos (2011).

<b>CONNECTION TYPE</b>	<b>Mean of <math>M_y/M_{y,p}</math></b>	<b><math>\sigma_{M_y/M_{y,p}}</math></b>	<b>Mean of <math>M_c/M_y</math></b>	<b><math>\sigma_{M_c/M_y}</math></b>
<b>RBS</b>	1.06	0.12	1.09	0.03

Likewise, Table 1.3 depicts the number of specimens with RBS connections (i.e.,  $d \geq 21$ ” classification) employed to calculate linear regressions for pre-capping rotation ( $\theta_p$ ), post-capping rotation ( $\theta_{pc}$ ), and cumulative rotation capacity ( $\mathcal{A}$ ) which is a parameter defining the rate of cyclic deterioration (Lignos & Krawinkler, 2011). On the same Table 1.3 the coefficient of determination  $R^2$  and dispersions ( $\sigma_m$ ) are presented. As can be seen, the coefficient of determination lies between 0.48 and 0.56 for the studied parameters, leading to a large uncertainty on the estimation of the parameters based on previous experimental research.

Table 1.3. Statistics of pre-capping rotation ( $\theta_p$ ), post-capping rotation ( $\theta_{pc}$ ) and cumulative rotation capacity ( $\lambda$ ) of steel components with RBS connections ( $d \geq 21''$ ), after Lignos (2011).

<i>PARAMETER</i>	<i># of specimens</i>	$R^2$	$\sigma_{In}$
$\theta_p$	72	0.56	0.24
$\theta_{pc}$	61	0.48	0.26
$\lambda$	55	0.486	0.35

The previous information leads to the motivation of the present dissertation, opening the discussion for the following questions: How accurate are the assumptions of the component properties of numerical models used to model collapse? How reliable are existing models given the induced epistemic uncertainty on the calibration of component parameters? And consequently, can we improve our ability to predict collapse utilizing hybrid testing via recalibration of the numerical component parameters during the simulation?

### 1.3. Literature review

In recent years, research efforts to develop model updating strategies to recalibrate the analytical subdomain of the HS models have been under development. Previous studies presenting updating schemes on simple structures (single-degree-of-freedom (SDOF) and up to 3DOF systems) have been developed. For instance Yang et al. (2012) presented an online optimization method for bridge dynamic hybrid simulations, where a bridge with two identical piers was studied. Information from one pier simulated experimentally with a fiber element was utilized to optimize the parameters of the remaining identical numerical pier, governed by a hysteretic model (Modified Giuffr -Menegotto-Pinto). A multi-variable nonlinear optimization process was employed (Nelder-Mead Simplex method implemented in Matlab®). The method proved to be

capable of improving the accuracy of HS with multiple identical substructures.

Hashemi, et al. (2013), presented an online model updating where a two-dimensional one-bay frame model, consisting of two elastic columns connected at the top by an elastic truss element and nonlinear rotational springs at the base, was tested utilizing HS. The column and base nonlinear spring of the left side was considered as the experimental substructure, whereas the remaining elements of the frame, inertia forces and damping were modeled numerically. The modified Bouc-Wen hysteretic model with degrading stiffness and strength was utilized to govern the behavior of the nonlinear springs. Also, the Unscented Kalman Filter (UKF) was employed to update the parameters of the nonlinear hinges. The updated data from the experimental left spring was directly and instantaneously fed into the numerical part (right spring).

Song and Dyke (2014) conducted a numerical study to update a hysteretic model (i.e., Modified Bouc-Wen) in real time. Proposed error indexes demonstrated that UKF for parameter identification can accurately capture the behavior of nonlinear models subjected to cyclic tests.

Kwon and Kammula (2013) presented another study on model updating with substructuring utilizing ten additional numerical models (five experimental and five numerical simulated substructures) to the original one. The modeling parameters varied from one numerical model to another to represent a possible range of hysteretic characteristics of the experimental substructure, adding weighting factors to identify the closest alternative model. A 2DOF structure with two nonlinear springs (Bouc-Wen-Babel-Noori hysteretic model) and two identical masses are utilized on a verification example. Certain limitations were reported: The number of parameters to update and amount of alternative structures increases as the complexity of the hysteretic models and additional number of DOF's are included; depending on the objective function selected, the results may be different; recalibration produces only slight changes to the models, the method

cannot drastically change parameters during simulation and; accuracy depends on how well a user can predict the behavior of a structural element allowing the possibility of initial calibration errors.

Wang and Wu (2013) pointed out that parameters in many applications are confined within certain ranges to make sense physically and avoid errors of possible divergent responses. Thus, a constrained unscented Kalman Filter (CUKF) algorithm was proposed to improve accuracy of numerical substructure modelling in real-time HS. A 2DOF system is utilized to validate the method. It was concluded that the CUKF improves the accuracy of simulations compared to conventional HT and decreases parameter fluctuation. The employment of the CUKF avoided parameter values to violate bound constraints since they are moved onto the initially declared bounds.

Mueller (2014) introduced an on-line model updating for real-time HS deploying the UKF for parameter identification. A 3DOF shear type building model and Bouc-Wen hysteretic model were employed. The procedure was implemented numerically and experimentally utilizing a test specimen that emulates a building under a quasi-static loading protocol.

Elanwar and Elnashai (2014) proposed to update the numerical substructure through its material constitutive relationships during the test based on the data obtained from the physically tested component. The approach is based on utilizing genetic algorithms as an optimization tool to identify the constitutive relationship parameters to be updated in the numerical model. The proposed model updating approach is verified through two analytical examples of steel and reinforced concrete frames (two-bay one story frame). The results show that updating the constitutive relationship of numerical substructures can reduce errors.

Chen et. al. (2013) presented a reliability assessment tool (model accuracy indicator, *MAI*) to quantify the cumulative effect of modelling errors in HS. A fully numerical HS utilizing a SDOF

system consisting of one experimental spring and one numerical spring without model updating was conducted. The benchmark case objective was to show that initial errors on the parameters of numerical substructures lead to inaccurate outputs. Then *MAI* was formulated based on the measured responses of the experimental substructures to refine the numerical models of similar parts within analytical substructures subjected to the same displacement response history. Numerical analysis indicated potential for reliability assessment of HS when actual structural response is not available for immediate comparison.

Yet none of these previous studies deals with the limit state of collapse. Thus, post-capping slopes are not observed in the verification examples and the efficiency of the techniques during high levels of nonlinearity (close to collapse) cannot be evaluated.

The present dissertation focuses on a numerical updating approach that is implemented as an add-on module to the HS architecture. It is applied during the analysis through performance levels associated with limit states (service, design, maximum considered, collapse, and imminent collapse levels). Hence, it does recalibrate the numerical components of the analytical part from elastic behavior to collapse. The verification case is a complex MDOF structure (four-story, two bays SMRF), with substructuring and overlapping domains (Hashemi, 2013).

## **1.4. Problem definition**

Maturation of the understanding of nonlinear structural behavior up to collapse under seismic events has been historically a difficult task. Even though advances in computer science in the last fifty years have led to the development of powerful nonlinear analysis programs, the accuracy of their results is still dependent on the assumptions made in the characterization of their member properties. Many of these analytical models are calibrated based upon experimental

observations from quasi-static tests.

Over the years, exhaustive experimentation has been carried out on structural systems, components and subassemblies to better understand behavior under extreme loading conditions. Nevertheless, a lack of knowledge and an associated high dispersion on the characterization of properties of structural members exists.

On the other hand, HT has become an alternative to investigate seismic performance of structural systems up to collapse in a safe, economical and reliable manner. Furthermore, this experimental testing technique requires calibration of the properties of numerical components to be utilized on the analytical subdomain, including uncertainty on the simulations inherited by the aforementioned dispersion.

This document focuses on fully simulated HT up to collapse applied to SMRF's. In this type of simulation, initial properties are assigned to the parameters of the numerical components (e.g., *CPM*). Generally, it is assumed that such initial properties are either well known or can be represented with a high degree of confidence. Nevertheless, this is not always the case due to uncertainties in material properties and analytical models.

The numerical updating procedure is introduced via analytical studies that simulate the experimental substructure through an experimental virtual (laboratory) specimen. The necessary algorithms for the implementation of the proposed numerical updating procedure within an HS are developed. At the same time, procedures to determine *when* (during the dynamic analysis), *what* (parameters) and *how* (algorithms) to update are also investigated.

## **1.5. Research objectives and scope**

The main research objective is to improve the ability to predict and simulate collapse

through hybrid testing with substructuring techniques in complex MDOF structures. The methodology proposed to accomplish this goal is to use the knowledge gained at key structural locations during the experimental test to update numerical models of the rest of the structure during the HS *as the test is running*. This improvement is accomplished through; (a) the reliable estimation of updated information of the most important parameters that control the response of multi-story structures especially when the system is near collapse and; (b) the reduction of epistemic uncertainty on the response of the numerical components in HS with substructuring that originate from the inaccurate estimation of initial modeling parameters..

## **1.6. Dissertation outline**

A description and validation of the numerical models employed during the implementation of the proposed numerical updating procedure is presented in Chapter 2. Results from a shake table test performed at the State University of New York at Buffalo on a 1:8 scaled two bay/four-story special moment resisting frame (Lignos, 2008) are utilized as benchmark case. A substructuring technique with overlapping domains (Hashemi, 2013) is utilized to subdivide the selected base case structure into an experimental substructure (i.e. virtual laboratory) consisting of the bottom 1.5 stories; and a numerical portion (3 upper stories and leaning column), in order to perform multiple fully numerical HS with substructuring.

Utilizing the selected substructured model, Chapter 3 presents the distinctions between a hybrid test performed in a real laboratory (i.e., physical specimen), and a fully numerical HS where the experimental part is also numerically modeled. The differences on the required testing equipment and controlling data flow are also addressed. At the same time the chapter describes common characteristics inherent to the hybrid testing philosophy when physical specimens or



virtual laboratories are employed. The chapter defines the limitations of the proposed numerical procedure, emphasizing the fact that experimental errors are not considered since a virtual laboratory is utilized for the simulations. Record-to-record variability is not addressed given that a single scaled ground motion is utilized. However, epistemic uncertainty is accounted for by inducing errors in the initial calibration of numerical components. An overview of the proposed numerical updating procedure is depicted, addressing globally the three basic stages of the updating procedure; *what to update*, *when to update*, and *how to update*. A case study containing induced initial calibration errors on the numerical components is presented and compared to the benchmark case to illustrate the procedure.

Chapter 4 describes the first stage of the updating procedure (i.e., Phase I). It consists on acquiring global first-story drift / base shear hysteretic information from the (virtual) experimental specimen at key steps during the analysis to determine *when to update*, until the system approaches to the limit state of collapse. This information is utilized to conduct a numerical fit of the main parameters of a phenomenological deterioration model used to represent this global response to determine *what to update*. Hence, a group of rules is designed and implemented to recalibrate the selected hysteretic model parameters along the simulation.

In Chapter 5 information on relevant global information obtained in Phase I is utilized to recalibrate individual local component parameters of the analytical subdomain. A numerical procedure to distribute damage from global to local domain (Phase II) is developed and implemented, thus providing guidelines on *how to update*. Some of the advantages of utilizing the updating technique when initial calibration errors (epistemic) may exist are as well discussed. Two illustrative examples are presented. Firstly a fully numerical HS of the benchmark case without initial calibration errors directed towards to demonstrate that the procedure is capable of

reproducing cyclic degradation effects and secondly, a study case with randomly generated numerical component parameter errors previously documented (Negrete, et al., 2014).

Chapter 6 explores the potential of the proposed updating procedure to minimize the effect of the uncertainty associated with the estimation of numerical component parameters. A set of cases with introduced initial random calibration component parameter errors is built. Fully numerical HS are performed utilizing this created bin, with and without the application of the proposed numerical approach. Outputs are examined on a case-by-case basis. A discussion of the most relevant observations observed from the simulations performed involving different initial conditions is presented.

A summary of the procedure and the findings of this investigation are discussed on Chapter 7. Future work and recommendations are also presented.

## **CHAPTER 2**

# **VALIDATION OF NUMERICAL MODELS EMPLOYED ON THE IMPLEMENTATION OF THE NUMERICAL UPDATING APPROACH**

### **2.1. Introduction**

This research proposes a numerical updating approach aimed at improving the responses obtained through hybrid simulations up to collapse. This updating approach can be incorporated as an add-on module into the established conventional hybrid simulation methodology. As it is the case with conventional hybrid simulation, the successful implementation of the proposed procedure necessitates the availability of reliable numerical models. In this context, results from shake table testing up to collapse with a scaled model of a four-story special moment resisting frame (Lignos, 2008) are used as a benchmark to validate numerical models and evaluate the outcomes of hybrid simulations. These results are illustrated in section 2.2. Extensive information from the test results is available and includes parameters such as: displacements, forces, accelerations at the base of the structure, and the collapse mechanism. As a starting point, section 2.3 describes a numerical model of the complete frame developed to reproduce the results of the shake table test utilizing a concentrated plasticity approach. The model on this first iteration reproduces the results of the shake table test employing a fully numerical hybrid simulation (i.e. the physical specimen is replaced with a numerical model). Section 2.4 presents a general description of an existing substructuring technique developed to better account for boundary conditions in complex structural systems using hybrid simulations (Hashemi, 2013). The

development and implementation of this substructuring technique is another component of the broader NSF-sponsored research project entitled: “NEESR-Collapse simulation of multi-story buildings through hybrid testing”. The aforementioned substructuring technique was developed by research-team members of the University at Buffalo. A calibrated version of the numerical model is utilized in section 2.5 to validate this substructuring technique, presenting several substructure alternatives for the four-story SMRF. One of the suggested substructured models presented in section 2.5 (1.5 stories as experimental specimen) is selected to develop, implement, and demonstrate the proposed numerical updating procedure in this dissertation.

## **2.2. Previous shake table studies**

The design of a prototype four-story steel structure was performed by Lignos (2008) as part of a study focused on investigating sidesway collapse of steel moment frames. The building is assumed to be located in Los Angeles, California. One of the perimeter frames that resist lateral loads primarily in the east-west (EW) direction is used in this study. The main characteristics of the investigated building are as follows:

- The structure was designed as an office building with movable partitions, a penthouse (Figure 2.1(a) and (b)), and floor system consisting of metal decks with 4 1/4” lightweight concrete slabs.
- The structural system is a SMRF with fully restrained reduced beam sections (RBS) designed in accordance with the 2003 International Building Code and FEMA-350 (2000) criteria.
- The first story of the building has a height of 15 feet while the upper stories have heights of 12 feet (Figure 2.1(c)).

- A992 Grade 50 steel is specified for all structural steel components.
- The first three modal periods in the EW direction are 1.33, 0.43, and 0.22sec.
- Columns are fixed at the base. All columns are spliced at mid-height of the third story (Figure 2.1(c)).

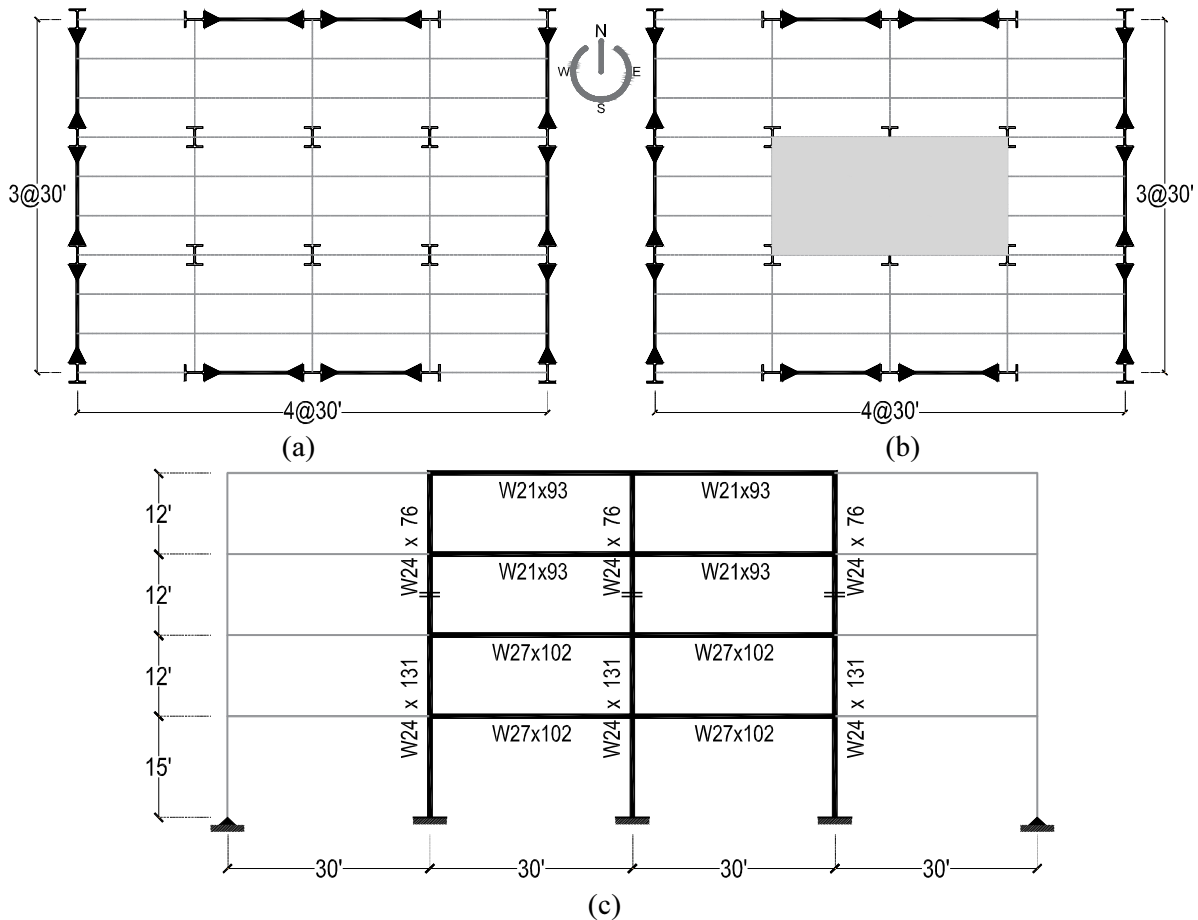


Figure 2.1. Prototype office building, (a) Plan view of a typical story, (b) Plan view of roof, penthouse highlighted in gray, (c) Elevation of EW SMRF (Lignos, 2008).

Two scaled models (1:8) of one of the EW perimeter moment resisting frames of the four-story steel prototype structure were designed, fabricated, and tested up to collapse using the shaking table of the Network for Earthquake Engineering Simulation (NEES) facility at the State University of New York at Buffalo. The prototype was scaled following similitude laws (Moncarz,

1981). The objective of the tests was to evaluate numerical collapse predictions for steel moment frames by explicitly addressing  $P-\Delta$  effects and component deterioration.

Two frames were tested as part of the study. In this dissertation, results from the second shake table test specimen are used as a benchmark for the comparative results to be presented in subsequent sections. The target periods of the scaled structure are 0.47sec, 0.14sec and 0.07sec respectively for first, second and third mode of vibration. The second frame reported an improved behavior compared to the first test (e.g., minimized amount of friction, change of collapse direction induced by a different set of ground motions utilized on frame 1). This second specimen was subjected to five consecutive scaled ground motions to investigate the effect of cumulative damage on the collapse capacity of the frame. The records were scaled from the same ground motion (Canoga Park record station, January 17 of 1994, Northridge, CA.) to five increasing intensities associated with various limit states (i.e., service level earthquake *SLE*, design based earthquake *DBE*, maximum considered earthquake *MCE*, collapse level earthquake *CLE* and imminent collapse level earthquake *CLEF*). The amplitude scale factors for the level of intensities were 0.4, 1.0, 1.50, 1.9 and 2.2 respectively. The accelerations at the base of the structure recorded from the shake table test (with a sampling rate of 128 Hz) are used as input for the hybrid simulations performed in the present research. It should be noted that for the particular case of the benchmark structure, axial loads are not included in the experimental models due to: 1) the frame being exposed to relatively small seismic axial load demands due to its geometry and aspect ratio, and 2) the tributary area/loads directly imposed on the selected frames are relatively small as most of the gravity loads are resisted by the interior gravity frames. Hence, since the benchmark case did not consider relevant the application of axial loads during the testing, the numerical models utilized on this dissertation did not account for these demands in order to conduct an evaluation

under similar testing conditions.

Figure 2.2(a) shows the experimental shake table test setup utilized by Lignos. The scaled model of the EW direction SMRF was connected through rigid links at each floor level to transfer the  $P-\Delta$  effect of the mass simulator (right hand side Figure 2.2(a)) to the test frame. The model specimen was built using aluminum members representing elastic elements (Figure 2.2(a)) connected to cruciform-shaped solid aluminum components joined to the aluminum members by pins and replaceable steel plates, simulating plastic hinges at the location of the RBS sections in beams and at points where plastic hinges have the potential to develop in columns (Figure 2.2(b)). While the aluminum elements remain elastic, replaceable steel plate coupons were inserted at plastic hinge locations to provide repeatable nonlinear simulations. The hinges were fabricated with a natural hinge and two reduced section steel plates (i.e., dog bone) as shown in Figure 2.2(c). An elevation drawing representing the 1:8 scaled frame assembly dimensions is depicted in Figure 2.2(d). This configuration aims to simulate the deteriorating strength and stiffness properties of plastic hinge regions of the prototype structure at all levels of deformations up to collapse.

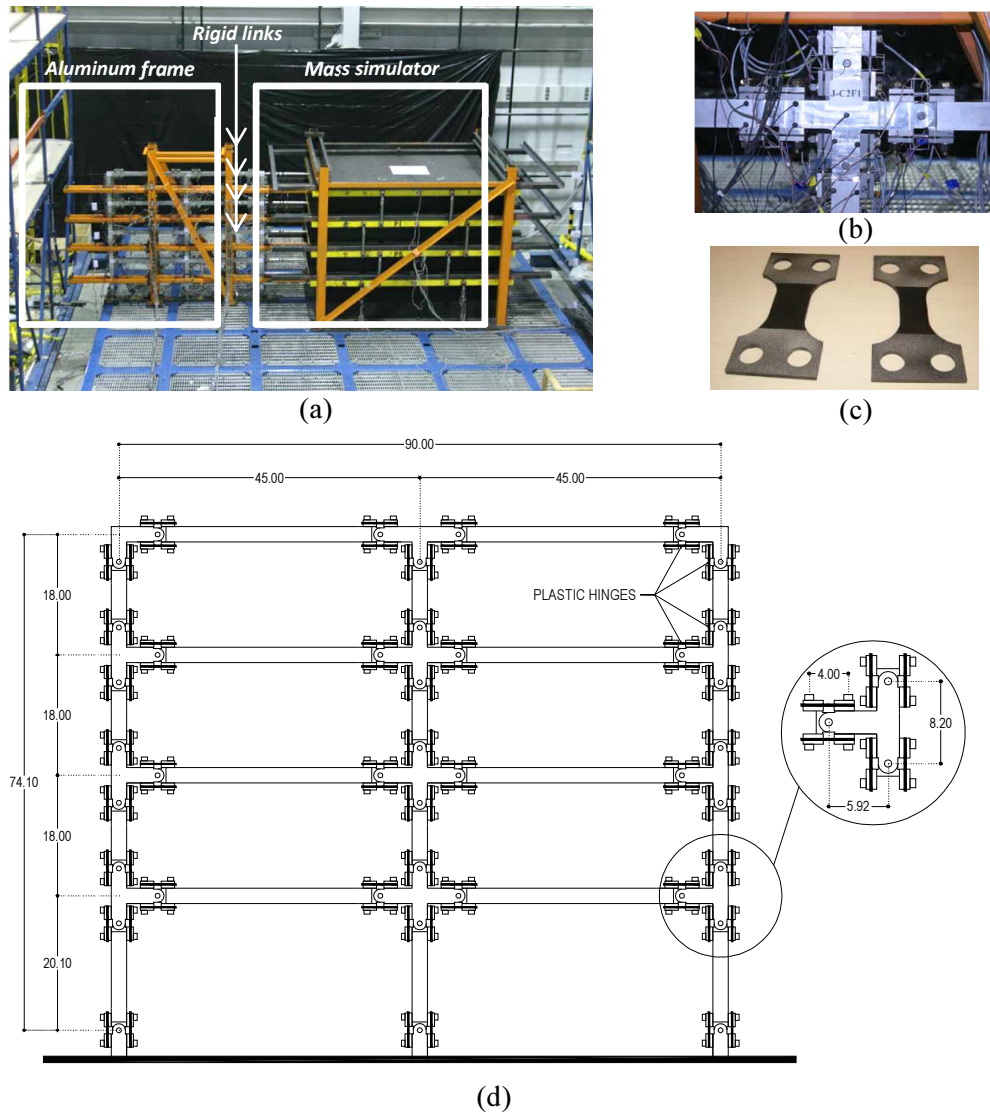


Figure 2.2. Four-story shake table test, (a) experimental setup, (b) natural aluminum hinges, (c) dog-bone steel hinge plates, after Lignos (2008), (d) 1:8 scaled frame assembly dimensions (in).

### 2.3. OpenSees full frame model results vs. shake table results

A numerical model was developed and calibrated using the Open System for Earthquake Engineering Simulation platform (McKenna, et al., 2000) to reproduce the obtained response of the shaking table test. A first version of the model was developed by Eads et al., (2012) as part of a study aimed to propose an efficient method for estimating the sidesway collapse risk of structures in seismic regions. This study focused on identifying for a given structure and location, the range



of ground motion intensities that controls the collapse risk. This goal was accomplished by deaggregating the mean annual frequency of collapse estimates for the structure. It was concluded that ground motion intensities consistent with the lower half of the collapse fragility curve (below the median) contributed the most to the collapse risk. The proposed technique by Eads et. al., leads to a significant reduction in computational effort and the uncertainty in the estimation of collapse risk.

A concentrated plasticity approach was used where beams and columns were modeled as elastic elements, utilizing nonlinear rotational springs located at the center of the reduced beam section and at the ends of the columns. The hysteretic behavior of the plastic hinges was governed by a modified version of the Ibarra-Medina-Krawinkler deterioration model (Lignos, 2008). A leaning column carrying gravity loads was used in the analytical model to simulate the  $P-\Delta$  effect. This leaning column was connected to the frame at each floor level via axially rigid links to: 1) reproduce the  $P-\Delta$  effect on the main frame by applying gravity loads that are taken by interior gravity frames, 2) simulate the lateral acceleration effect produced by the tributary building masses during a seismic event. The approach is numerically equivalent to the mass simulator connected through rigid links to the scaled aluminum model frame used for the shaking table studies (Figure 2.2 (a)).

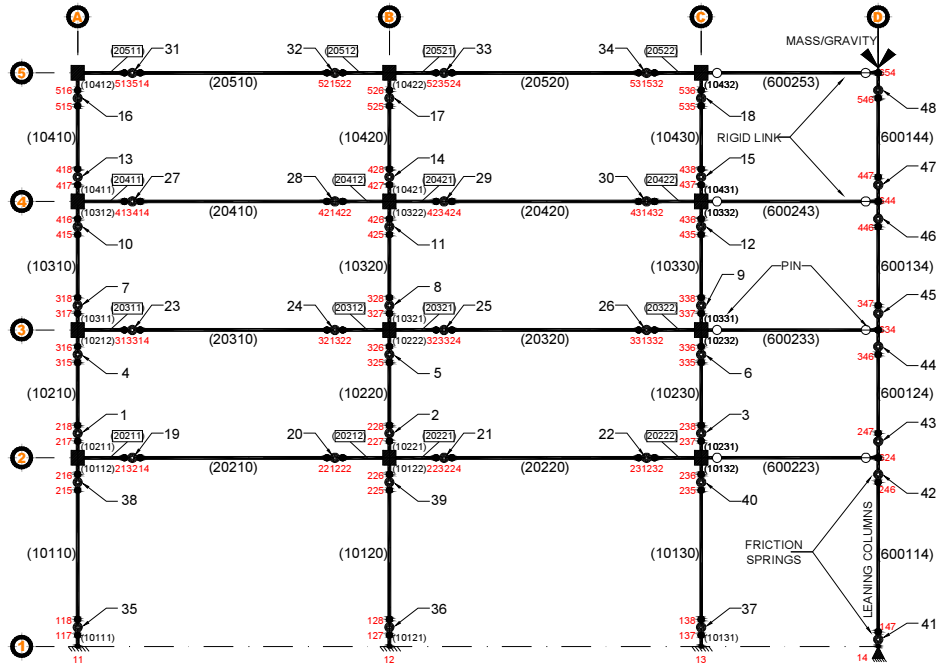


Figure 2.3. Numerical model of the scaled structure.

The present dissertation uses numerical models useful for hybrid simulation that were calibrated by reproducing the interstory drift ratios and story shear forces from the shake table tests. The utilization of these metrics led to matching the global behavior of the base case and at the same time providing a direct source for checking during the implementation on a laboratory since the information can be acquired from actuators and other measuring devices during the experiment. These hybrid models consist of a virtual experimental (simulated laboratory) and a numerical substructure, as shown in Figure 2.4, so they differ from the full numerical model of Figure 2.3. The experimental portion of the hybrid models consists of the scaled 1:8 four-story SMRF, whereas the numerical part includes the leaning column with added gravity loads to simulate the structure  $P-\Delta$  effect. The initial hybrid model was calibrated by Hashemi (2013) by adding friction elements (i.e. rotational springs with elasto-plastic behavior) at every story on the leaning column to simulate the energy dissipation mechanisms. Additionally, Rayleigh damping ratios were of 2% and 5% were assigned to the first and third vibration modes respectively.

Detailed explanations of the calibration results can be found in Hashemi (2013). The Newmark's method with fixed number of iterations integration scheme was employed on the hybrid simulations.

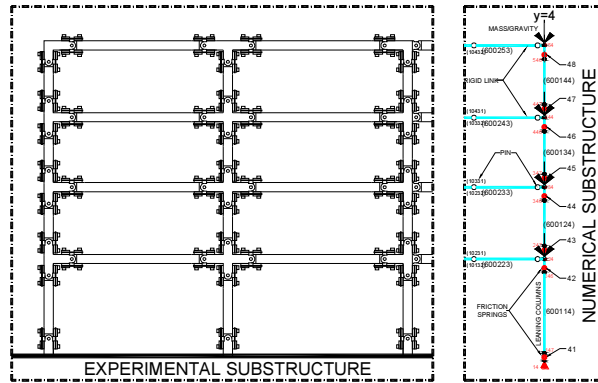


Figure 2.4. Hybrid simulation substructures, four-story SMRF model.

As described in Ahmadizadeh (2007) in order to minimize the likelihood of numerical instability and systematic error propagation, a proper selection of the integration time step for numerical simulations should be considered. The selected time step should satisfy the stability conditions of the utilized integration algorithm, at the same time that must be small enough to accurately capture the nonlinear behavior of the test structure. The time step should meet the available communication capacity with the testing equipment for the intended experiment rate. MDOF systems would necessitate small integration time intervals to satisfy the required numerical stability criterion (Yamada & Iemura, 1992). Hence, decisions on the optimal time step size must be made.

As part of the calibration process carried out by Hashemi (2013), it was confirmed that when too small time step sizes are considered, experimental instability can arise in the linear elastic range due to the inability of the testing system to control displacements, inadequate instrumentation, setup procedures, or misalignment of the physical setup. Also, Hashemi (2013)

reports that limited resolution of the available actuators may lead to the inaccurate application of displacements when the time step is too small. However, the use of large analysis step sizes can cause numerical instability, especially when high levels of nonlinearity are achieved due to convergence issues. Table 2.1 presents the final analysis steps obtained for the hybrid simulations discussed on this research, where  $dt$  is the recording sampling rate of the shake table acceleration equal to 128Hz (i.e., 0.0078125 sec). The time steps and number of iterations were selected to minimize the potential for numerical instability. In addition, delays in network communication, computation process, and instrumentation filtering on the State University of New York at Buffalo (Hashemi, et al., 2013) were accounted for. The first set of values was later modified during the implementation of the proposed numerical approach to achieve convergence during the analyses.

Table 2.1. Analysis step size information, recalibrated model.

Analysis/Record	Step Size	Increment (Sec)	Analysis steps/Record	Limit State
$dt_{\text{Analysis1}}$	0.50 dt	0.00391	2560	Service level (SLE)
$dt_{\text{Analysis2}}$	0.13 dt	0.00098	10240	Design base (DBE)
$dt_{\text{Analysis3}}$	0.10 dt	0.00078	12800	Maximum considered (MCE)
$dt_{\text{Analysis4}}$	0.06 dt	0.00047	21333	Collapse level (CLE)
$dt_{\text{Analysis5}}$	0.06 dt	0.00047	21333	Imminent collapse (CLEF)

For the hybrid tests conducted as part of this study, the same final sequence containing the five scaled earthquakes was used, adding a minute of free vibration between each scaled record. Rayleigh damping ratio of 20% was applied to the free vibration stages to bring the structure to rest before the next excitation.

Figure 2.5 depicts a comparison of the inter-story drifts obtained from the calibrated numerical model, including the aforementioned characteristics, subjected to the final earthquake sequence from the recorded shake table results (Hashemi, 2013). All hybrid simulations conducted

as part of this study were based on exposing the calibrated model to the same sequence of support excitations recorded on the shake table tests, which are used as benchmark for comparison.

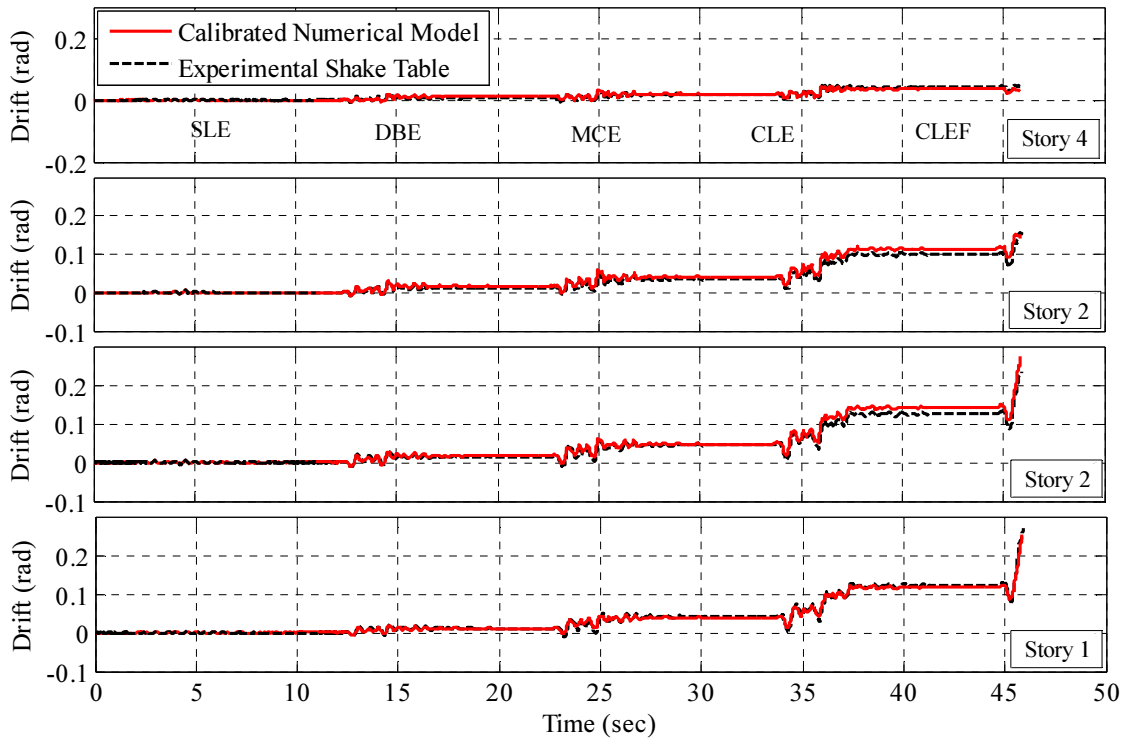


Figure 2.5. Comparisons of inter-story drifts of numerical model vs. shake table test, after (Hashemi, 2013).

## 2.4. General description of substructuring technique

In hybrid simulations, the physical specimen can consist of the full structural system. Nevertheless, limitations on size, loading carrying capacity and availability, capacity of testing equipment (e.g., actuators), as well as limited resources to build large-scale-full-system specimens, are constraints that can lead to the application of substructuring techniques where only critical portions of the structure are physically constructed and tested. Thus, substructuring techniques allow separating the complete structural system into several parts (Mosqueda, et al., 2005). In this sense, the portions of the structure that exhibit a more complex behavior, and consequently are

more difficult to model with a high degree of precision, can be physically tested. Those sections with a consistent and well-defined behavior can be numerically analyzed (Saouma & Sivaselvan, 2008).

The substructuring procedure presented in Hashemi (2013) is utilized in this study and is briefly explained next. This procedure introduces a technique developed to better account for boundary conditions in complex structural systems using hybrid simulations. The main 1:8 four-story SMRF model is subdivided into an experimental sub-domain containing the lower one-and-a-half levels of the structure and a numerical part comprising the upper full three levels plus the leaning column, not including first level columns, as shown in Figure 2.6. The substructuring approach introduces overlapping domains and shares redundant elements between the numerical and experimental substructures, interacting by more than the boundary interface. Therefore, it is possible to enhance the subassemblies boundary interface interactions.

In the overlapping substructuring technique, the actuators are used to impose the command displacements on the boundary of the experimental substructure (nodes of  $n_1$ ,  $n_2$  and  $n_3$ , Figure 2.6). The internal member forces are then obtained inside the experimental portion on a location sufficiently far from the loading boundary to reduce the effect of the pin assumption at the midheight of columns. Assuming that the point of inflection is located at the column midheight throughout the response history could significantly change the response and collapse mechanism of the structure. The experimental specimen extends beyond its intended boundaries (half story-height on this investigation) to apply the concentrated actuator loads. This way, the feedback forces are measured away from the loading boundary, which is significantly influenced by the assumption of zero bending moments at the column cuts. At the same time the overlapping of numerical and experimental substructures enhance the subassembly interface interactions, sharing redundant

elements.

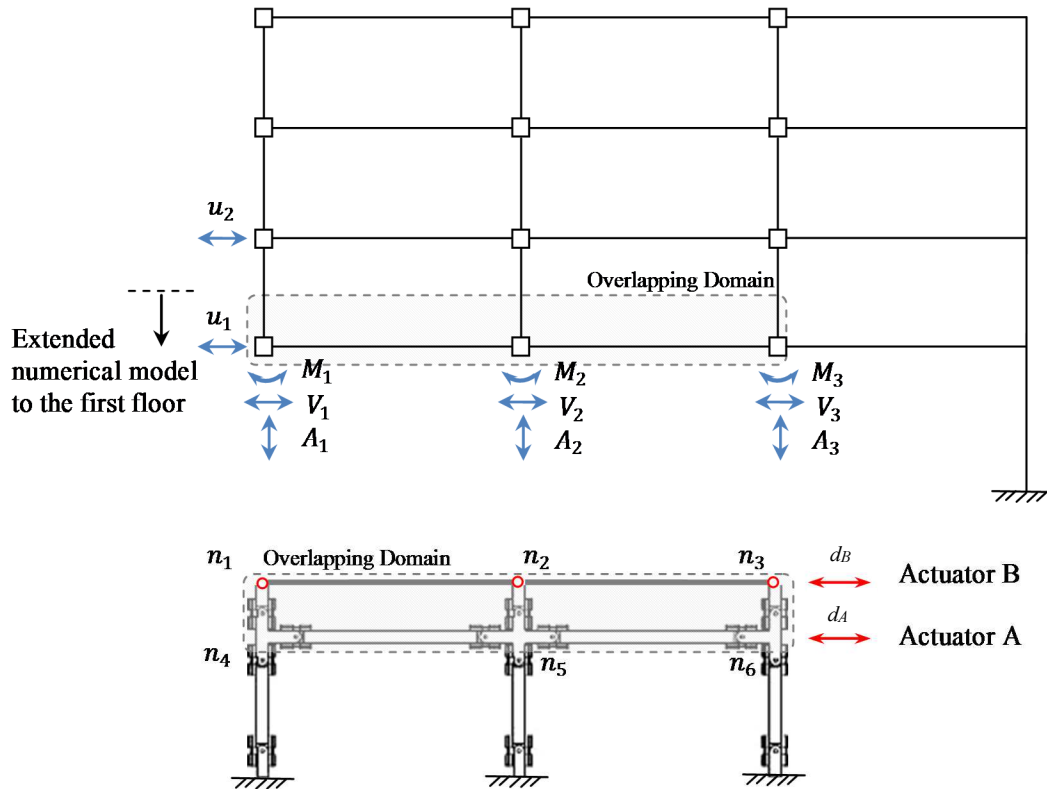


Figure 2.6. Experimental and numerical substructures and their overlapping interface, after (Hashemi, 2013).

In this substructuring approach, the command displacements are imposed to the boundary of the experimental substructure (midheight of the columns of the second story). As can be seen in Figure 2.6, the rotational DOFs at the interphase are not controlled in the experimental substructure to minimize the number of actuators needed to perform the simulation. The translational DOFs are assumed to be the same in the interface of  $n_1$ ,  $n_2$  and  $n_3$  and are horizontally constrained by a rigid truss element. Thus, the initial nine DOFs are reduced to one unidirectional horizontal DOF controlled by one actuator (Actuator B, Figure 2.6). One additional actuator (Actuator A, Figure 2.6) controls the first floor horizontal displacement. The actuator command displacements are calculated as:

$$d_A = u_1 \quad (3.1)$$

$$d_B = \frac{u_1 + u_2}{2} \quad (3.2)$$

where  $d_A$  and  $d_B$  are Actuator A and B command displacements, and  $u_1$  and  $u_2$  are first and second floor displacements, respectively, which are calculated from the numerical model. Next, the restoring forces are measured and transferred back to the numerical model. Furthermore, axial, shear and moment demands for each first-story columns at the location of nodes  $n_4$ ,  $n_5$  and  $n_6$  are computed ( $A_i$ ,  $V_i$ , and  $M_i$ ;  $i = 1, 2, 3$ ) and fed back from the experimental substructure to the numerical finite element model.

## 2.5. Numerical substructuring technique vs. full numerical model

The initial decision on the implementation of a substructuring technique is to determine the most advantageous subdivision of the structural system. The choice is based on engineering judgment supported by previous numerical studies and/or previous knowledge of the structural system in terms of its inherent deterioration behavior and potential collapse mechanism. Also, the availability of equipment on the testing facility must be strongly considered. For instance, when dealing specifically with the four-story SMRF model used in this study, several options on selection of sub-domains are available. Some possible scenarios (illustrative but not limitative) are presented in Figure 2.7. One first option is to use the full frame as an experimental specimen without overlapping elements with the numerical part (Figure 2.7(a)). This approach is consistent with conventional pseudo-dynamic testing. In this case, four actuators would be necessary to apply horizontal displacements at each floor level. A second scenario is to consider the 3.5 bottom levels



as physical specimen and the upper two levels and leaning column as numerical sub-domain (Figure 2.7(b)), overlapping 2.5 levels. In this configuration, four actuators are also needed to apply floor displacements on each floor level in addition to the displacements at the interphase (i.e., level 3.5). A third possibility is to use 2.5 levels as experimental portion and the remaining elements as numerical domain (Figure 2.7(c)). In this setup 1.5 levels are overlapped between domains. Three actuators are needed to perform the test with this arrangement. Lastly, 1.5 levels can be considered as the physical specimen, needing only two actuators, one at the second-floor level story and another at the sub-domains interphase (Figure 2.7(d)). The smallest overlapping domains are attained with this configuration (only a half story level).

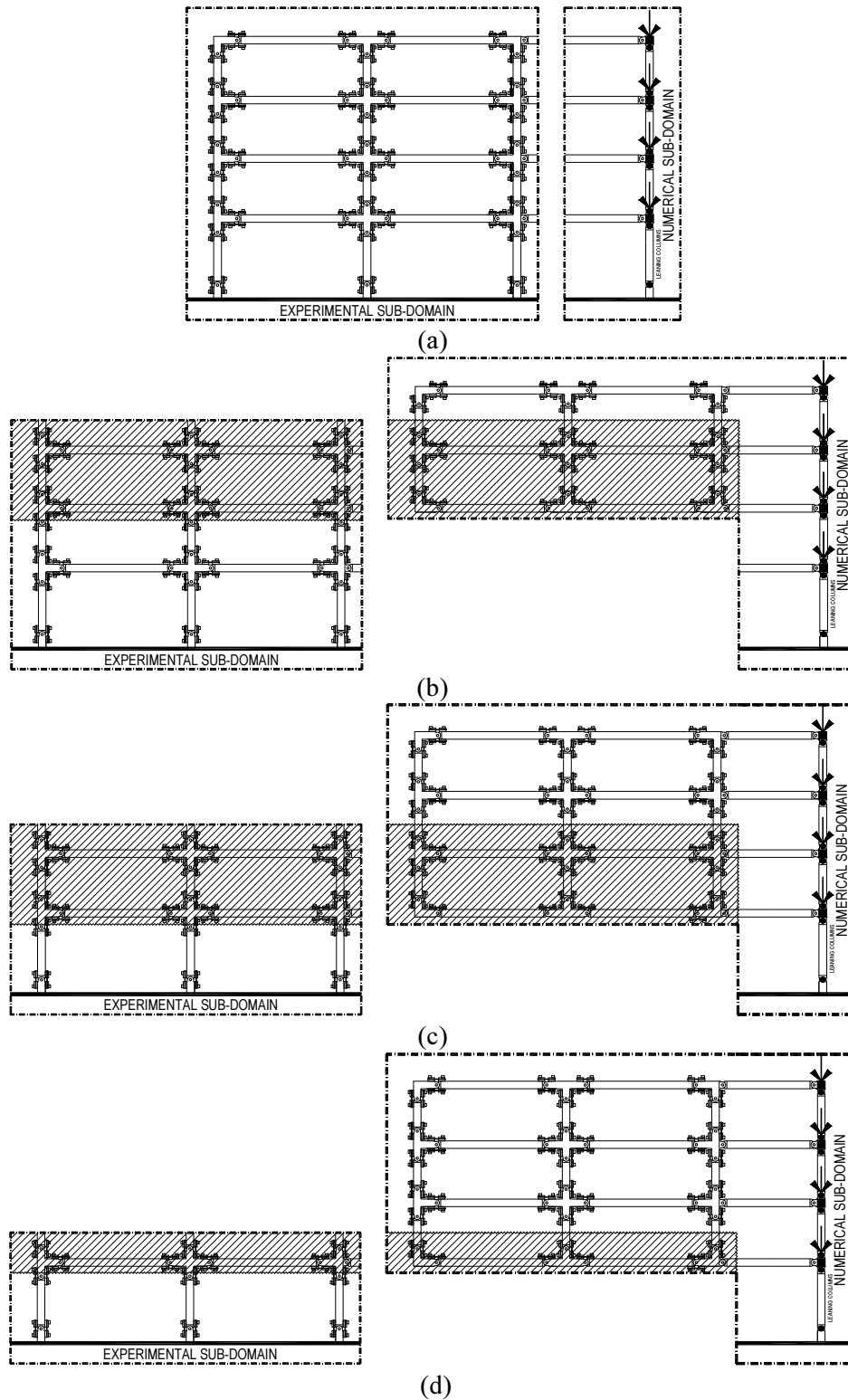


Figure 2.7. Substructuring options: (a) full SMRF experimental w/o/overlapping, (b) 3.5 stories SMRF experimental w/overlapping, (c) 2.5 stories SMRF experimental w/overlapping, (d) 1.5 stories SMRF experimental w/overlapping.

An evaluation of differences between story drift ratios obtained from shake table tests and hybrid simulations were conducted with experimental specimens corresponding to: i) full numerical calibrated model (Figure 2.7(a)), ii) 2.5 floor levels (Figure 2.7(c)) and, iii) 1.5 floor levels (Figure 2.7(d)), and is shown in Figure 2.9. As can be observed, good agreement exists among the compared results. However, the highest deviation is observed with the 1.5-story substructure at the *CLE* and *CLEF* ground motions due primarily to the approximations induced by the substructuring technique at the boundary of the experimental substructure. However, even if this deviation is the highest, the relative differences with respect to the full numerical calibrated model are relatively small (e.g., deviations of 5% for the first story with respect to the base case).

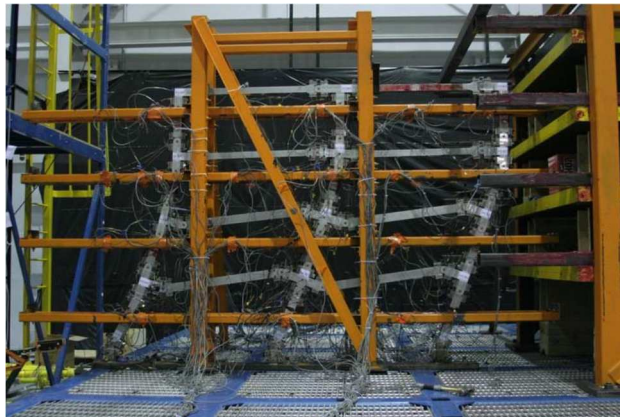


Figure 2.8. Collapse mechanism of the four-story SMRF after a shake table test, after Lignos (2008).

Previous knowledge about the four-story structure is available. Moreover, the collapse mechanism obtained from the shake table test performed by Lignos (2008) utilizing the same ground motions and SMRF model is presented in Figure 2.8. As it can be seen, the deterioration is mainly concentrated on the first three levels. Based on this information, on the present research, the numerical updating approach is implemented using the 1.5-story substructure (Figure 2.7(d)) for which the numerical errors are still relatively small as can be observed in Table 2.2. In addition,

this configuration offers a suitable experimental setup in the laboratory because it requires the least number of actuators of the suggested configurations. Hence, the amount of equipment and instrumentation required to perform the test is significantly reduced. Another reason to choose this substructure as the target case is the relatively high level of nonlinearity present at the bottom story (see Figure 2.8), which is consistent with the hybrid-testing philosophy of experimentally testing the portions of the system with the highest degree of nonlinearity.

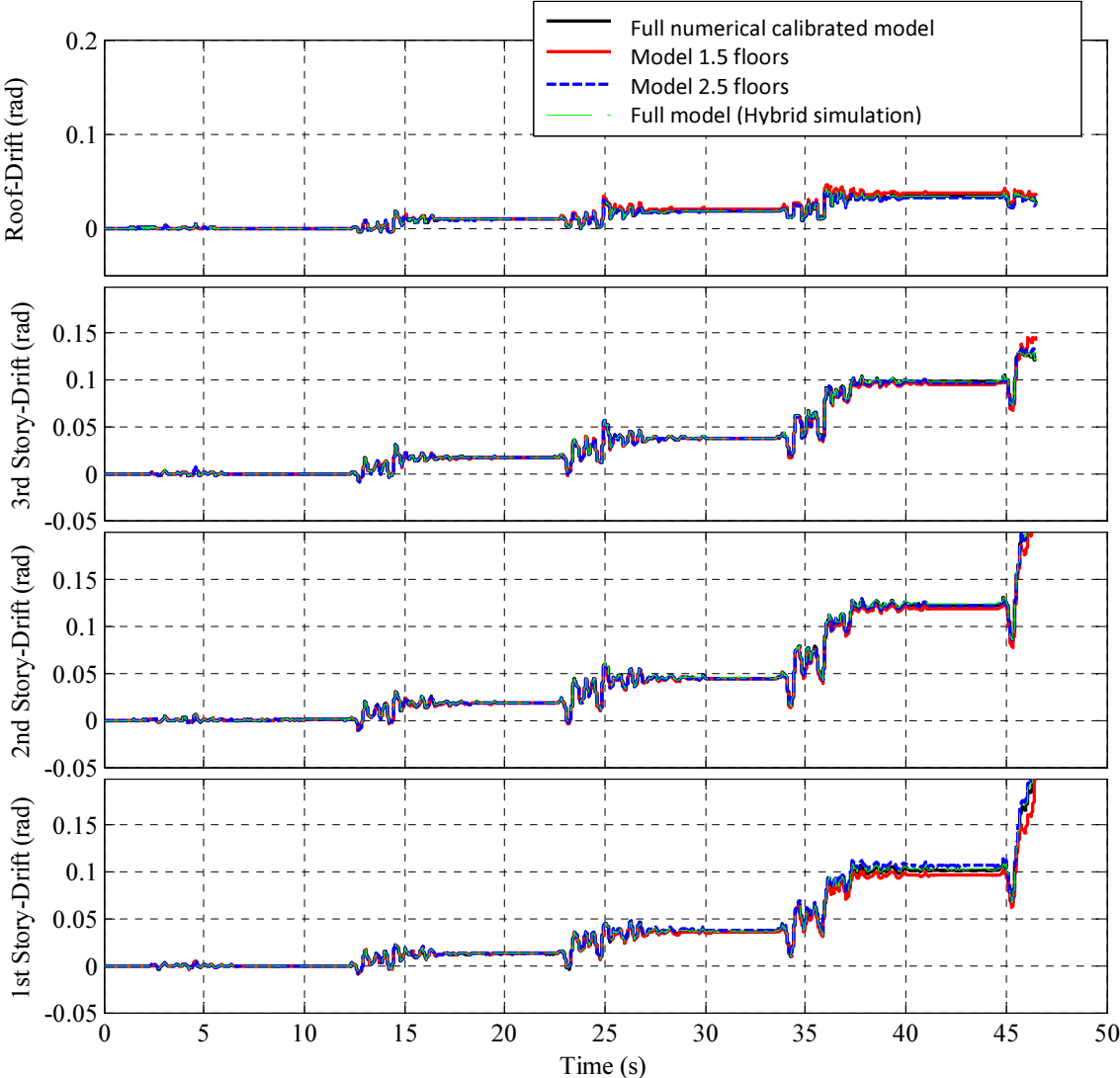


Figure 2.9. Comparison of inter-story drifts for suggested substructures, after (Hashemi, 2013).

Table 2.2. Absolute error ratios from substructured hybrid models to base case.

<i>MODEL</i>	<i>ROOF</i>	<i>3<sup>RD.</sup> STORY</i>	<i>2<sup>ND.</sup> STORY</i>	<i>1<sup>ST.</sup> STORY</i>
<i>2.5 Floors</i>	5%	1%	0%	4%
<i>1.5 Floors</i>	12%	4%	3%	5%

## 2.6. Summary and Conclusions

In order to implement the numerical updating approach developed and proposed in this dissertation, reliable numerical models are needed. As a departure point for this research, previous results from a shake table test study conducted to evaluate the seismic collapse potential of steel moment frames (Lignos, 2008) were used as benchmark. This process was facilitated because of available information on the frame design; main geometric, material, and structural properties; recorded support excitation from the shake table experiment; documented collapse mechanism; and the specimen itself.

The numerical models employed on this dissertation were developed based on previous research from team members ((Eads, et al., 2012), (Hashemi, 2013)). These models started with an initial iteration with the properties of the benchmark case. Later a recalibration of the model was carried out to perform hybrid simulations and developed a substructuring technique for complex structural systems (Hashemi, 2013).

In the present research the substructuring technique with overlapping domains, as proposed by Hashemi (2013), is employed to conduct the development and implementation of the proposed numerical approach.

From several presented possible scenarios of substructured arrangements for the four-story SMRF, the 1.5-bottom-stories configuration was selected to implement and illustrate the proposed numerical updating technique. In this configuration, the four top stories plus the leaning column are used as numerical subdomain. It is considered as an advantageous configuration to illustrate

the approach and eventually implement it on a real laboratory since it offers a suitable experimental setup, preserving good accuracy with respect to the benchmark case.

## CHAPTER 3

### NUMERICAL UPDATING APPROACH - A GENERAL OVERVIEW

#### 3.1. Introduction

The preceding chapter dealt with model validation and the selection of a suitable substructuring option for the implementation of the numerical updating approach (NUA). Based on the results presented in Chapter 2, substructuring is performed using the bottom 1.5 stories of the 1:8 scaled SMRF as the experimental substructure. In this approach, the upper three stories of the SMRF are used in the numerical subdomain. Thus, the overlapping domain consists of the bottom half of the second-story columns. In order to develop and implement the proposed NUA add-on hybrid simulation module, multiple numerical simulation trials are carried out. In these trials, the experimental substructure is modeled numerically (*i.e.* virtual experimental substructure). Alternatively, one could perform numerous hybrid simulations with a physical experimental substructure in a laboratory; however, this approach is impractical, inefficient, and costly. The following sections include a discussion of the overall approach to implement numerical updating, including the incorporation of fully numerical simulation trials.

#### 3.2. Implementation of fully numerical hybrid simulation

This study is part of a broader research project entitled: “NEESR-Collapse simulation of multi-story buildings through hybrid testing” funded by the National Science Foundation (NSF) (<http://nees.org/warehouse/project/912>). An overall objective of this NSF-funded research project

was to validate hybrid testing through collapse using hybrid simulations with a 1:8 scale SMRF structure built on a physical laboratory (NEES@Buffalo). To achieve this goal, a conventional hybrid testing architecture was implemented taking into account the available floor space and equipment at the NEES@Buffalo laboratory (see Figure 3.1). The selected physical substructure consists of the bottom 1-½ stories (as described in Chapter 2), which was attached to the laboratory strong floor. Two servo-controlled actuators were used; one was attached to the strong wall of the laboratory and a second one to a steel reaction frame. The second actuator was hanging from an auxiliary supporting frame designed to carry the self-weight of the actuator and at the same time, allow it to rotate when necessary (Figure 3.1(a)). Additionally, having overlapping domains as part of the substructuring technique, as explained in the preceding chapter, is aimed to prevent the restoring-force measurements to be influenced by the common assumption of points of inflection at the midheight columns. The actuators are only used to impose the command displacements, and other transducers (*e.g.* load cells used at the top of the subassembly to measure distribution of inters-story shear forces, and strain gauges located on the elastic members of the frame) are used to obtain the internal member forces at locations other than the boundary of the experimental substructure (Figure 3.1(b)). This is useful to determine restoring forces necessary to feed the numerical model during the hybrid simulation through a data acquisition (DAQ) system.



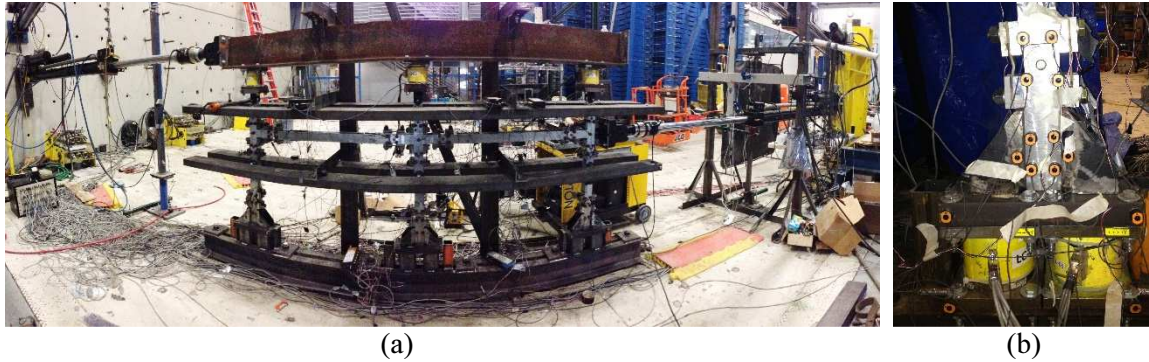


Figure 3.1. NEES@Buffalo hybrid testing setup; a) panoramic view of 1.5 story substructure, b) measuring devices (load cells and strain gauges) on columns (Hashemi, 2013).

The communication information loop is represented in Figure 3.2 as implemented in the laboratory (NEES@Buffalo) during hybrid simulation. It follows the SCRAMNet (Shared Common RAM Network) experimental control architecture presented by Schellenberg et al., (2010), who introduced its implementation at NEES@Berkeley. The DAQ system (6) is integrated in the SCRAMNet (3) loop along with the xPC (Simulink real-time) used for the hybrid control system. The Servo-Control Loop contains the Flex Test controller (2). The Flex Test controller is responsible for sending command displacements to the actuators (1) attached to the specimen and for reading back measured displacements and forces. Then, an intermediate loop runs the Predictor-Corrector actuator command generator (5) on the xPC-Target real-time digital signal processor (4) and delivers the command displacements to the Flex Test controller (2) in real-time through the shared memory SCRAMNet (3). Finally the xPC-Host PC (7) runs and includes OpenSees numerical models, Matlab®, and OpenFresco communicating with the xPC-Target through TCP/IP connection. The solution of the equation of motion for every analysis step takes place in the outer integrator loop (7).

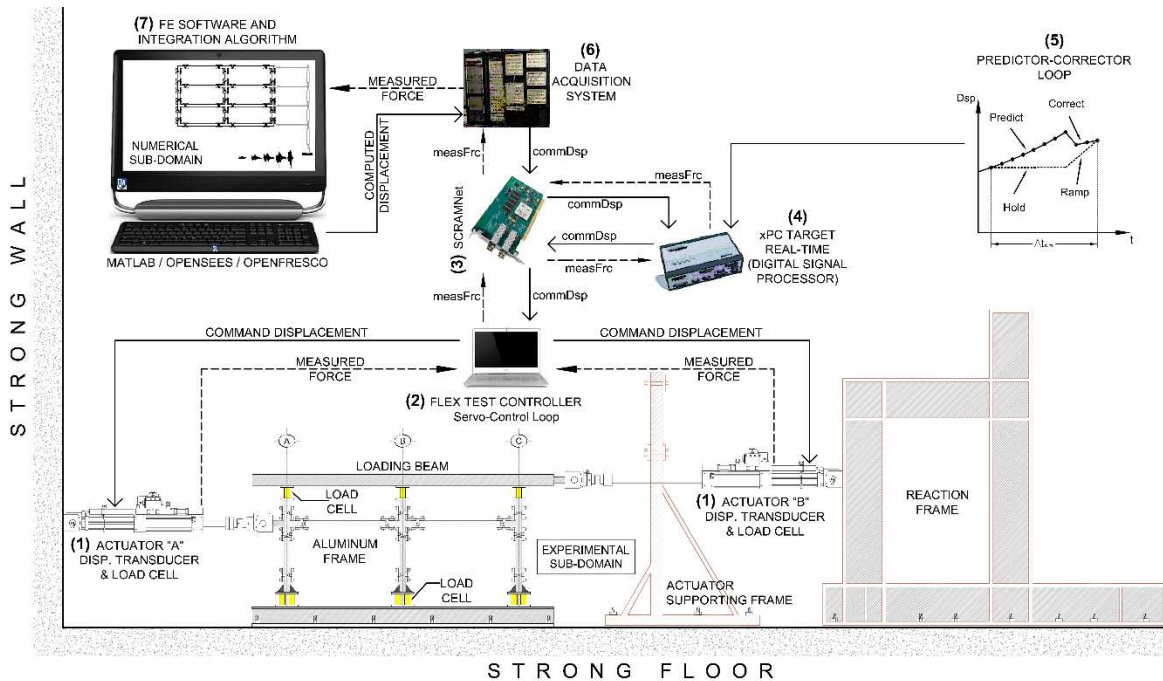


Figure 3.2. Hybrid simulation architecture.

As stated before, the development of the proposed numerical updating procedure requires multiple numerical simulation trials before the approach can be eventually implemented with a physical substructure, especially when many degrees of freedom (DOF) are involved. The Open Framework for Experimental Setup and Control (OpenFresco) (Schellenberg, et al., 2010) offers capabilities for experimental simulation control and data acquisition objects. As described on the coupling simulation method by Schellenberg, et al. (2008), the control is enabled through a Simulation Finite Element Adapter (SimFEAdapter) class. The adapter allows users to simulate physical subassemblies and specimens, acting as interfaces to the slave finite element software, where the subassemblies are simulated. One advantage of utilizing this technique is that all the connected codes run continuously without the need to shut down and restart the involved programs, given that the adapter does not make use of any file system, thus hybrid simulations can be performed steadily. In our case (see Figure 3.3) two counterparts are declared, a master model where the system is solved (numerical subdomain) and one linked program modeling and

analyzing the subassembly acting as slave (virtual experimental substructure). Both substructures are modeled in OpenSees. The slave subassembly acts as a generic super-element (Figure 3.3(1)) and is connected to the master model via interface degrees of freedom to establish interactions between master and slave models for the substructuring technique applied on this research. Thus, an adapter element (Figure 3.3(2)) is added to the slave model providing the interfaces to the master programs. OpenFresco acts as a middleware server between these two elements, providing data storage, communication methods, system control, optimization, and data transformation (Schellenberg, et al., 2008).

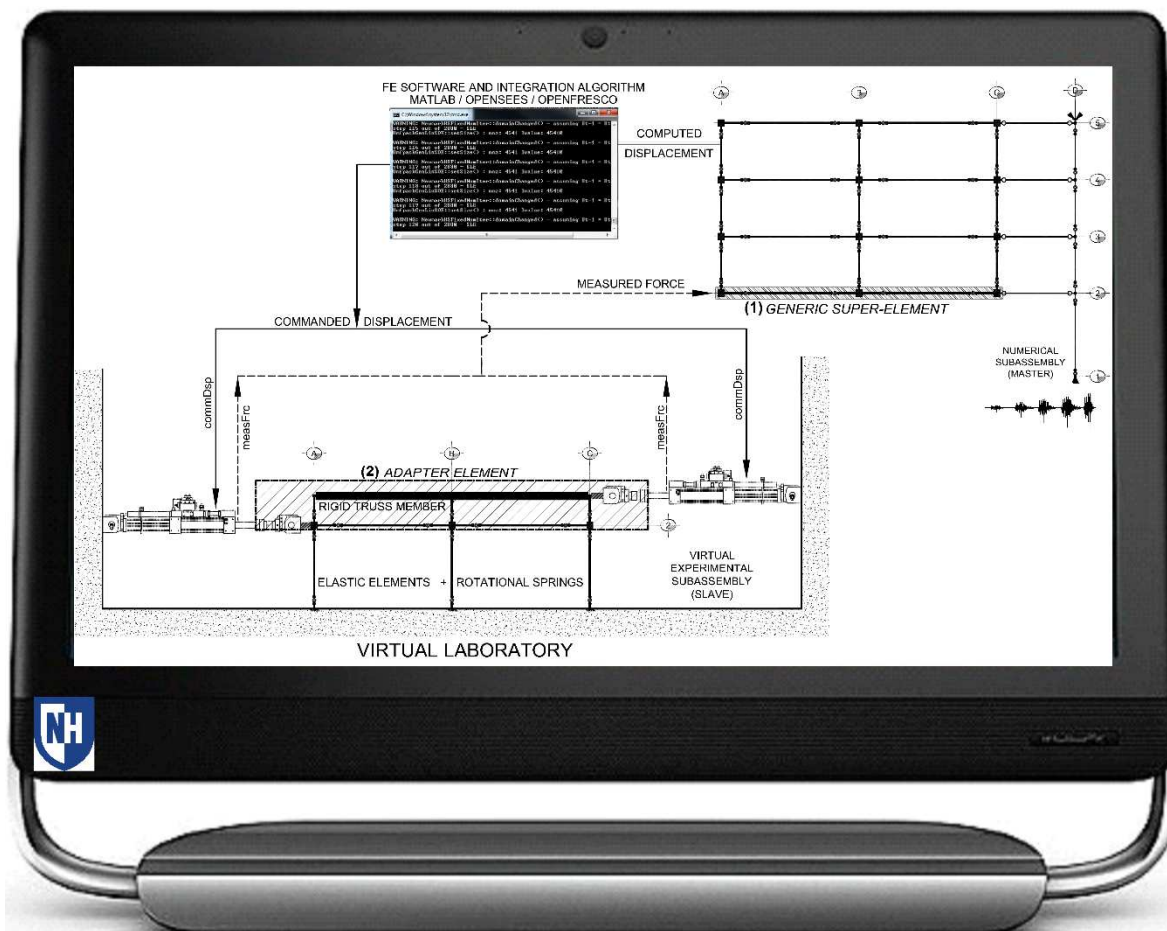


Figure 3.3. Fully numerical hybrid simulation architecture.

To couple the slave and master programs, displacements are prescribed at the interface degrees of freedom of the slave subassembly, and the resultant forces are measured and returned back to the master program (Figure 3.3). The adapter element providing the interfaces to the slave subassembly is connected to the three interface nodes at the middle height of the second-story columns (Figure 3.3(2)). As explained in section 2.4, only the horizontal degrees-of-freedom nodes were utilized while the vertical and rotational ones were restrained. The initial nine DOF's are thus reduced to one unidirectional horizontal DOF controlled by one actuator (Hashemi, et al., 2013). The 8x8 initial stiffness matrix of the super-element (Figure 3.3(1)) is determined from the 1½ substructure by imposing unit displacements at one interface degree-of-freedom at a time while restraining the remaining interface degrees of freedom. Figure 3.4 shows the degrees of freedom considered on the virtual experimental subassembly leading to the super-element initial stiffness matrix (Equation 3.1).

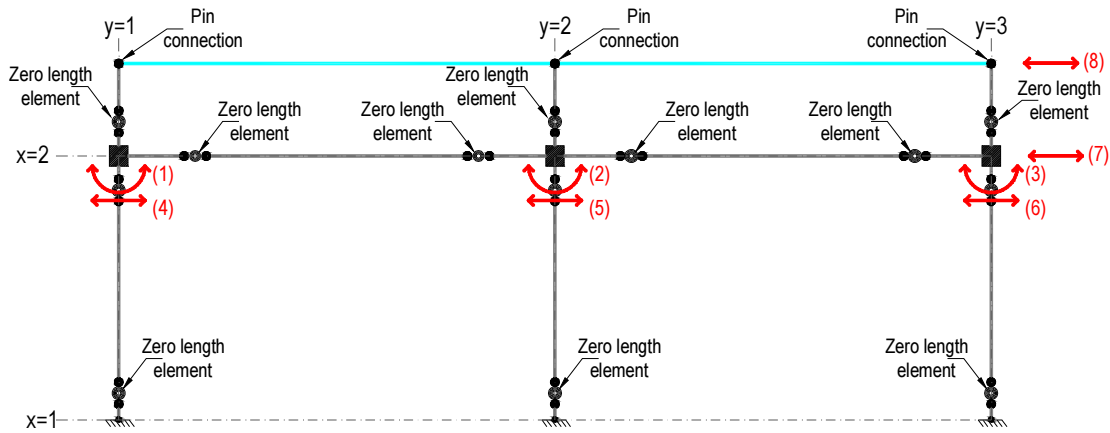


Figure 3.4. Degrees of freedom utilized on the generic super-element initial stiffness matrix calculations.

$$\mathbf{K}_{\text{super}} = \begin{bmatrix} 3599.98 & 0 & 0 & 230.69 & 0 & 0 & 0 & 0 \\ 0 & 3672.95 & 0 & 0 & 237.28 & 0 & 0 & 0 \\ 0 & 0 & 3599.98 & 0 & 0 & 230.69 & 0 & 0 \\ 230.69 & 0 & 0 & 20.82 & 0 & 0 & 0 & 0 \\ 0 & 237.28 & 0 & 0 & 21.42 & 0 & 0 & 0 \\ 0 & 0 & 230.69 & 0 & 0 & 20.82 & 0 & 0 \\ 0 & 0 & 0 & 0 & 0 & 0 & 0 & 0 \\ 0 & 0 & 0 & 0 & 0 & 0 & 0 & 0 \end{bmatrix} \text{ (Kips/in)} \quad (3.1)$$

The generic super-element represents the virtual experimental subdomain in the master finite element subassembly, connected to the three interface nodes (Figure 3.3(1)). A linear elastic adapter element (Figure 3.3(2)) connected to the nodal interface degrees of freedom is added to the slave program with high stiffness values compared to the one of the subassembly. The adapter acts as actuators to control the degrees of freedom in the slave model, similar to a laboratory setup where actuators usually possess a larger stiffness compared to the specimen. Differently from the super-element, the stiffness matrix of the adapter element acting in the slave finite element subdomain (Figure 3.3(2)) is not determined from the (virtual) physical properties of the master subassembly. According to Schellenberg et al., (2008), values of 1.0E+12 for the diagonal elements have shown to be adequate for this type of elements, since higher values may lead to numerical problems and smaller ones to loss of accuracy on the imposed displacements. The stiffness matrix of the adapter element is presented on Equation 3.2.

$$\mathbf{K}_{\text{adapter}} = \begin{bmatrix} 1.0E+12 & 0 & 0 & 0 & 0 & 0 & 0 & 0 \\ 0 & 1.0E+12 & 0 & 0 & 0 & 0 & 0 & 0 \\ 0 & 0 & 1.0E+12 & 0 & 0 & 0 & 0 & 0 \\ 0 & 0 & 0 & 1.0E+12 & 0 & 0 & 0 & 0 \\ 0 & 0 & 0 & 0 & 1.0E+12 & 0 & 0 & 0 \\ 0 & 0 & 0 & 0 & 0 & 1.0E+12 & 0 & 0 \\ 0 & 0 & 0 & 0 & 0 & 0 & 1.0E+12 & 0 \\ 0 & 0 & 0 & 0 & 0 & 0 & 0 & 1.0E+12 \end{bmatrix} \text{ (Kips/in)} \quad (3.2)$$

During the simulation, the adapter element sends trial displacements using a TCP/IP socket to the OpenFresco simulation application server. Transmission control protocol (TCP) / Internet protocol (IP) socket is a mechanism for data delivery between two IP addresses one local and another remote. It is defined by a transport protocol with one local and one remote port address that identify a program in a computer (e.g., OpenSees). The objective of the TCP/IP socket is to

establish a client-server architecture, where the client (master subdomain) starts the communication while the server (slave subdomain) awaits. This process is internally implemented in the same computer in order to persistently couple master and slave models information during fully numerical simulations. The information flow loop for one analysis step based on the NEES@Berkeley implementation (Schellenberg, et al., 2010) is graphically presented in Figure 3.5 and summarized on the following steps:

- a) On the master program, the super-element receives a vector of global displacements for all its degrees of freedom:

$$\{u_{super}\} = \{u_{el}\}.$$

- b) The master program communicates these displacements using a TCP/IP socket to the simulation application middleware server (OpenFresco).
- c) The displacements are next transferred from OpenFresco to the SimFEAdapter experimental control object. This object is responsible for the connection to the adapter element, again using a TCP/IP socket.
- d) The adapter element combines the received displacements  $\{u_{imp}\}$  from the master subassembly with its own element displacements  $\{u_{adpt}\}$ .
- e) The element force vector  $\{p_{el}\} = \{p_{adpt}\}$  is updated utilizing the equation  $\{p_{adpt}\} = [K_{adpt}](u_{adpt} - u_{imp})$  and returned to the subassembly.
- f) OpenFresco returns the negative of the resisting force vector  $-\{p_{adpt}\}$  to the master program, once the slave program performs an equilibrium solution process and achieves convergence, through the TCP/IP socket.
- g) The super-element saves them as element forces and sends them back to the master integration method, in order to determine the new trial displacements and proceed to the

next time step.

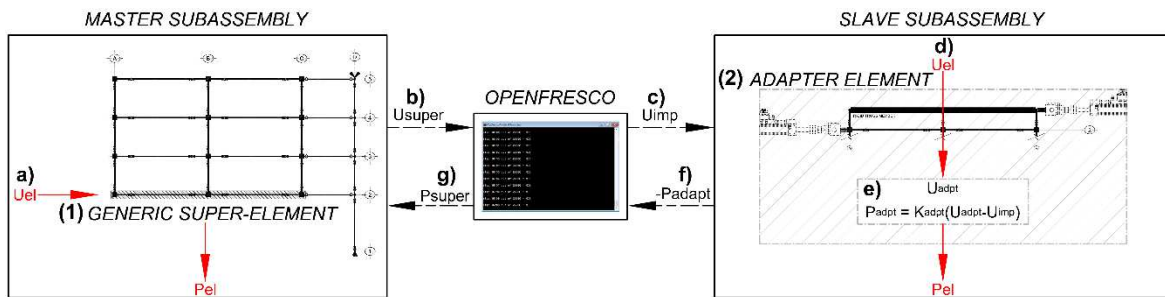


Figure 3.5. Hybrid simulation information flow loop, adapted from Schellenberg et al., (2010).

Consequently, during the implementation of the proposed numerical approach the described procedure depicted on its general form in Figure 3.3 and Figure 3.5 is utilized. In this document, “fully numerical hybrid simulation” refers to the fact that the experimental subdomain is also numerically formulated as well as the master substructure.

### 3.3. Update parameter commands in OpenSees

The OpenSees platform (McKenna, et al., 2000) incorporates a parameter updating function to support application of reliability, optimization, system identification, and sensitivity studies. These studies need to “parameterize” a finite element model in order to compute sensitivity and map probability distributions with respect to uncertain parameters (Scott & Haukaas, 2008). Two possible approaches to tag and update specific parameters of a defined element of material are available. The first one incorporates the parameters to be updated, and then new parameter values are introduced when instructed to do so by a model updating application. Thus, first the *parameter* command is used to identify the element, section, material, load, etc., as follows:

<i>Parameter \$tag &lt;specific object arguments&gt;</i>	
<i>\$tag</i>	integer tag identifying the parameter
<i>&lt;specific object arguments&gt;</i>	depend on the object in the FE model encapsulating the desired parameters

Once the target parameters are tagged and the arguments identified, a second step is invoked to update the selected factors. The *updateParameter* command is used to assign a new value to the tagged parameter:

<i>updateParameter \$tag \$newValue</i>	
<i>\$tag</i>	integer tag identifying the parameter
<i>&lt;specific object arguments&gt;</i>	the updated value to which the parameter needs to be set

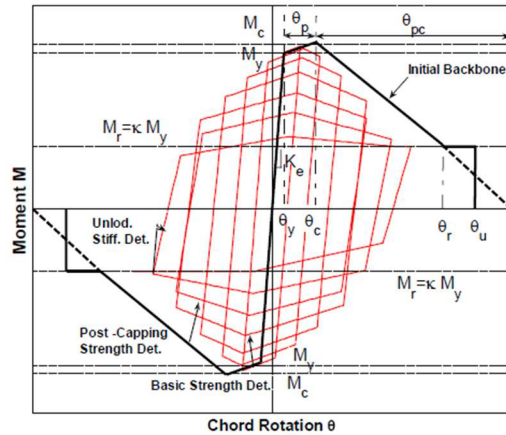
The second approach is to utilize the *setParameter* command, which is built with the same purpose. This command can be employed at the element, section, or material level. In this case, there is no need to tag the elements prior to the updating event and the values are implemented directly in one step, when a model updating application commands the change:

<i>setParameter (const char **argv, int argc, Parameter &amp;param)</i>	
<i>**argv</i>	integer tag identifying the parameter
<i>int argc</i>	element or range of elements to be updated
<i>&amp;param</i>	parameter to update

These updating commands were previously applied on sensitivity analysis utilizing frictional contact interfaces, soil analysis, inelastic truss elements, and bilinear materials, among others. The modified Ibarra-Medina-Krawinkler (*IMK*) deterioration model with bilinear hysteretic response (bilinear material) is utilized in this research to represent the behavior of the rotational springs of the main four-story frame. The model contains 24 factors that can potentially be subjected to parameter updating during a response-history analysis. Nevertheless, in this dissertation nine parameters are used to control hysteretic responses with deterioration during the



implementation of the proposed approach. This subset of parameters is:  $SK0$ ,  $SMY\_Pos$ ,  $SMY\_Neg$ ,  $Sas\_Plus$ ,  $Sas\_Neg$ ,  $Stheta\_p\_Plus$ ,  $Stheta\_p\_Neg$ ,  $Stheta\_pc\_Plus$  and,  $Stheta\_pc\_Neg$ . The full set of parameters that describe the *IMK* model shown in Figure 3.6 are presented next.



- Effective yield strength and rotation ( $M_y$  and  $\theta_y$ )
- Effective stiffness  $K_e = M_y/\theta_y$
- Capping strength and associated rotation for monotonic loading ( $M_c$  and  $\theta_c$ )
- Pre-capping rotation capacity for monotonic loading  $\theta_p$
- Post-capping rotation capacity  $\theta_{pc}$
- Residual strength  $M_r = \kappa M_y$
- Ultimate rotation capacity  $\theta_u$

uniaxialMaterial Bilin \$matTag \$K0 \$sas_Plus \$sas_Neg \$My_Plus \$My_Neg \$Lamda_S \$Lamda_C \$Lamda_A \$Lamda_K \$c_S \$c_C \$c_A \$c_K \$theta_p_Plus \$theta_p_Neg \$theta_pc_Plus \$theta_pc_Neg \$Res_Pos \$Res_Neg \$theta_u_Plus \$theta_u_Neg \$D_Plus \$D_Neg <\$nFactor>	
\$matTag	integer tag identifying material
\$K0	elastic stiffness
\$sas_Plus	strain hardening ratio for positive loading direction
\$sas_Neg	strain hardening ratio for negative loading direction
\$My_Plus	effective yield strength for positive loading direction
\$My_Neg	effective yield strength for negative loading direction (negative value)
\$Lamda_S	Cyclic deterioration parameter for strength deterioration
\$Lamda_C	Cyclic deterioration parameter for post-capping strength deterioration
\$Lamda_A	Cyclic deterioration parameter for acceleration reloading stiffness deterioration
\$Lamda_K	Cyclic deterioration parameter for unloading stiffness deterioration
\$c_S	rate of strength deterioration. The default value is 1.0
\$c_C	rate of post-capping strength deterioration. The default value is 1.0
\$c_A	rate of accelerated reloading deterioration. The default value is 1.0
\$c_K	rate of unloading stiffness deterioration. The default value is 1.0
\$theta_p_Plus	pre-capping rotation for positive loading direction (often noted as plastic rotation capacity)
\$theta_p_Neg	pre-capping rotation for negative loading direction (often noted as plastic rotation capacity) (positive value)
\$theta_pc_Plus	post-capping rotation for positive loading direction
\$theta_pc_Neg	post-capping rotation for negative loading direction (positive value)
\$Res_Pos	residual strength ratio for positive loading direction
\$Res_Neg	residual strength ratio for negative loading direction (positive value)
\$theta_u_Plus	ultimate rotation capacity for positive loading direction
\$theta_u_Neg	ultimate rotation capacity for negative loading direction (positive value)
\$D_Plus	rate of cyclic deterioration in the positive loading direction (this parameter is used to create asymmetric hysteretic behavior for the case of a composite beam)
\$D_Neg	rate of cyclic deterioration in the negative loading direction (this parameter is used to create asymmetric hysteretic behavior for the case of a composite beam)
\$nFactor	elastic stiffness amplification factor, mainly for use with concentrated plastic hinge elements (optional, default = 0)

Figure 3.6. Modified Ibarra-Medina-Krawinkler deterioration model, implemented in OpenSees, after (Lignos & Krawinkler, 2011).

From the parameters shown above, the subset of parameters used during the proposed NUA is:  $SK0$ ,  $SM_y\_Pos$ ,  $SM_y\_Neg$ ,  $Sas\_Plus$ ,  $Sas\_Neg$ ,  $Stheta\_p\_Plus$ ,  $Stheta\_p\_Neg$ ,  $Stheta\_pc\_Plus$  and,  $Stheta\_pc\_Neg$ . Given that parameter-updating commands were not used in the past with the *IMK* bilin model in OpenSees, no previous problems were reported. Nevertheless, at the time of implementing the *setParameter* command on the hybrid simulations, only the first three selected listed parameters were working appropriately. As part of this study, the functionality of the *setParameter* command with all other bilin model parameters was corrected and new executable

files were compiled directly from the OpenSees source code. In this manner, the subset of nine model parameters could be updated during the analysis without having to revert to the beginning of the analysis. An example of the writing instruction within the OpenSees environment for the *setParameter* command employed in this study is presented next for the variables subjected to updating in the finite element models developed in the present research. In addition, this list provides an illustration of the required OpenSees syntax for the *IMK* bilin material model.

```
setParameter -value [expr $Kc12PO*($j1+($k1-$j1)*$upd_frac)] -ele 1 Ke }
setParameter -value [expr $Myc12PO*($j35+($k35-$j35)*$upd_frac)] -ele 1 My_pos }
setParameter -value [expr -$Myc12PO*($j69+($k69-$j69)*$upd_frac)] -ele 1 My_neg }
setParameter -value [expr $b1PO*($j103+($k103-$j103)*$upd_frac)] -ele 1 As }
setParameter -value [expr $b1PO*($j137+($k137-$j137)*$upd_frac)] -ele 1 AsNeg }
setParameter -value [expr $th_pP1PO*($j171+($k171-$j171)*$upd_frac)] -ele 1 Thetap_pos }
setParameter -value [expr $th_pN1PO*($j205+($k205-$j205)*$upd_frac)] -ele 1 Thetap_neg }
setParameter -value [expr $th_pcP1PO*($j239+($k239-$j239)*$upd_frac)] -ele 1 Thetapc_pos }
setParameter -value [expr $th_pcN1PO*($j273+($k273-$j273)*$upd_frac)] -ele 1 Thetapc_neg }
```

Thus, the *setParameter* command is called to update specific parameters of selected hinges required to be recalibrated according to the procedure detailed in Chapter 5. It should be noted that quantities  $F$  and  $\delta$  are generic force and deformation parameters. For plastic hinge regions (component-level responses)  $F = M$  and  $\delta = \theta$  (Lignos, 2008), which implies that the *IMK* model is also used to represent moment-rotation responses in this dissertation.

### 3.4. Experimental errors and epistemic uncertainty in hybrid simulations

As stated by Mahin and Shing (1985), Thewalt and Mahin (1987), Mahin, et. al. (1989), Mosqueda, et. al. (2005), Yang, et. al. (2008), Saouma and Sivaselvan (2008), among the main sources of errors in hybrid simulation are structural modeling errors, numerical methods errors (idealization of the equation of motion), approximate numerical integration methods errors, and experimental errors. The latter having the most important impact on the simulation results. This is

the case mainly because these errors are unknown prior to testing and the sources of errors may vary from test to test. For example, one of these sources of experimental errors include feedback to the numerical model from measured restoring forces that could exhibit noise, which may induce the systematic propagation of errors, as well as unstable or spurious dynamic responses. Experimental errors can arise from displacement control of hydraulic actuators, force relaxation (Thewalt & Mahin, 1987) or strain rate effects due to the slow rates of testing, calibration errors in the instrumentation, noise generated in the instrumentation, and analog to digital converters (Yang, et al., 2008).

Additionally, boundary condition assumptions of the physical specimens must be made, as well as idealization of the support components in the laboratory. For example, if the specimen is to be tested in plane (*i.e.* as a two-dimensional structure) and it is connected to actuators on opposite sides, one set of actuators can be attached to a strong wall and others to a less rigid support, which could lead to differences on the stiffness of the structure to be tested. Furthermore, the fixity of the specimen supports assumed in the numerical models may not be accurately reproduced in the laboratory. Thus, turning a conceptual numerical model with ideal support conditions, optimal application of loads and measurement of feedback forces, “perfect” structural sections, and full restriction of out of plane deformations among others exists, into a real physical specimen and its respective emplacement in a laboratory, may result in experimental errors associated with instrumentation and testing equipment.

Errors due to discrepancies in parameter properties of components may be present when initial values cannot be accurately defined or because of human error. Moreover, as stated by (Benjamin & Cornell, 1970) “uncertainty” can be formally classified as aleatory (also called natural, intrinsic, irreducible or fundamental) uncertainty and epistemic or model uncertainty.

Aleatory uncertainty is related to the randomness in the behavior of the system under study (*e.g.*, record-to-record variability due to earthquake event characteristics such as duration, accelerations, displacements, and frequency content, among others). Aleatory uncertainty is irreducible. On the other hand, epistemic uncertainty characterizes the lack of knowledge on the form of the model itself and about the appropriate value to use for a quantity that is assumed to have a fixed value in the context of a specific application. Epistemic uncertainties are reducible through improved understanding, refining models, increased or more relevant data.

The epistemic (or state-of-knowledge) uncertainty could also arise from different sources. For instance, in the particular case of steel structures, properties of steel components might not be measured with sufficient precision, which might be related to equipment sensitivities, and in some cases, deficiencies present in the calibration of testing equipment. In addition, geometrical differences in rolled shape elements occur from lot to lot, localized imperfections, as well as uncertainties in material properties (*e.g.*, due to steel incoming from several sources to blast furnaces during the production of rolled shapes), may lead to different strength and strain properties of structural elements. The latter acquiring more importance when distributed hybrid testing is conducted (Mosqueda, et al., 2005) due to availability of rolled steel shapes from region to region or even country to country. Human error also adds uncertainty that cannot be fully quantified or completely mitigated, previous to, as well as during testing.

In the present research, aleatory uncertainty due to record-to-record variability is not accounted for, given that only one scaled ground motion is used. At the same time, experimental errors are simulated, since a virtual experimental structure is employed. The proposed approach directly deals with the reduction of the epistemic uncertainty associated with the lack of knowledge in the accurate calibration of component properties in the numerical models used for hybrid testing

with substructuring.

It is postulated herein that epistemic uncertainty can be reduced through recalibration of the properties of the numerical substructure based on the response of the experimental substructure during the analysis.

### **3.5. Numerical updating approach - general scope**

Conventional hybrid simulation in earthquake engineering consists of dividing the structural system into a numerical portion and one or more experimental (virtual experimental in this research) substructures that interact with one another during the solution of the equations of motion of the system. A flowchart illustrating conventional hybrid testing, as it applies to earthquake engineering, is depicted in Figure 3.7. Displacements calculated from the solution of the equation of motion of the numerical portion of the model are applied to the virtual experimental substructure(s) at the interface between numerical and physical elements. Next, restoring forces obtained from the application of the calculated displacements to the physical substructure(s) are measured and fed back to the numerical substructure. Then, new relative velocity and relative accelerations on the numerical portion of the structure are computed. At the beginning of the next ground motion time step, restoring forces and the current state deformation state of the structure are applied to solve for the next displacement vector. The process is repeated until the end of the simulation is found; the structure experiences collapse; or the structure reaches a predefined deformation threshold.

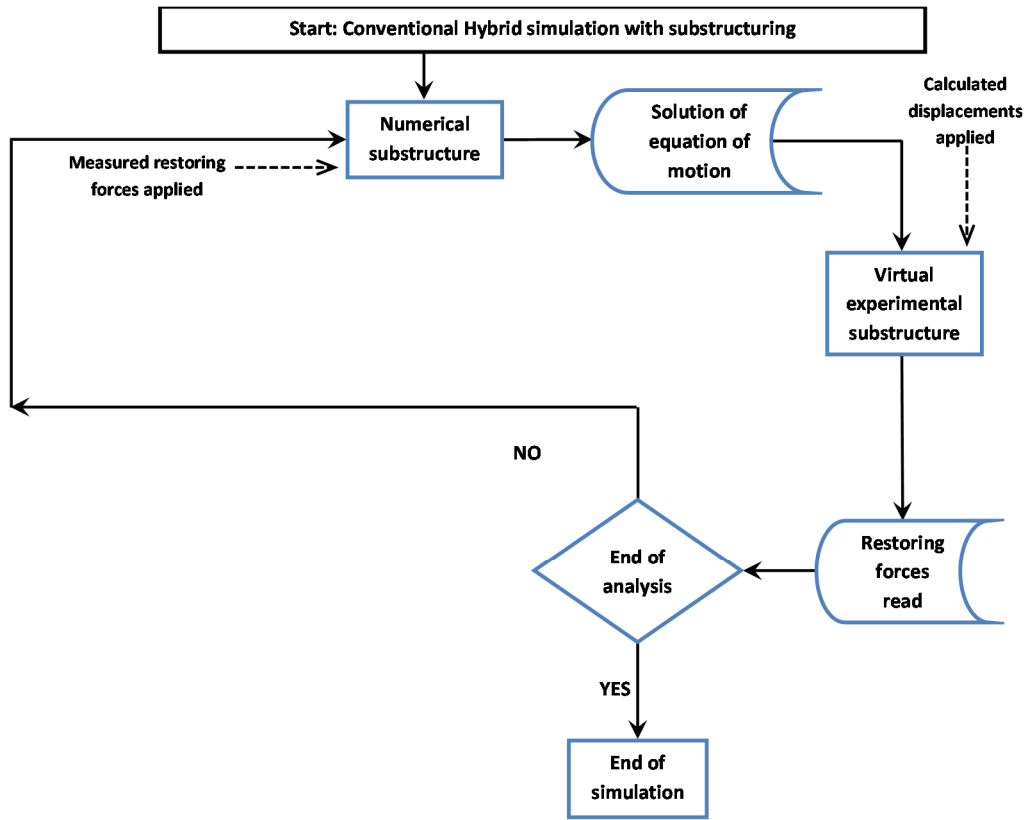


Figure 3.7. Flowchart for implementation of conventional hybrid simulation with substructuring.

The NUA proposed in this study can be implemented as an add-on module into the well-established hybrid simulation architecture in order to improve the ability of hybrid simulation to trace dynamic responses up to collapse. The location of the add-on module on a conventional hybrid simulation framework is shown in Figure 3.8. As can be seen, when numerical updating is not deemed to be necessary, the simulation is carried out following the conventional hybrid simulation approach shown in Figure 3.7.

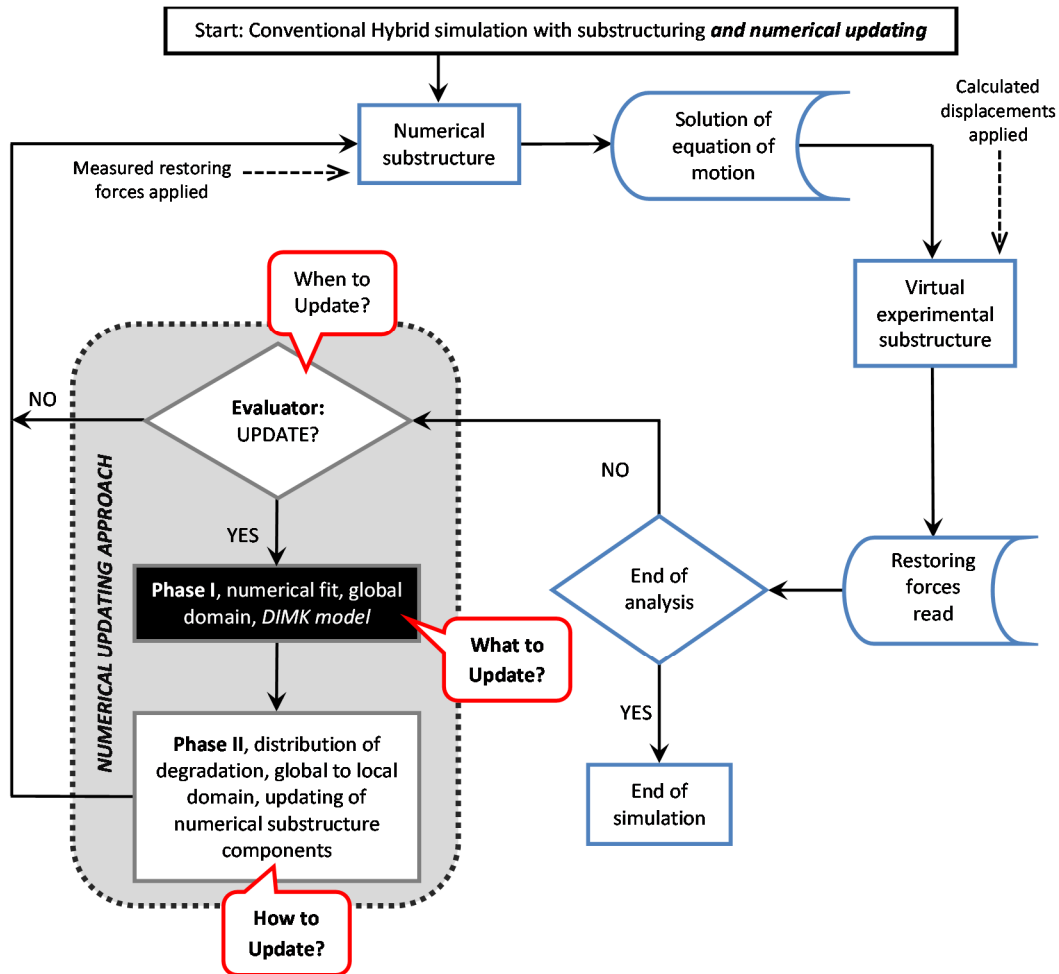


Figure 3.8. Flowchart for implementation of numerical updating approach.

The NUA consists of two phases preceded by an evaluation stage (Figure 3.8). First, measures of story-strength/story-drift values (i.e., global response) for the virtual test substructure are obtained *during the analysis*. At the beginning stages of the simulation in the evaluation module, a change of elastic stiffness ( $K_e$ ) in the current cycle with respect to the value in the previous cycle ( $\Delta K_e \geq 10\%$ , where  $\Delta K_e$  is the change in stiffness) activates the start of the updating process. Additional triggers are utilized in subsequent stages of the analysis to complete the updating of the selected subset of nine parameters for every component. The evaluator module is called at every analysis step equal to one time the fundamental period of the structure ( $1.0T_1$ ). The time interval utilized to call the evaluator module at appropriate ground motion steps is presented



on Table 3.1, where  $dt$  is the ground motion time increment ( $\frac{1}{128} sec$ ). This time increment is based on sensitivity studies previously conducted as part of this research, firstly suggested by the team-members of this broad sponsored project. From these studies, it was learned that updating at closer intervals does not show significant improvement on the accuracy of the results. Conversely, closer updating intervals in some cases resulted in numerical instability in addition to longer computational times. Largely spaced updating events would result in loss of accuracy of the hybrid simulation due to recalibration information that might be acquired late in time to update the required parameters.

Table 3.1. Interval of analysis steps for evaluator stage.

Limit State	Step Size	Increment (sec)	Analysis points/Record	Evaluator interval (analysis steps)
<b>SLE</b>	0.50 dt	0.00391	2560	<b>120</b>
<b>DBE</b>	0.13 dt	0.00098	10240	<b>480</b>
<b>MCE</b>	0.10 dt	0.00078	12800	<b>600</b>
<b>CLE</b>	0.06 dt	0.00047	21333	<b>1000</b>
<b>CLEF</b>	0.06 dt	0.00047	21333	<b>1000</b>

Once *when to update* is defined by the evaluator module (Figure 3.8), Phase I starts by using global response information from the experimental substructure to apply a numerical fit to update each relevant parameter (subset of nine factors) at the global level. The global hysteretic response is fitted using the *IMK* hysteretic model during the analysis (*DIMK* model). Hysteretic model parameters necessary to characterize story-level behavior are then identified. The objective of Phase I is to translate experimental global information into measurable global parameters related to a hysteretic model with deterioration in order to define *what to update*. On Phase II, the global history of deterioration is translated into component-level deterioration. Component-level parameters that replicate the fitted story-level responses from the virtual test substructure are

obtained. Finally, these sets of local values are used to update, when needed, the parameters of the numerical substructure during the hybrid simulation. The goal of Phase II is to determine *what component parameters to update* to appropriately distribute damage on the global domain within the local components of the numerical substructure (Figure 3.8).

In-house computational optimization interfaces programmed in Matlab® run in parallel with OpenSees and OpenFresco to implement the proposed approach. These interfaces are designed to apply the numerical fits to the hysteretic responses, and optimize the acquisition and classification of updated information of the local parameters of the numerical portion of the structure.

As part of the implementation process and verification of the numerical approach results, one case study with induced random initial errors on the calibration of the *IMK* numerical model parameters is presented for illustration purposes. The initial error ratios (i.e. deviation in percentage from the correct values) for all the plastic hinges on the numerical model are:

- Elastic stiffness  $K_e$ : -50.0%.
- Yield moment  $M_y$ : + 35.0%.
- Rotation capacity previous to capping limit  $\theta_p$ : +35.0%.
- Softening post-capping slope  $\alpha_c$ : + 35.0%.

Figure 3.9 shows the first-story drift ratio response history of the hybrid simulation with substructuring, performed on the 1:8 scaled SMRF utilized on this investigation. The structure was subjected to the set of increasingly scaled ground motions described in subchapter 2.2. Drift time history responses for three simulations are shown in Figure 3.9: 1) simulation of the base case with

no errors on the estimation of parameters is shown in red line; 2) simulation with the initial induced errors on the parameters and no updating is shown in gray line and; 3) simulation with the add-on NUA module is shown in black line.

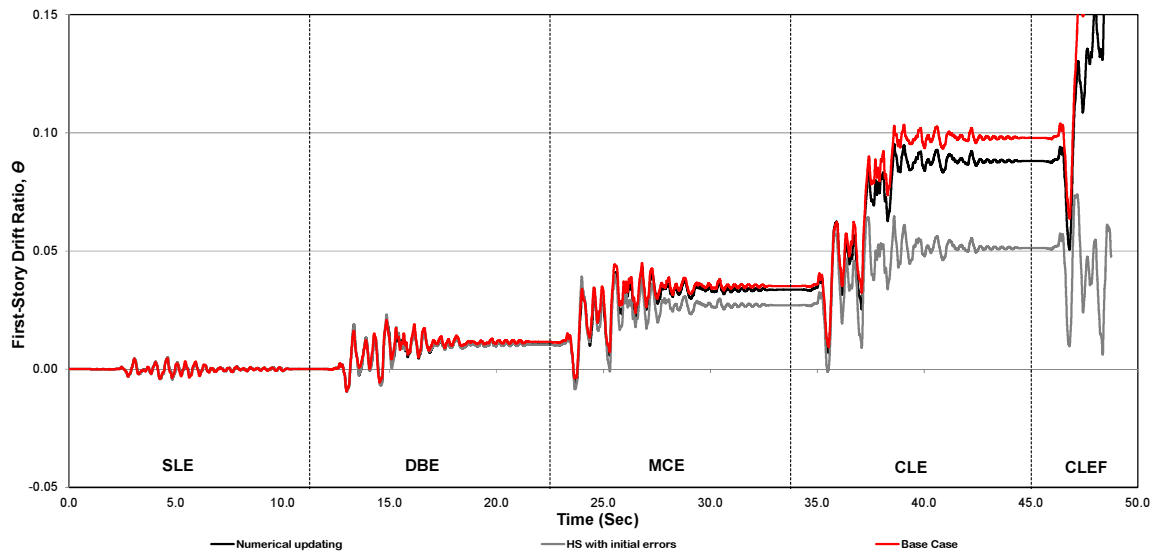


Figure 3.9. First-story drift for a hybrid simulation case study with initial calibration errors through collapse.

As can be observed from Figure 3.9, if initial errors are included into the numerical components, the results of the simulation may deviate from the base case up to the point to be considered not satisfactory. The main reason to discard the results of the simulation with induced initial errors is that the structure does not approach the onset of numerical instability (no sideways collapse is achieved) and the errors on the residual drifts are remarkably large (e.g. 48% after *CLE* ground shake). Contrariwise when the add-on updating module is incorporated, the time at which imminent collapse is approached is closely captured and the errors on the interstory drift are minimized (e.g. 10% after *CLE*). In this sense, utilizing an updating approach like the one presented on this research may lead to the minimization of errors on drifts and forces (detailed information is presented on Chapters 5 and 6), as well as improving our ability to simulate collapse

via recalibration of the numerical subdomain based on acquired information of the experimental subassembly during the simulation.

### 3.6. Summary and conclusions

The main topic of the present dissertation is to develop and implement a *numerical updating approach* to conduct more accurate fully numerical hybrid simulation with substructuring through collapse. In this process, the proposed approach was developed through virtual hybrid simulations in which the physical substructure was modeled numerically. Multiple trials were performed in a practical and efficient way before the approach can be eventually implemented on an experimental facility. In this research, the same scaled SMRF specimen used by Lignos (2008) was modeled numerically in the OpenSees platform to reproduce the shake table results, but this time utilizing hybrid simulation. The overall setup of the hybrid simulation at NEES@Buffalo was explained, utilizing the substructuring technique developed by Hashemi (2013). The bottom 1½ stories of the 1:8 scaled SMRF is employed as the experimental substructure, whereas the upper three levels with a leaning column added to simulate the  $P-\Delta$  effects is employed as the numerical subdomain. A fully numerical hybrid simulation was achieved, through the implementation of an experimental subdomain also modeled numerically (virtual laboratory). The coupling method presented by Schellenberg et al., (2010) was utilized on the implementation of the fully numerical hybrid simulation with substructuring to communicate between the virtual experimental and numerical counterparts.

The functionality of the updating command (*setParameter*) incorporated on the OpenSees platform was corrected from the source code to be properly applied with bilin models (*IMK* in this research). Hence, the drawback of reverting the simulation history to the beginning of the analysis

to update the component parameters was avoided.

Modeling (epistemic) uncertainty is investigated on this research. Given that the present research focuses on fully numerical simulations and utilizes a set of one increasingly scaled single ground motion (five intensities related to limit states), aleatory uncertainty due to record-to-record variability is not accounted for. Also experimental errors are neither considered since the setup utilized is a numerically modeled virtual laboratory. Epistemic uncertainty is expected to be reduced through the implementation of the proposed add-on hybrid simulation module, minimizing the initial calibration error values of component parameters.

A global overview of the proposed approach was presented, serving as a guide for its detailed explanation on the subsequent chapters of this dissertation. The main portions of the numerical updating and its general objectives are covered and explained; *when to update* dictated by an evaluation module, followed by a parameter identification through the use of a numerical fitting to discover *what parameters to update*. Also, a procedure to distribute the global deterioration identified on the experimental substructure into component deterioration via recalibration of the numerical subdomain was implemented. This latter task is achieved by enforcing updating events to address the issue of *how to update*. Finally a case study was presented where random parameter errors were implemented on the initial calibration of component parameters. HS with the initial errors and with the implementation of the proposed numerical updating were performed. Results for first-story drift showed the advantages of using the NUA, leading the system with initial errors to correct a non-collapse behavior to capture collapse at adequate timing, and minimizing the deviations in interstory drift when the structure is near to collapse.

## CHAPTER 4

### NUMERICAL UPDATING APPROACH: PHASE I

#### 4.1. Introduction, definition, and scope

Hybrid testing consists of dividing the structural system into experimental and numerical portions, which interact during the full simulation. The numerical updating procedure proposed in this research is introduced via analytical studies that simulate the experimental substructure through a virtual experimental specimen/laboratory. This fully numerical updating approach is based on utilizing the measured response from the experimental substructure to update during the test the parameters of the components of the numerical substructure. The approach consists of two primary phases, highlighted in gray on the flowchart in Figure 4.1. Initially, global (first-story drift / base shear) hysteretic information is acquired from the virtual experiment during the analysis. The data is used to conduct a numerical fit of the parameters of a phenomenological deterioration model used to represent this global response. Then, this calibrated global response is used to find the parameters of component models that form part of the virtual experimental substructure to distribute damage from global to local domain. These global component parameters are then used to update during the analysis local component parameters corresponding to the numerical portion of the structural system that is being tested. This updating approach is conducted at key steps during the analysis until the limit state of collapse is approached, and it is referred herein as the *numerical updating approach* (NUA). Therefore, the objective of Phase I is to translate experimental global information into measurable global parameters related to a hysteretic model with deterioration capabilities, followed by the identification of local component parameters

consistent with the history of the target global response of interest.

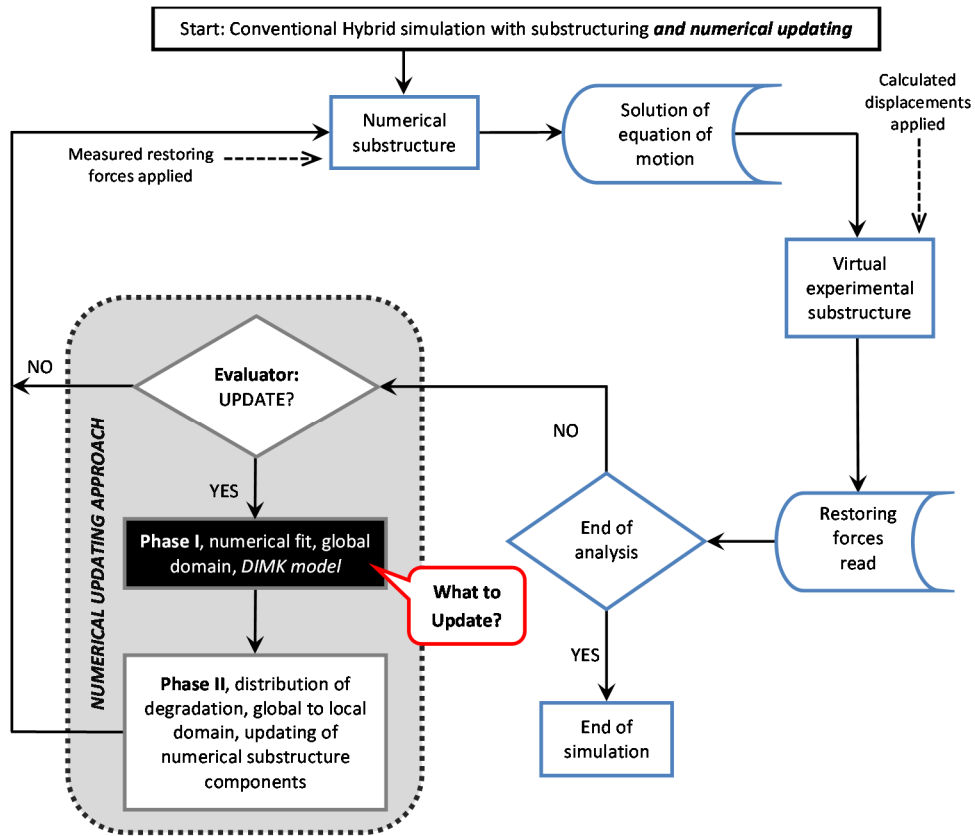


Figure 4.1. Flowchart of proposed numerical updating approach.

In this study the NUA is based on the implementation of the same phenomenological deterioration model at both the global and local levels. The Ibarra-Medina-Krawinkler (*IMK*) model is used for this purpose (Ibarra, et al., 2005). This model is capable of characterizing the main modes of monotonic and cyclic strength and stiffness deterioration with a relatively small number of parameters. The properties of the model are briefly discussed in subsequent sections. A set of rules were designed in this study to identify, during the analysis, the parameters of the *IMK* model necessary to capture the response of the virtual experimental substructure at each vibration cycle until the limit state of collapse is approached.

## 4.2. Hysteretic model selection

Different hysteretic models have been proposed over the years to describe mechanical behavior of structural systems. The available models vary from simple elasto-plastic models to complex strength and stiffness degrading curvilinear hysteretic models. Table 4.1 summarizes the capabilities of some of the hysteretic models historically used in seismic research.

A literature review of the main hysteretic models historically used in earthquake engineering research is presented in FEMA (2009). Some conclusions of comprehensive studies reported in this document regarding several types of models indicate that hysteretic models with strength and stiffness degradation capabilities are more suitable for collapse assessment of structures. Some of these conclusions are summarized below:

- A wide range of structural components and systems will develop some level of stiffness degradation when subjected to reverse cyclic loading. Differences in peak displacements between stiffness-degrading and non-degrading systems increase as the period of vibration decreases and as the lateral strength decreases.
- Cyclic strength deterioration can lead to significant increases in peak displacement demands in short-period systems. In moderate and long-period systems, cyclic strength deterioration effects have been shown to be relatively small, and in many cases can be neglected.
- In-cycle strength deterioration is characterized by a loss of strength within the same cycle in which yielding occurs. As additional lateral displacement is imposed, a smaller lateral resistance is developed. This results in a negative post-yield stiffness within a cycle.



- Dynamic response of systems with cyclic strength deterioration is generally stable, while in-cycle strength and stiffness degradation are critical in determining the possibility of lateral dynamic instability (i.e., collapse) of a structural system.

Due to the fact that one of the goals of this study is to simulate collapse, it is essential to use a hysteretic model able to account for the aforementioned strength and stiffness deterioration modes, cyclic and in-cycle. As can be observed from Table 4.1, the Ibarra-Medina-Krawinkler models, original (Ibarra, et al., 2005) and modified (Lignos & Krawinkler, 2011), include the required characteristics to be used in collapse-simulation studies. Thus, the *IMK* model is utilized in the present research.

Table 4.1. Capabilities of hysteretic models, modified from Lignos (2008).

MODEL	CYCLIC HARDENING	BAUSCHINGER EFFECT	STRENGTH CAPPING	RESIDUAL STRENGTH	CYCLIC DETERIORATION			
					BASIC STRENGTH	POST-CAPPING	UNLOADING STIFFNESS	ACCELERATED STIFFNESS
Clough and Johnston and Modifications	-	-	-	-	-	-	☑	☑
Takeda Model	-	-	-	-	-	-	☑	☑
Bouc-Wen and Modifications	☑	☑	-	-	☑	-	☑	☑
Ramberg-Osgood	☑	☑	-	-	☑	-	☑	-
Kunath et. Al.	☑	☑	-	-	☑	-	☑	☑
Syvaselvan and Reinhorn	☑	☑	-	-	☑	-	☑	-
FEMA-356	☑	-	☑	☑	-	-	-	-
Yield-Line Plastic Hinge Models	☑	☑	☑	☑	☑	☑	☑	☑
Song-Pincheira	-	-	☑	☑	-	-	☑	☑
Ibarra-Medina-Krawinkler	-	-	☑	☑	☑	☑	☑	☑
Modified Ibarra-Medina-Krawinkler	-	-	☑	☑	☑	☑	☑	☑

Nevertheless, challenges with the implementation of the *IMK* model on collapse simulations exist. One of the major drawbacks of using a piecewise linear model versus smooth curvilinear models (e.g., Bouc-Wen) is achieving numerical convergence particularly when stiff structures are used. For instance, a portion of a moment-rotation hysteresis history of a steel component test is depicted on Figure 4.2. In the left hand side (Figure 4.2(a)) the simulation is implemented using a large analysis step ( $\Delta t_{analysis}$ ). As can be seen, a considerable deviation in strength (*ii*) on the current analysis step (*i*) is calculated due to the large size of  $\Delta t_{analysis}$ . Thus, the simulation applies a value of moment located on the elastic stiffness path when the desired constitutive relationship to be represented by the *IMK* model should be consistent with the strain-

hardening trajectory, creating a numerical moment unbalance. These large deviations in strength may lead to numerical instability on the simulation. On Figure 4.2(b), the same portion of the hysteretic response is used. As can be observed, the use of smaller  $\Delta t_{\text{analysis}}$  helps reduce the magnitude of possible deviations (ii) on strength when abrupt changes in stiffness are found within the *IMK* model, which also minimizes the likelihood of numerical instability. On the present research, sensitivity studies were performed to determine the pertinent  $\Delta t_{\text{analysis}}$  values to avoid numerical instability during simulations. Appropriate values of  $\Delta t_{\text{analysis}}$  and their influence on hybrid simulation results are discussed in Chapter 3.

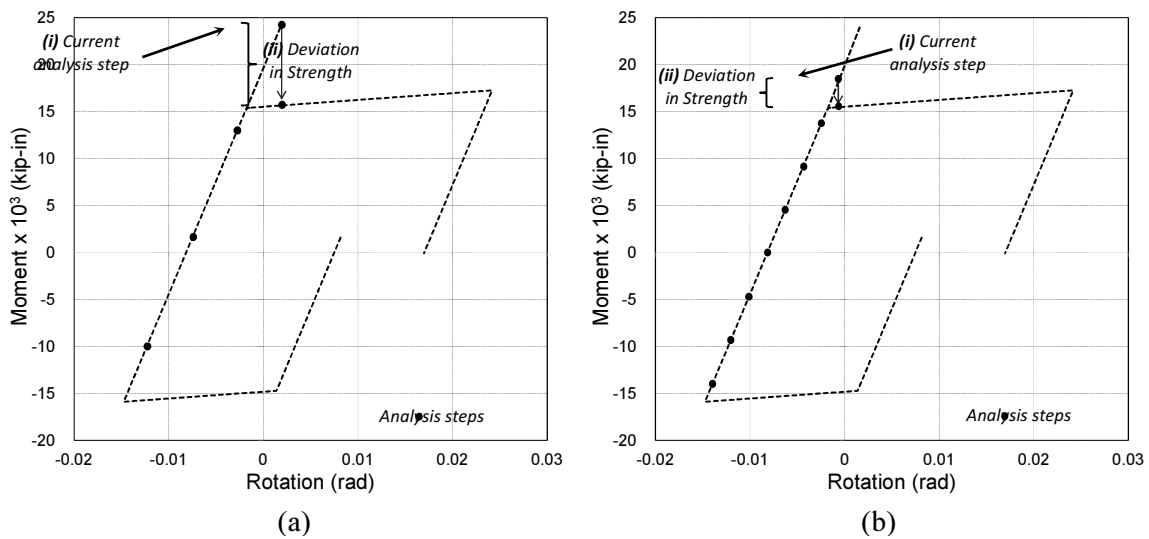


Figure 4.2. Deviation in strength due to analysis step increment size: (a) large  $\Delta t_{\text{analysis}}$ , (b) small  $\Delta t_{\text{analysis}}$ .

### 4.3. Ibarra-Medina-Krawinkler Hysteretic Model

The *IMK* model on its original form incorporates a backbone curve (Figure 4.3) that represents the monotonic response of a component or substructure without cyclic deterioration. The rate of cyclic deterioration of the parameters that control the backbone curve is based on an energy-based rule developed by Rahnama and Krawinkler (1993). The expression is based on the

hysteretic energy dissipated when the component is subjected to cyclic loading.

The cyclic deterioration in excursion  $i$  is defined by the parameter  $\beta_i$  given in Equation 4.1.

$$\beta_i = \left( \frac{E_i}{E_t - \sum_{j=1}^i E_j} \right)^c \quad (4.1)$$

Where:

$E_i$  = hysteretic energy dissipated in excursion  $i$ ,

$E_t$  = reference hysteretic energy dissipation capacity,  $E_t = \gamma F_y \delta_y$ ,

$\sum E_i$  = hysteretic energy dissipated in all previous excursions,

$\gamma$  = hysteretic energy dissipation capacity as a function of twice the elastic strain

energy at yielding ( $F_y \delta_y$ ), it is calibrated from experimental results,

$c$  = exponent defining the rate of deterioration, suggested values are between

1.0 (almost constant rate) and 2.0 (lower rate in early cycles, accelerated rate in later cycles).

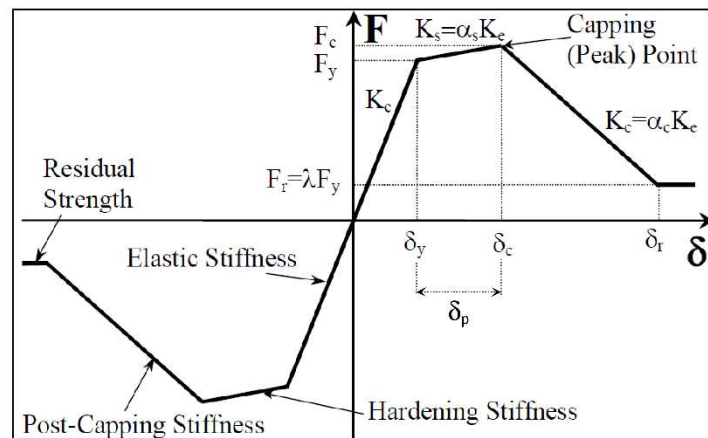


Figure 4.3. Backbone curve, *IMK* model (Ibarra, et al., 2005).

The salient properties of the model are set by the parameters that define the backbone

curve: elastic (initial) stiffness  $K_e$ , yield strength  $F_y$ , strain-hardening stiffness  $K_s = \alpha_s K_e$ , capping deformation  $\delta_c$ , which corresponds to the peak strength  $F_c$  of the load-deformation curve, post-capping stiffness,  $K_c = \alpha_c K_e$  and residual strength,  $F_r = \lambda F_y$ , representing the fraction of the yield strength of the component that is preserved once a given deterioration threshold is achieved. Moreover,  $\alpha_s$  represents the work hardening in the specimen through plastic deformation, leading to an increase on the specimen strength. The amount of strain (or work) hardening depends on the spread of plasticity on the specimen, the member cross section, as well as the material properties and loading protocols. On the other hand,  $\alpha_c$  represents the softening trend of the specimen after having reached the maximum resistance moment (capping point). After the capping point is attained, the specimen stops increasing its strength. Nevertheless, as long as a brittle failure mode is not present (i.e., fracture), an important amount of deformation is available before the capacity of the system reaches a residual strength or approaches the limit state of collapse. In steel structures, this softening could be due to a combination of material non-linearity with severe local buckling and, if torsional restraints are not provided, with lateral torsional buckling (Karakostas, 2000). Theoretically, values for steel components are in the ranges of  $0\% \leq \alpha_s \leq 100\%$  and  $-\infty \leq \alpha_c \leq 0\%$  of the elastic stiffness. Typical median values for beams with reduced beam sections (RBS) calculated from 52 steel component tests reported on Lignos (2008) are 3.5% for strain hardening ratio and -4.5% for post-capping ratio (Table 4.2).

Table 4.2. Test results of beams RBS, modified from Lignos (2008).

TEST ID	REFERENCE	BEAM SIZE	K (kips-in/rad)	My (Kips-in)	McMy	Mc (Kips-in)	Øp (rad)	Øpc(rad)	α <sub>c</sub>	α <sub>c</sub>
1	Uang et al. (2000a)	W30x99	2790995	15200	1.11	16872	0.025	0.160	2.40%	-3.78%
2	Uang et al. (2000a)	W30x99	2700000	15800	1.11	17538	0.028	0.200	2.30%	-3.25%
3	Uang et al. (2000a)	W30x99	2500000	14000	1.11	15540	0.025	0.240	2.46%	-2.59%
4	Uang et al. (2000a)	W30x99	2790995	15300	1.11	16983	0.026	0.200	2.32%	-3.04%
5	Uang et al. (2000b)	W36x150	7460000	30500	1.15	35075	0.020	0.210	3.07%	-2.24%
6	Uang et al. (2000b)	W24x62	1011000	7400	1.10	8140	0.019	0.170	3.85%	-4.74%
7	Uang et al. (2000b)	W36x150	7412000	30000	1.10	33000	0.013	0.090	3.11%	-4.95%
8	Uang et al. (2000b)	W36x150	7412000	30000	1.15	34500	0.015	0.140	4.05%	-3.32%
9	Engelhardt et al. (2000)	W36x150	8890000	20000	1.10	22000	0.025	0.320	0.90%	-0.77%
10	Engelhardt et al. (2000)	W36x150	8890000	20000	1.10	22000	0.025	0.320	0.90%	-0.77%
11	Tremblay et al. (1997)	W21x62	840000	5340	1.08	5767.2	0.045	0.220	1.13%	-3.12%
12	Tremblay et al. (1997)	W21x62	700000	5200	1.10	5720	0.031	0.210	2.40%	-3.89%
13	Herrick, Smith-Emery (1996)	W27x94	924000	9160	1.07	9801.2	0.029	0.170	2.39%	-6.24%
14	Ivankiw and Carter (1996)	W30x99	550000	11500	1.10	12650	0.031	0.130	6.74%	-17.69%
15	Ivankiw and Carter (1996)	W30x99	550000	11500	1.10	12650	0.031	0.130	6.74%	-17.69%
16	Herrick, Smith-Emery (1996)	W33x169	2200000	18100	1.10	19910	0.023	0.240	3.58%	-3.77%
17	Herrick, Smith-Emery (1996)	W36x135	1800000	17500	1.10	19250	0.022	0.210	4.42%	-5.09%
18	Herrick, Smith-Emery (1996)	W36x135	1800000	17000	1.10	18700	0.018	0.170	5.25%	-6.11%
19	Ivankiw and Carter (1996)	W36x150	955000	21600	1.10	23760	0.025	0.300	9.05%	-8.29%
20	Engelhardt et al. (1996)	W36x194	2250000	28500	1.10	31350	0.025	0.310	5.07%	-4.49%
21	Engelhardt et al. (1996)	W36x170	2240000	29800	1.10	32780	0.029	0.290	4.59%	-5.05%
22	Engelhardt et al. (1996)	W36x150	2240000	20200	1.08	21816	0.020	0.260	3.61%	-3.75%
23	Anderson and Duan (1998)	W21x68	700000	8900	1.12	9968	0.021	0.230	7.27%	-6.19%
24	Popov et al. (1998)	W36x135	2450000	20000	1.10	22000	0.019	0.150	4.30%	-5.99%
25	Popov et al. (1997)	W33x130	2220000	17400	1.08	18792	0.018	0.170	3.48%	-4.98%
26	Popov et al. (1997)	W33x130	2220000	18000	1.09	19620	0.020	0.170	3.65%	-5.20%
27	Popov et al. (1997)	W36x194	3510000	34500	1.06	36570	0.024	0.300	2.46%	-3.47%
28	Tsai and Chen (2000)	H100x200x11x17	837013	24900	1.07	26643	0.033	0.350	6.31%	-9.09%
29	Tsai and Chen (2000)	H600x200x11x17	837013	22900	1.07	24503	0.035	0.350	5.47%	-8.36%
30	Tsai and Chen (2000)	H600x200x11x17	837013	23100	1.10	25410	0.034	0.250	8.12%	-12.14%
31	Tsai and Chen (2000)	H600x200x11x17	837013	22900	1.10	25190	0.036	0.240	7.60%	-12.54%
32	Tsai and Chen (2000)	H600x200x11x17	837013	27500	1.10	30250	0.038	0.240	8.65%	-15.06%
33	Zekioglu et al. (1996)	W27x178	1800000	23200	1.08	25056	0.035	0.260	2.95%	-5.35%
34	Zekioglu et al. (1996)	W27x178	1800000	27500	1.06	29150	0.035	0.350	2.62%	-4.63%
35	Zekioglu et al. (1996)	W36x150	2000000	24500	1.06	25970	0.022	0.230	3.34%	-5.65%
36	Zekioglu et al. (1996)	W33x152	4000000	34000	1.06	36040	0.021	0.240	2.43%	-3.75%
37	Zekioglu et al. (1996)	W33x152	4000000	32500	1.06	34450	0.021	0.230	2.32%	-3.74%
38	Suita et al. (1998)	WF-500x200x10x16	750000	5800	1.08	6264	0.042	0.380	1.47%	-2.20%
39	Suita et al. (1998)	WF-500x200x10x16	750000	5600	1.08	6048	0.041	0.320	1.46%	-2.52%
40	Suita et al. (1998)	WF-500x200x10x16	750000	6200	1.08	6696	0.038	0.360	1.74%	-2.48%
41	Suita et al. (1998)	WF-500x200x10x16	900000	5900	1.08	6372	0.039	0.280	1.34%	-2.53%
42	Suita et al. (1998)	WF-500x200x10x16	900000	6250	1.08	6750	0.040	0.320	1.39%	-2.34%
43	Lee et al. (2005)	H700x300x13x24	2000000	18000	1.12	20160	0.035	0.280	3.09%	-3.60%
44	Lee et al. (2005)	H700x300x13x24	2000000	18000	1.12	20160	0.031	-	3.48%	-
45	Lee et al. (2005)	H700x300x13x24	2000000	13000	1.25	16250	0.013	-	12.50%	-
46	Lee et al. (2005)	H700x300x13x24	2000000	16000	1.11	17760	0.015	-	5.87%	-
47	Lee et al. (2005)	H600x200x11x17	807000	7900	1.11	8769	0.028	0.180	3.85%	-6.04%
48	Lee et al. (2005)	H600x200x11x17	780000	7900	1.10	8690	0.024	0.165	4.22%	-6.75%
49	Lee et al. (2005)	H600x200x11x17	950000	8100	1.11	8991	0.025	0.260	3.75%	-3.64%
50	Lee et al. (2005)	H600x200x11x17	1000000	9600	1.11	10656	0.026	0.220	4.06%	-4.84%
51	Shin et al. (2008)	H506x201x11x19	685056	7500	1.13	8475	0.044	0.400	3.23%	-3.09%
52	Shin et al. (2008)	H506x201x11x19	628247	8100	1.07	8667	0.041	0.310	2.20%	-4.45%
<b>MEDIAN</b>									<b>3.48%</b>	<b>-4.49%</b>

Four cyclic deterioration modes with respect to the backbone curve are considered:

- Basic strength deterioration; captures the deterioration in yield strength and strain hardening slope, independently in the positive and negative directions (Figure 4.4(a)).
- Post-capping strength deterioration; unlike basic strength deterioration, the post-capping branch is kept constant and is moved towards the origin (inwards) by an amount equivalent to the relative reduction of the reference strength ( $F_C$ ) (Figure 4.4(b)).
- Unloading stiffness degradation, the unloading stiffness ( $K_u$ ) is degraded according to a deterioration parameter  $\beta_k$ . Particularly, this parameter is computed when a load reversal takes place in the inelastic range, unlike the other deterioration parameters that are computed when the loading path crosses the horizontal axis. This is the only model parameter that is updated (deteriorated) simultaneously in both directions. Consequently, the unloading stiffness deteriorates about twice as fast as the other model parameters for a symmetric cyclic response (Figure 4.4(c)).
- Accelerated reloading stiffness degradation; it is applied only for peak-oriented and pinching models. It increases the absolute value of the target displacement used to reload, which is originally defined as the maximum positive or negative displacement of past cycles, according to the direction of loading (Figure 4.4(d)).

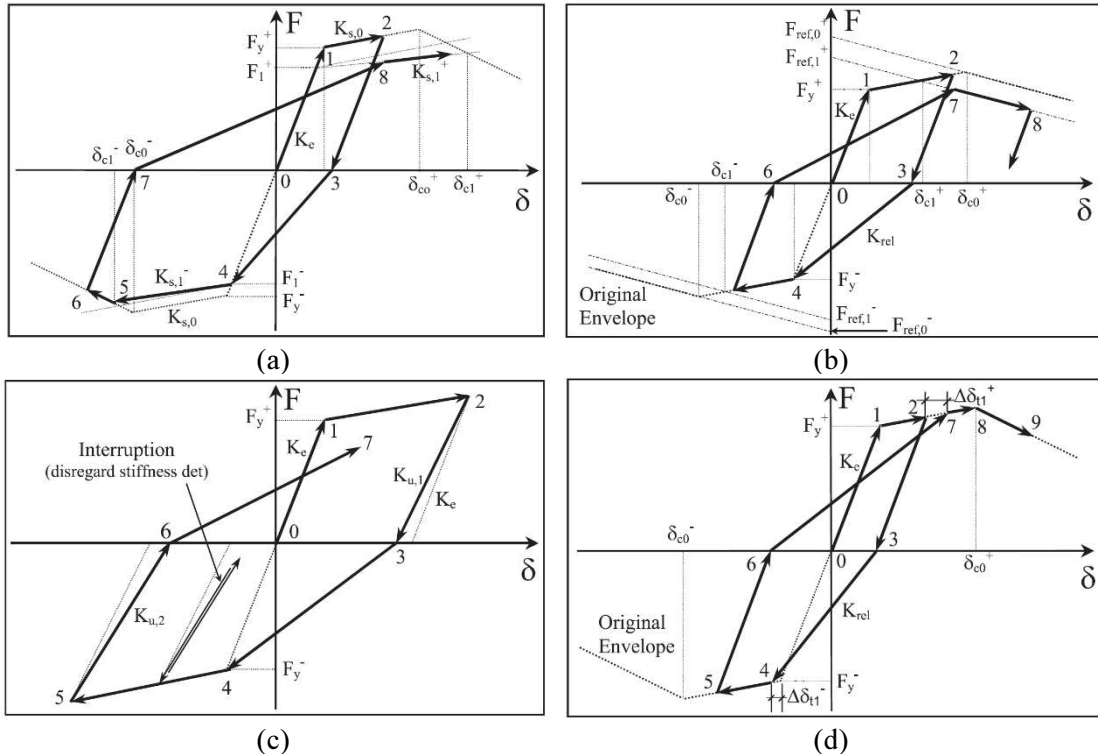


Figure 4.4. Individual deterioration modes, illustrated on a peak-oriented model (Ibarra, et al., 2005): (a) basic strength deterioration; (b) post-capping strength deterioration; (c) unloading stiffness degradation; and (d) accelerated reloading stiffness degradation.

Some additional advantages of using the *IMK* model are: 1) its availability in OpenSees (McKenna, et al., 2000), including modifications made by Lignos (Lignos & Krawinkler, 2011); and 2) the relatively small number of parameters used to control hysteretic responses with deterioration, implying a minor number of main parameters to update during the implementation of the proposed NUA. In the present study the parameters to update are  $K_e$ , using information obtained from the early elastic cycles of vibration (to be applied on both positive and negative directions);  $F_y$ ,  $\alpha_s$ ,  $\delta_p$  and  $\alpha_c$ , which are updated independently on both positive and negative quadrants (i.e., a total of nine parameters are updated for each component).



#### 4.4. Modifications to *IMK* model

It is general practice to calibrate hysteretic model parameters once the complete response histories are available after an experiment. For the specific case of the *IMK* model, once the parameters of the backbone curve and those that control cyclic deterioration are calibrated, the model will behave as predicted by predefined rules.

One of the main features of the NUA implemented in this study is to update the main model parameters *during the analysis*. Since it is clear that the complete histories of local or global responses are not available at the start of the simulation, rules to make the *IMK* model capable of characterizing responses and changes in modeling parameters during the analysis were designed and implemented. The modified *IMK* model that incorporates the aforementioned set of rules is referred to herein as the Dynamic *IMK* model (*DIMK*). The parameters that define the backbone of the *DIMK* model change continuously during the analysis in order to capture the history of the response during the experiment.

Deformation compatibility between the global response measured from the virtual experiment and its numerical fit constitutes the departure point to establish rules to identify the parameters of the *DIMK* model. It also should be noted that the numerical fit is calculated one analysis step behind with respect to the experimental response. Because the time increments used in this approach are small, this time lag is not deemed to be critical in terms of the accuracy of the proposed approach. For instance, the largest analysis time increment utilized in the updating procedure is  $\Delta t_{analysis} = \frac{1}{128}(0.50) = 0.0039sec$  (see Table 3.1).

In principle, the initial parameter values of the backbone at the component level could be based on *a priori* knowledge based on testing of components and structural sections to be used on the experimental substructure, and on previous research of similar components reported in the

literature. One example is the report by Lignos and Krawinkler (2011), which includes a database of most of the available cyclic steel component tests conducted prior to 2008. Moreover, Lignos and Krawinkler developed empirical formulae based on statistical regression analysis to estimate the most important parameters of the *IMK* model that control the moment-rotation response of primarily steel beams and some columns. The equations proposed by Lignos and Krawinkler were used in this study to estimate the initial parameters of the backbone curve of the numerical models.

#### **4.5. Proposed rules for *DIMK* numerical fit.**

The rules proposed to update each relevant parameter of the *DIMK* model at the global level are summarized below. These rules are implemented in the in-house Matlab® optimization interfaces developed as part of this study.

The deterioration modes in the original *IMK* model are governed by hysteretic energy dissipation capacity factors ( $\gamma_{s,c,k,a}$ ), that form the basis for the calculation of cyclic deterioration parameters  $\beta_{s,c,k,a}$ , which control cyclic strength deterioration and stiffness degradation, as shown in Equation 4.1. Appropriate values of  $\gamma_{s,c,k,a}$  are obtained through calibration approaches geared toward providing the best possible numerical fit to existing experimental data that incorporate the complete response history. The approach implemented in this dissertation involves utilizing the original *IMK* model to apply a numerical fit based on a set of rules to estimate the time evolution of the parameters that describe the backbone curve at each cycle of vibration. In this procedure, the  $\gamma$  factors that control the rate of cyclic deterioration in the original model are kept inactive. This is deemed to be a reasonable approach given that the experimental data used to carry out the aforementioned numerical fit are being generated during the simulation. Therefore, not enough information exists at the start of the test to calibrate  $\gamma$  factors based on the complete response

history of the specimen. Keeping the cyclic deterioration inactive is achieved by assigning high values to hysteretic dissipation capacity parameters ( $\gamma$ ). As shown in Equation 4.1 and based on the definition of the reference hysteretic energy dissipation capacity  $E_t = \gamma F_y \delta_y$ , it is evident that by assigning a high value ( $\rightarrow \infty$ ) to the  $\gamma_{(s,c,k,a)}$  factors, a relatively large value of  $E_t$  is also obtained. This results in the parameters  $\beta_{(s,c,k,a)}$  tending to zero, leading to a system without cyclic deterioration. This technique is implemented during the development of *DIMK* rules and its posterior application on the NUA. Moreover, the residual force is defined as zero ( $F_r = \lambda F_y = 0.0$ ), providing added flexibility to the *DIMK* model to follow the response history up to the last stages of resistance of the specimen, especially when the specimen approaches the limit state of collapse.

Furthermore, relevant parameters ought to be updated from one value to another incrementally over a reasonable number of analysis time steps to prevent numerical instability. Thus, “emotional” changes must be avoided along the simulation. These emotional changes can be described as the instantaneous updating of numerical parameters most likely based on local changes in the response. These changes could be provoked by several possible reasons, among them, local spurious behavior on the hysteretic information possibly due to noise in the recorded responses, higher-mode effects, or local forces induced by limitations associated with the resolution of the actuator load cells. The importance of avoiding this abrupt updating of parameter values relies on the fact that some of the local changes shown in the hysteretic response of the system are “spurious” and may lead to erroneous recalibration of values when fitting the *IMK* model to the hysteretic response.

Some of the criteria adopted to avoid emotional updating errors are as follows:

1) Implementation of algorithms that incorporate local filters based on the backbone of the *IMK* model. The function of the filters is to check if the response obtained is not a local spurious force/displacement response e.g., one provided by noise associated with the data-acquisition process. This is met via force and displacement verifications. For instance, after a change from the current linear branch to the next portion of the *IMK* model is identified (e.g, from elastic- $K_e$  to  $\alpha_s K_e$ ), several displacement data points are accumulated until it is verified that the trajectory effectively shifted and is following the subsequent *IMK* path, hence, avoiding a change immediately after the first indication of a variation. This verification is linked to a confirmation of the direction of the force. The associated force should meet the same criteria; it also ought to follow the construction of the backbone after the accumulation of some analysis steps results. For example, if the simulation is located on the strain-hardening branch, the force should be increasing in intensity. Conversely, if the analysis is on the post-capping slope, the force must be decreasing. Hence, if both filters are satisfied, then a change from branch to branch is accepted and applied to the model. If,, on the other hand, responses are deemed to be related to spurious effects, the parameters that characterize the backbone of the *IMK* model during this cycle are not modified. It is also pointed out that the numerical fitting follows the *IMK* model backbone construction sequence at all times. In this sense, once a piecewise linear branch of the backbone fitting curve (elastic- $K_e$ , strain-hardening- $\alpha_s K_e$  or post-capping- $\alpha_c K_e$ ) is entered, any change estimated due to spurious forces commanding to return to a previous linear branch (e.g., post-capping- $\alpha_c K_e$  to strain-hardening- $\alpha_s K_e$ ) on the same loading cycle without completing the *IMK* backbone or finding a loading reversal is neglected. In this case, the parameters from previous branches of the backbone curve are not modified during the current cycle. This process is followed until a load reversal takes place or the structure approaches the limit state of collapse;

2) A strength approach is adopted to command a change from the elastic to the strain-hardening branch during the numerical fitting. A tolerance is established on the deviation of strength between the numerical fit and the experimental response at a given step. If the prescribed tolerance is exceeded, a change from  $K_e$  to  $\alpha_s K_e$  takes place, as explained in more detail later in this section. Thus, due to the fact that criteria based on stiffness variations are more suitable to emotional/impulsive reactions and given the high frequency content and associated noise that might exist on hybrid testing of complex structures, the strength-based approach is applied along the present research.

A hysteretic moment-rotation history obtained from a full-scale steel test specimen reported in Uang et. al. (2000), is used to illustrate the design and implementation of the *DIMK* rules. The steel specimen tested is referred to as “LS-1” and it was built according to the setup presented on Figure 4.5(a) and tested to failure. The A992 steel shapes utilized were a W30x99 beam section and a W14x176 column section. The beam-to-column connection was designed using reduced beam sections (RBS), which were also used in the main structure tested as part of this study. The standard SAC loading history protocol developed by Krawinkler (1996) was applied to the specimen. The complete moment-rotation hysteretic response obtained from the test is presented in Figure 4.5(b). In this context, the bending moment was obtained by the product of the hydraulic actuator force and the distance from the point of application of the load to the face of the column. The rotation was estimated via the ratio of the displacement at the tip of the beam to the original beam length.

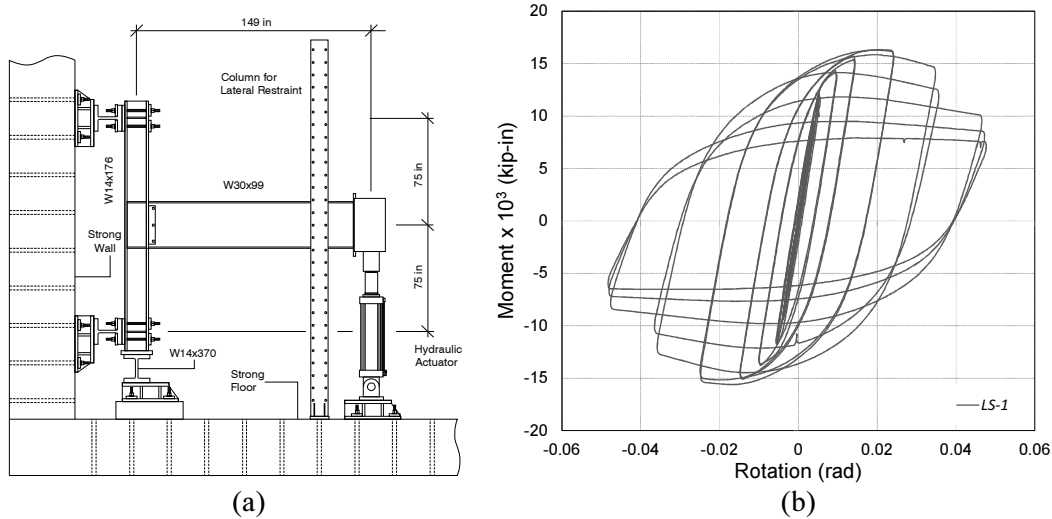


Figure 4.5. Specimen LS-1: (a) test set-up full-scale steel specimen, (b) moment vs. rotation, after Uang et. al., (2000).

In the numerical updating process, updated parameters used to define the *DIMK* model are labeled with the subscript “*n*” ( $K_{en}$ ,  $M_{yn}$ ,  $\theta_{pn}$ ,  $\alpha_{sn}$ , and  $\alpha_{cn}$ ) to distinguish them from the original *IMK* model nomenclature.

It should be note that differences in the predicted ( $K_e$ ,  $M_y$ ,  $\theta_p$ ,  $\alpha_s$ , and  $\alpha_c$ ) versus measured parameters ( $K_{en}$ ,  $M_{yn}$ ,  $\theta_{pn}$ ,  $\alpha_{sn}$ , and  $\alpha_{cn}$ ) are computed on the current cycle and applied at the start of the following loading cycle in the same direction.

#### 4.6. Modifications to the elastic stiffness $K_{en}$

Given that the stiffness parameters defining the backbone of the *IMK* model are fractions of the elastic stiffness ( $K_e$ ), a change of at least 10% on this parameter in the current cycle with respect to the previous one, triggers an update to *DIMK* stiffness parameters. In the case of the elastic stiffness ( $K_e$ ), a linear fit is applied to calculate the updated value of the elastic stiffness slope ( $K_{en}$ ). The data used for the calculations consists of the hysteretic response history of the current cycle, from the beginning of the loading path up to a value smaller than or equal to the

yield strength value of that specific cycle ( $M_{yn}$ ). The elastic stiffness value is updated on the *DIMK* model at the step following the initiation of a reversal loading on the subsequent cycle. From this analysis step on, the actual  $K_{en}$  value is utilized on the *DIMK* model on both positive and negative loading quadrants. This value is kept constant until another change in elastic stiffness of at least 10% is estimated and the described process is carried out again.

In Figure 4.6 a portion of the LS-1 moment-rotation hysteresis results is plotted with a continuous gray line. The dotted red line represents the *DIMK* numerical fit. An induced calibration error on the initial elastic stiffness and its corresponding inaccurate numerical fit are shown in Figure 4.6(a), where no correction rule is employed. In Figure 4.6(b), the application of the correction rule is depicted. First, the induced erroneous initial stiffness value of 50,000 kips/ft is shown (*i*). Next, data collected to calculate a linear fit and obtain  $K_{en}$  for the specific loading cycle is also shown (*ii*). The data collection begins with the start of the positive loading path (*iii*) and ends when the maximum strength in the current cycle ( $M_{yn}$ ) is found (*iv*). This can occur when a deviation on the elastic path towards the strain hardening trajectory or a loading reversal is encountered. On Figure 4.6(b)  $M_{yn}$  adopts the value of the maximum strength identified at the loading reversal, but in other instances when the system or component enters the nonlinear range  $M_{yn}$  would take the maximum moment value achieved on the elastic loading path at the current cycle. It should be mentioned that  $M_{yn}$  can take any value, lesser, equal or greater than the yield strength ( $M_y$ ) at the given cycle. Then, the  $K_{en}$  updated value of 200,100 kips/ft is applied on the first step of the subsequent reversal loading (*v*), which is also identified in Figure 4.6(b). As can be noticed in the same Figure 4.6(b), the application of the corrected value (*vi*) is clearly observed as a sudden change from the  $K_e$  with the induce initial error to the updated  $K_{en}$  slope value. The updated value  $K_{en}$  is used in the

following cycles until another updating event is triggered.

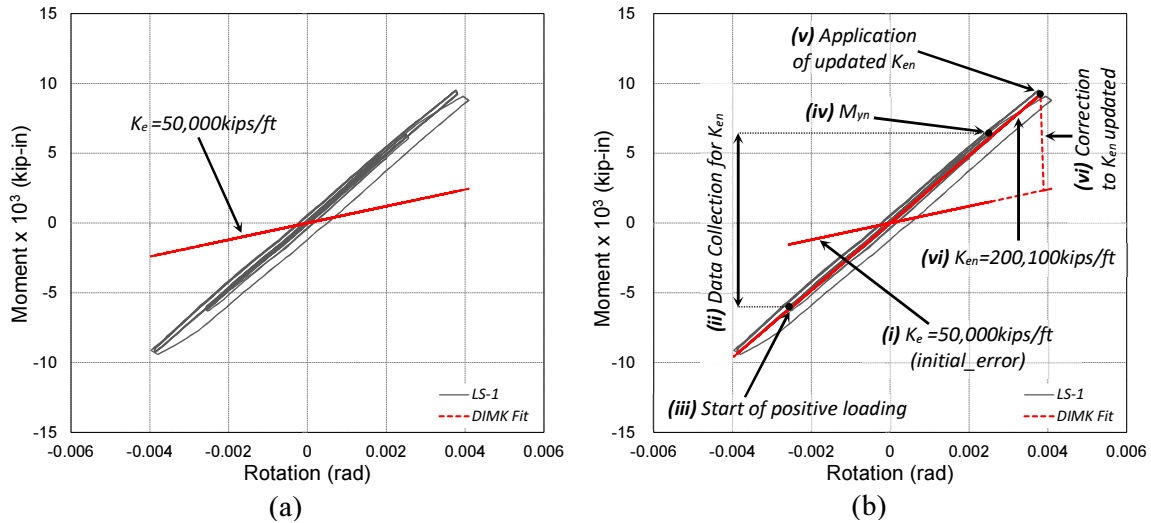


Figure 4.6. Elastic stiffness modification rule: (a) no correction, (b) corrected.

#### 4.7. Modifications to yield strength demand $M_{yn}$

A strength-based criterion is implemented in order to update the yield strength demand  $M_{yn}$ . An initial deviation tolerance is established (e.g., 35% of initial  $M_y$ ) between the strength of the *DIMK* model fit based on existing parameters, and the strength of the global hysteretic response at the current cycle. If this tolerance is exceeded, the parameter  $M_{yn}$  is updated in the numerical model by setting its value equal to the strength demand on the current cycle from the experimental response at the point where the tolerance is exceeded.

An excerpt of the LS-1 specimen moment-rotation hysteresis is plotted in Figure 4.7 with a continuous gray line. The numerical fit using the *DIMK* model is shown in dotted red line to illustrate the yield strength modification rule. As can be observed, once the predefined deviation tolerance in strength is exceeded during the loading branch (i), a change in path is enforced from the elastic loading branch ( $K_{en}$  slope) to the hardening stiffness branch (ii). This is part of the dynamic recalibration procedure in which the yield strength is capped to its new yield value  $M_{yn}$ .



The rule applies for both positive (Figure 4.7(a)) and negative (Figure 4.7(b)) quadrants.

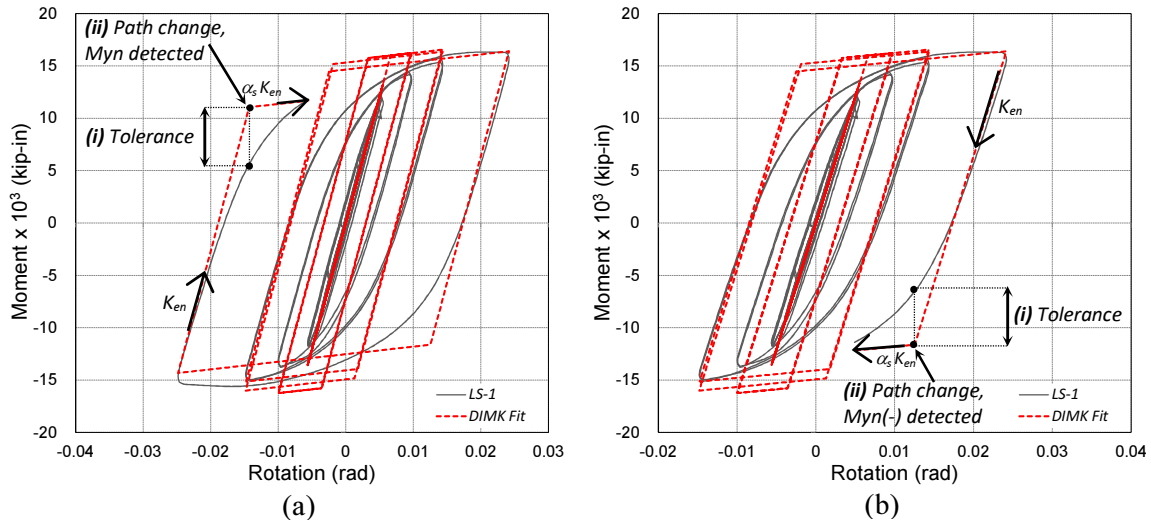


Figure 4.7. Basic strength *DIMK* rule model yield strength larger than experimental: (a) positive loading, (b) negative loading.

Figure 4.7 illustrated the application of this rule when the  $M_{yn}$  value in the *DIMK* is ahead (greater than) the required one based on the experimental global hysteretic response. When the existing *DIMK* yield strength value is behind (smaller than) the one observed in the experimental response, the fitted numerical strength value is gradually increased at each analysis step, to follow closer the experimental response. The rule is applied up to the desired value of strength demand estimated from the experiment during that cycle of vibration. This gradual increase is implemented in order to prevent sudden changes in strength and avoid numerical instability issues.

Two supplementary variables are introduced for clarification, 1) Strength value of the experimental substructure  $M_{exp}$  and, 2) Numerical fitted strength value,  $M_{fit}$ . Both variables store smaller values than  $M_{yn}$  and correspond to the current analysis step. The additional increment in strength ( $\Delta M_{fit}$ ) is defined as the product of the factor  $\eta$  times the difference of the rotation ( $\Theta_i$ ) on the current step minus the rotation from the previous step ( $\Theta_{i-1}$ ) multiplied by the current

elastic stiffness  $K_{en}$ , as written in Equation 4.2. Based on sensitivity studies, recommended values are in the order of  $2\% \leq \eta \leq 5\%$ .

The increment in strength calculated through Equation 4.2, is added up to the actual value of  $M_{fit}$  on the current step as shown in Equation 4.3, to obtain the incremented value of strength,  $M_{fit}'$ .

$$\Delta M_{fit} = \eta(\Theta_i - \Theta_{i-1})K_{en} \quad (4.2)$$

$$M_{fit}' = M_{fit} + \Delta M_{fit} \quad (4.3)$$

This increment is applied at each analysis step up to when: 1) the *DIMK* model fitting overtakes the experimental part – the strength value does not need to be further increased; 2) a loading reversal in the experimental hysteresis is found, or 3) the slope in the experimental response deviates from the elastic stiffness ( $K_{en}$ ), entering into the hardening stiffness branch.

Figure 4.8 shows examples of the three possible scenarios of the application of the rule. In Figure 4.8(a) it can be seen that due to the previous loading history, at the start of the current loading path, the experimental response is already ahead of the numerical fit (*i*). Thus, a series of step-wise increments in strength are needed and applied during a portion of the analysis history where ( $M_{exp} > M_{fit}'$ ), as described in Equations 4.2 and 4.3. This portion of the history (*(ii)* enclosed in a square bracket) comprises several analysis steps where the numerical fitting strength should be increased through the application of the rule. Later in the analysis (*(iii)*), the experimental and increased numerical fit strengths equal their values ( $M_{exp} = M_{fit}'$ ). After this step a strength increment is no longer needed. Lastly, the numerical fit overtakes the experimental response ( $M_{fit}$

$> M_{exp}$ ) on the analysis steps subsequent to point (iv) of the current loading cycle.

The second possible scenario is depicted in Figure 4.8(b). The current loading path starts (i) with the numerical fit strength ahead of the experimental value ( $M_{fit} > M_{exp}$ ). Later in the analysis (ii), the experimental strength equals the numerical fit strength ( $M_{exp} = M_{fit}$ ). After this step, the experimental response overtakes the numerical fit ( $M_{exp} > M_{fit}$ ) providing evidence of the need of application of the rule. The basic strength increment rule is applied during several analysis steps (iii) enclosed on the square bracket. In this scenario, even though the experimental strength is been increased through the application of the rule, a loading reversal is reached (iv) and consequently the end of the application of the strength increment rule. Also at this point (iv)  $M_{fit}'$  becomes  $M_{yn}$ .

The third possible scheme is exemplified in Figure 4.8(c). The numerical fit is ahead of the experimental response (i) at the start of the loading trajectory ( $M_{fit} > M_{exp}$ ). Afterward, a point of equilibrium (ii) between responses is found ( $M_{exp} = M_{fit}$ ). Alike the previous scenario, after this step the experimental strength overtakes the numerical fit ( $M_{exp} > M_{fit}$ ). The rule is applied during the analysis steps bounded in the bracket (iii). Finally, the experimental response exits the limit of proportionality, leading to a change on the numerical fit course into the hardening branch (iv) and therefore finalizing the application of the strength increment rule.  $M_{yn}$  adopts the value of the  $M_{fit}'$  associated with the strength value of point (iv). On the last two scenarios the experimental response completes the loading path (up to a loading reversal or the end of the elastic stiffness) ahead of the numerical fit ( $M_{exp} > M_{fit}'$ ), with minimized differences by virtue of the operation of the basic strength increment rule.

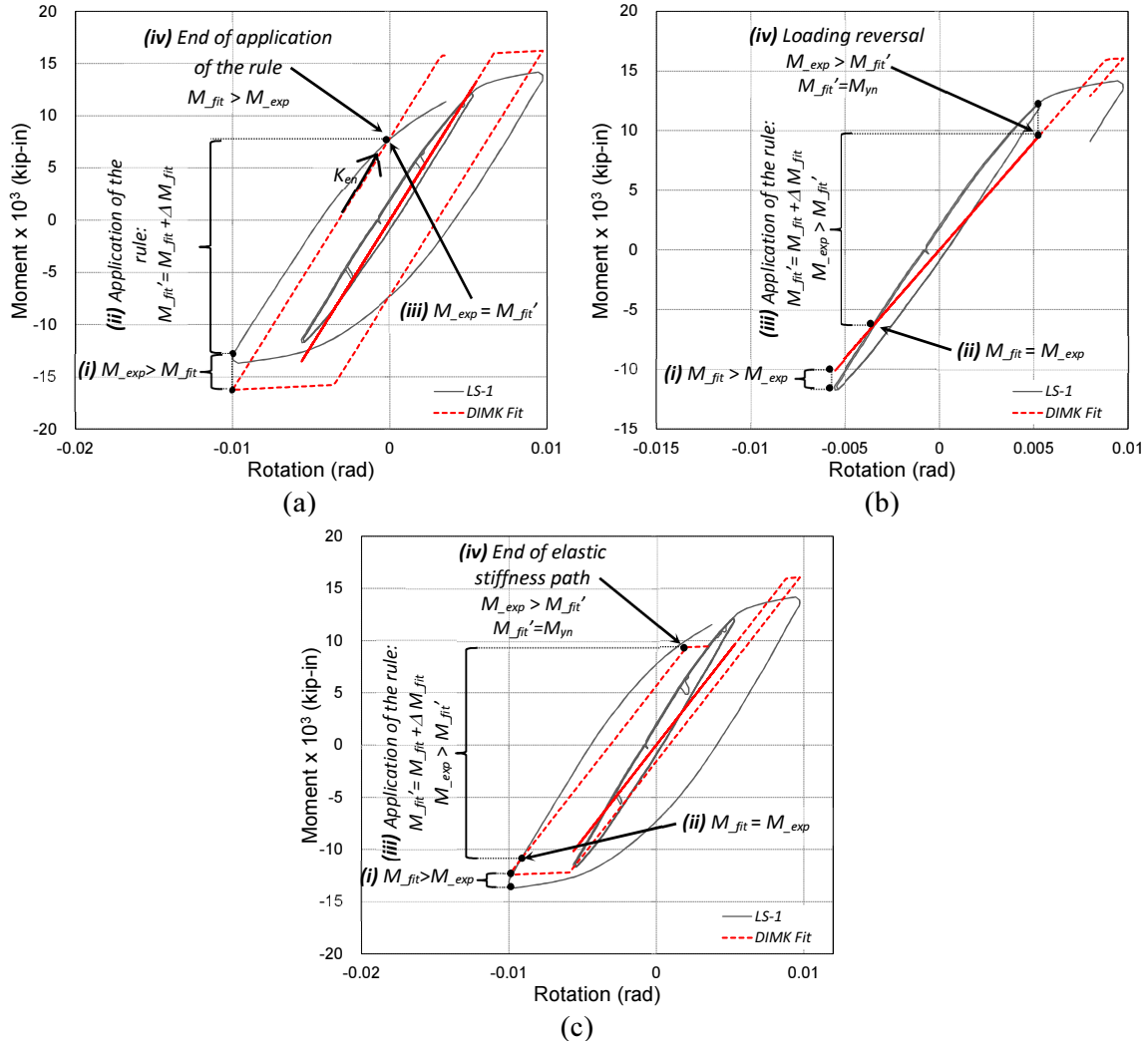


Figure 4.8. Basic strength increment *DIMK* rule, model yield strength lower than experimental: (a) numerical fit overtaking experimental response, (b) loading reversal and, (c) end of limit of proportionality.

#### 4.8. Modifications to plastic deformation capacity $\delta_{pn}$

Given that the hysteretic response is load dependent, the original value of the plastic rotation capacity parameter,  $\theta_p$ , should vary according to the imposed demand. Physical specimens intrinsically possess a characteristic value of this parameter that could be determined through a monotonic load test. However, once the specimen is under high levels of non-linearity with cumulative deterioration, the initial value could be significantly modified.

Similarly during seismic-type reversal loading, short and long pulses are imposed on the substructure due to the aleatory nature of the input signal. Therefore, the proposed rule is intended to recalibrate dynamically the parameter  $\theta_p$  according to the required demands imposed to the experimental model, increasing or decreasing its value during the analysis ( $\theta_{pn}$ ).

Based on the deformation compatibility criterion previously explained, once the *DIMK* model attains the yield deformation ( $\Theta_{yield}$ ) and enters the strain hardening branch ( $\alpha_s K_{en}$ ) as pointed out in Figure 4.9 (i), rotation data is recorded to determine the new value of  $\theta_{pn}$  on the current cycle. This data collection finalizes at point (ii) of Figure 4.9 ( $\Theta_c$ ) when a maximum moment value ( $M_c$ ) on the present cycle is reached (iii), which is estimated from a change in slopes from positive to negative in the experimental response. After this step the specimen enters into the post-capping stiffness region ( $\alpha_c$ ). The same approximation is conducted to calculate  $\theta_{pn}$  on the negative loading direction as also depicted in Figure 4.9 (i, ii, iii).

The updated value of  $\theta_{pn}$  is then calculated making use of the collected data (points (i, ii, iii) in Figure 4.9) applying Equation 4.4. The updated value is applied on the first step of the reversal negative loading path following the present cycle (Figure 4.9 (iv)). The rule is applied to both, positive and negative loading quadrants independently. The parameter is calculated every time updated data is available (i.e., maximum strength  $M_c$  is reached) in order to follow closely the history of degradation of the experimental response and to correct possible inaccurate initial values at early stages of deterioration.

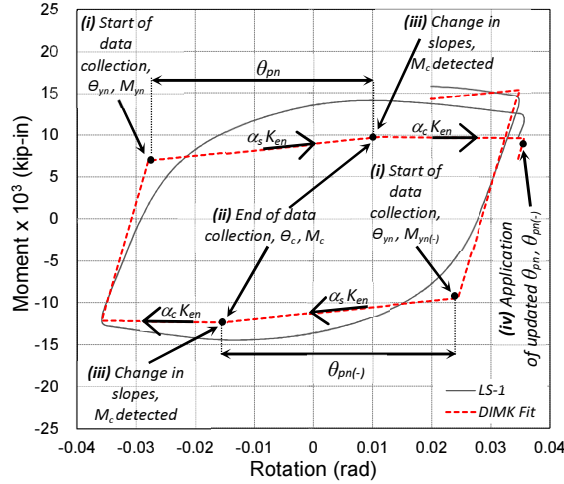


Figure 4.9. Plastic rotation capacity ( $\theta_{pn}$ ) DIMK rule.

$$\theta_{pn} = (\theta_c - \theta_{yn}) \quad (4.4)$$

#### 4.9. Modifications to strain-hardening ( $\alpha_{sn}$ ) and post-capping ( $\alpha_{cn}$ ) slopes

Updated values of the strain-hardening ratio ( $\alpha_s$ ) can be obtained from geometric relationships based on the previously acquired updated information. The available updated data is illustrated in Figure 4.10 and consists of the elastic stiffness ( $K_{en}$ , point (i) in Figure 4.10); force and deformation values associated with the yield strength (( $\theta_{yn}$ ,  $M_{yn}$ ) point (ii) in Figure 4.10); recalibrated cycle maximum plastic rotation capacity ( $\theta_{pn}$ , point (iii) in Figure 4.10(a)); capping limit strength (( $\theta_c$ ,  $M_c$ ) point (iv) in Figure 4.10(a)) or in the absence of this information, the maximum strength (( $\theta_{max}$ ,  $M_{max}$ ) point (iv) in Figure 4.10(b)) previously obtained on the cycle, where  $M_{max} < M_c$ . The latter case is used only for the strain hardening slope calculations, given that the capping strength was not reached and enough information is unavailable to recalibrate the post-capping branch.

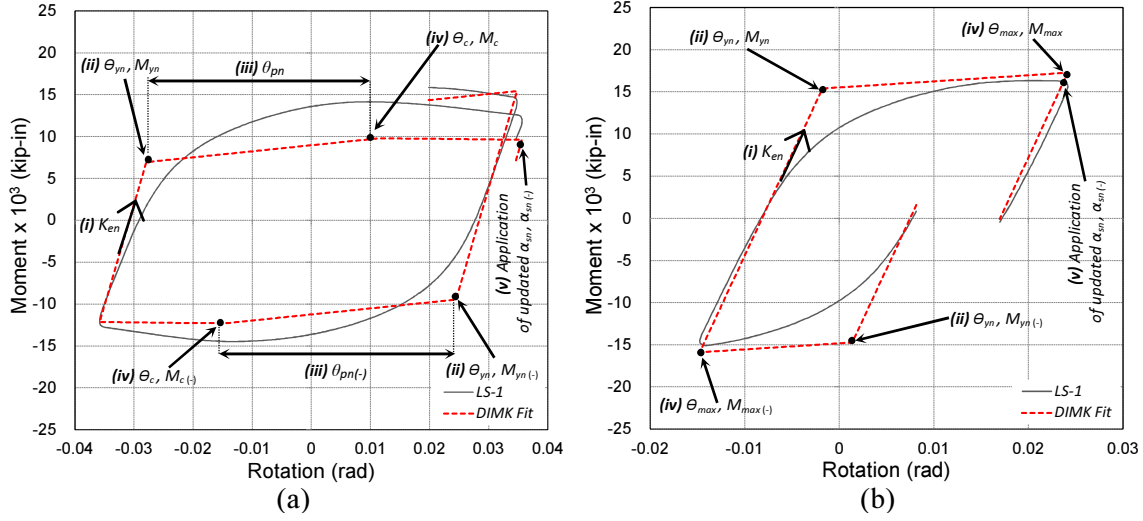


Figure 4.10. Updated available information for calculation of  $\alpha_{sn}$ : (a) capping strength ( $M_c$ ) detected, (b) loading reversal detected, no  $M_c$  found.

Making use of the described information, the strain-hardening slope is calculated according to Equations 4.5 (Figure 4.10(a)) and 4.6 (Figure 4.10(b)). Then, the calculated slope is normalized to  $K_{en}$  following the original formulation of the *IMK* model based on Equation 4.7. Calculations of strain hardening slopes ( $\alpha_s$ ) are run independently for both positive and negative loading paths. Analogously as with the previously readjusted parameters, the updated value of  $\alpha_s$  is applied on the first step after a load reversal takes place in the current cycle (point (v) in Figure 4.10), i.e., changes will apply when the response enters the next loading cycle in the direction of interest.

$$K_{sn} = \frac{(M_c - M_{yn})}{\theta_{pn}} \quad (4.5)$$

$$K_{sn} = \frac{(M_{max} - M_{yn})}{(\theta_{max} - \theta_{yn})} \quad (4.6)$$

$$\alpha_{sn} = \frac{K_{sn}}{K_{en}} \quad (4.7)$$

As stated in section 4.3, post-capping strength deterioration in the original *IMK* model is applied through a translation of the post-capping branch towards the origin while the slope of this branch is kept constant. For the case of the *DIMK* model used in this study, the post-capping branch can shift towards the origin while the value of the post-capping slope can be simultaneously recalibrated (i.e., rotated). Only in the event that  $M_c$  has been reached on the current cycle,  $\alpha_{cn}$  is calculated and updated during the first step after a deformation reversal occurs.

Similarly as defined in the original *IMK* model, the post-capping rotation capacity ( $\theta_{pcn}$ , (iii) in Figure 4.11) is calculated as the difference between the maximum cycle rotation ( $\Theta_{pc}$ , point (ii) in Figure 4.11) and the one associated with the capping strength ( $\Theta_c$ , point (i) in Figure 4.11), as described in Equation 4.7. A linear fit starting from ( $\Theta_c, M_c$ ) (point (i) in Figure 4.11) up to the end of the loading cycle ( $\Theta_{pc}, M_{pc}$ ) (point (ii) in Figure 4.11) is then applied to find the post-capping slope ( $K_{cn}$ ) as detailed in Equation 4.9. Once the post-capping stiffness slope ( $K_{cn}$ ) is derived, the original formulation of the *IMK* model is applied to normalize the post-capping slope, as stated in Equation 4.10.

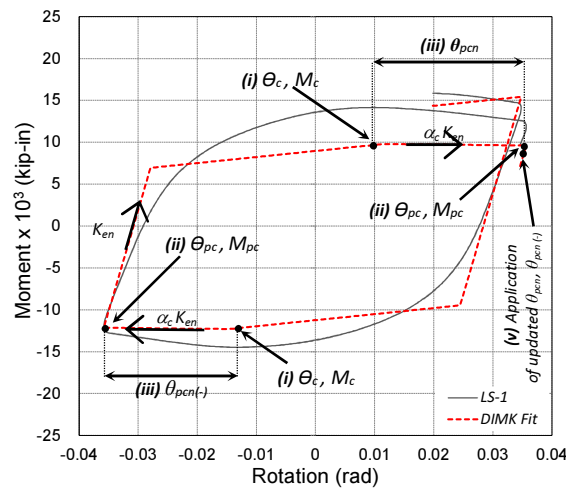


Figure 4.11. Updated available information for  $\alpha_{cn}$  calculations.



$$\theta_{pcn} = (\theta_{pc} - \theta_c) \quad (4.8)$$

$$K_{cn} = \frac{(M_{pc}) - (M_c)}{\theta_{pcn}} \quad (4.9)$$

$$\alpha_{cn} = \frac{K_{cn}}{K_{en}} \quad (4.10)$$

The recalibrated values of  $\alpha_{sn}$  and  $\alpha_{cn}$  in the positive and negative directions are updated in the model on the first step of the following loading reversal ( $\nu$ ), and they are kept constant until a new updating event is needed.

A benchmark numerical fit without the application of modifications to the strain-hardening ( $\alpha_{sn}$ ) and post-capping ( $\alpha_{cn}$ ) slopes is plotted in Figure 4.12(a) for illustration. Points (i) and (ii) show the  $\alpha_s$  and  $\alpha_c$  branches without recalibration. Meanwhile, Figure 4.12(b) presents a *DIMK* numerical fit in which the modification rules for  $\alpha_{sn}$  and  $\alpha_{cn}$  are applied. Points (i) in Figure 4.12(b) focus on the effect of implementing the recalibrated values of  $\alpha_{sn}$ . As can be observed, the numerical fit with the application of the rules (Figure 4.12(b)) follows closer the experimental hardening stiffness slope (points (i)) when the updating is applied. Strain hardening is relevant in the general response of the system since it is directly linked with the increase on resistance of the specimen through plastic deformation. Nonlinear analysis supposes that this characteristic ought to manifest during the analysis, since sections suitable for plastic design should not buckle before strain hardening occurs (Kuhlmann, 1989).

Furthermore, points (ii) on Figure 4.12(b) highlight the repercussion of the application of the updated values of  $\alpha_{cn}$ , both in positive and negative quadrants. Again the fitting is able to mimic the post-capping slopes of the experimental response on zones when the specimen exhibits

softening after having reached the maximum moment resistance ( $M_c$ ). The post-capping stiffness is as well a key parameter in the simulation of the behavior of structures up to the limit state of collapse. This is reported on a study aimed to evaluate global collapse of frame structures under seismic excitations (Ibarra, 2005), which revealed that softening of the post-capping stiffness and the displacement at where this softening commences are the two system parameters that most influence the collapse capacity of a system.

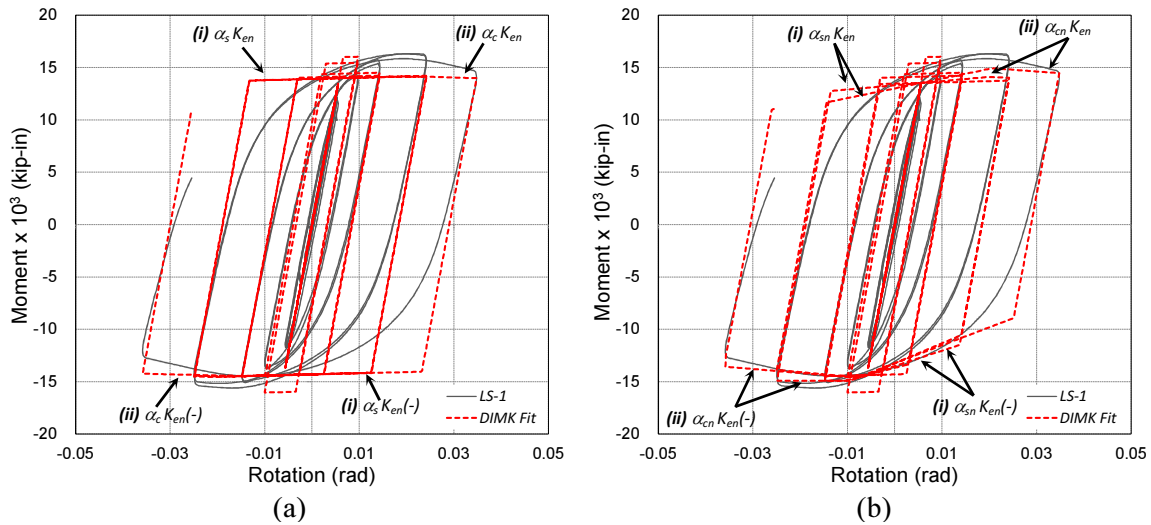


Figure 4.12. Effect of the application of strain-hardening and post-capping stiffness *DIMK* rules: (a) base case, no correction, (b) corrected.

#### 4.10. Summary and conclusions

The NUA proposed on the present research consists of two main stages. The first phase is the topic of this chapter.

Initially, from the available hysteretic models with and without degradation capabilities historically used on seismic research, the Ibarra-Medina-Krawinkler (*IMK*) model was selected.

Advantages and drawbacks of employing a piecewise linear hysteretic model were addressed, as well as the strategies employed on this research to avoid numerical instability using this type of model, such as the implementation of reasonably small analysis step increments. Additional advantages of the selected *IMK* hysteretic model were highlighted. For instance, the model is already implemented in the OpenSees platform and contains a relatively small number of parameters to control and consequently to update.

In Phase I, global hysteretic information (e.g., first-story drift ratio *vs* first-story shear force) is acquired from the virtual experimental substructure. In order to calibrate relevant hysteretic model parameters for seismic collapse assessment, the complete response history of the experiment should be available. Due to the lack of response information at the start of the test, the main contribution of this phase is the development and implementation of a set of rules to recalibrate the selected hysteretic model parameters that characterize the backbone of the *IMK* during the simulation. These algorithms are aimed to readjusting the elastic stiffness ( $K_e$ ), yield strength demand ( $M_y$ ), plastic deformation capacity ( $\theta_p$ ), strain-hardening ( $\alpha_s K_e$ ) and post-capping ( $\alpha_c K_e$ ) slopes.

Thus in Phase I, the main parameters are updated when required based on the fitted story-level experimental hysteretic response of a given cycle addressing the fact of *what to update*.

## **CHAPTER 5**

### **NUMERICAL UPDATING APPROACH: PHASE II**

#### **5.1. Introduction**

Hybrid simulation makes use of calculations and on-line controls, which together with experimental measurements of the physical substructure behavior provides a realistic simulation of the dynamic response. In conventional hybrid testing with substructuring, initial properties are assigned to the parameters of the numerical substructure components (e.g., concentrated plasticity models). Generally, these initial component properties are calibrated and assumed to have a high degree of correlation with the studied prototype structure. Nevertheless, this is not always achievable.

As stated in Mosqueda (2005), reliable results can be obtained from hybrid simulation only if the propagation of experimental errors is properly mitigated. Another source of error is found with the inaccurate assignment of initial parameters of numerical components. Thus, one research objective of the NUA presented is to reliably estimate updated information of the most important parameters that control the response of the system, especially when the structure is near collapse. The completion of the objective is intended to minimize the epistemic uncertainty on the calibration of numerical component parameters, minimizing errors in the hybrid simulation.

A flowchart of the proposed numerical updating procedure is illustrated on Figure 5.1. , where the numerical approach is highlighted in gray. This approach is based on utilizing the measured response of the experimental portion (Phase I), to update during the analysis the component parameters (Phase II) of the numerical subdomain of the structural system. In Phase I

(see Chapter 4) a set of fitted global parameters defined the hysteretic response of the virtual experimental substructure. Next, the distribution of global (story-level) damage into the local components of the numerical portion of the structure is needed. Thus, the goal of Phase II is to answer the question: *how to update* the local parameters that contribute to the global damage history of the system?

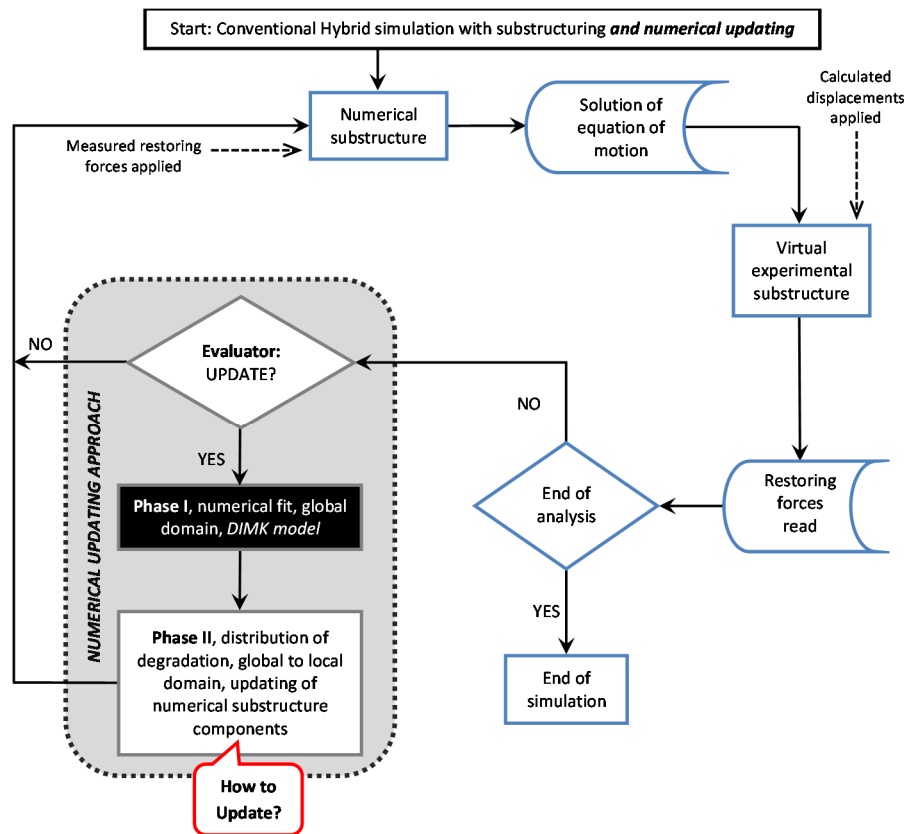


Figure 5.1. Flowchart of proposed numerical updating approach.

## 5.2. Identification of main parameters to update

The purpose of Phase II is to complete a numerical updating event initiated on a selected vibration cycle (Phase I). The obtained recalibrated local parameters are applied on the following cycle in the same direction, finalizing the current updating event. Phase II estimates the most important model parameters of the local components of the numerical portion based on the

acquired global structural response of the experimental substructure. Combinations of different model parameter values are evaluated to build the most adequate array of factors for the current updating event. An updating event is defined as a numerical recalibration process of the local components of the numerical substructure, initiated by a detected change (evaluator module, Figure 5.1) on the elastic stiffness between the current cycle with respect to its value in the previous cycle (e.g.,  $\Delta K_e \geq 10\%$ , where  $\Delta K_e$  is the difference in elastic stiffness). Then, this assemblage of parameter values is applied to the numerical part of the structure and utilized during the solution of the equation of motion of the system until a new updating event is required.

In order to conduct the mapping between global (story-level) responses and the responses of local components (plastic hinges), and hence, obtain adequate local parameters for updating, a numerical model of the full four-story scaled steel structure is utilized (i.e., 4PO-model). The 4PO-model consists of a 1:8 scale, four-story/two-bay steel moment resisting frame linked to a leaning column with gravity loads, modeled with elastic beam-column elements connected by plastic hinges, as described in section 2.3. Given that a concentrated plasticity approach is used, rotational springs are used to represent the nonlinear behavior of the structure. Therefore, rotational springs become the target numerical components to update.

Figure 5.2 shows the numbering of elastic elements and plastic hinges of the 4PO-model, containing the four stories of the SMRF and leaning column. The full frame (Figure 5.2) contains 18 plastic hinges on columns from levels 2 to 5 (1-18), 16 springs on beams also from levels 2 to 5 (19-34) and 6 on the first level columns (35-40). The numbering follows the same pattern as in the selected hybrid simulation substructures (Figure 5.3), thus hinges that need to be updated are consistently mapped on all models. It should be noted that this model is in addition to the virtual experimental and numerical substructures used during the hybrid simulation, and it is built with

their same original geometry and properties.

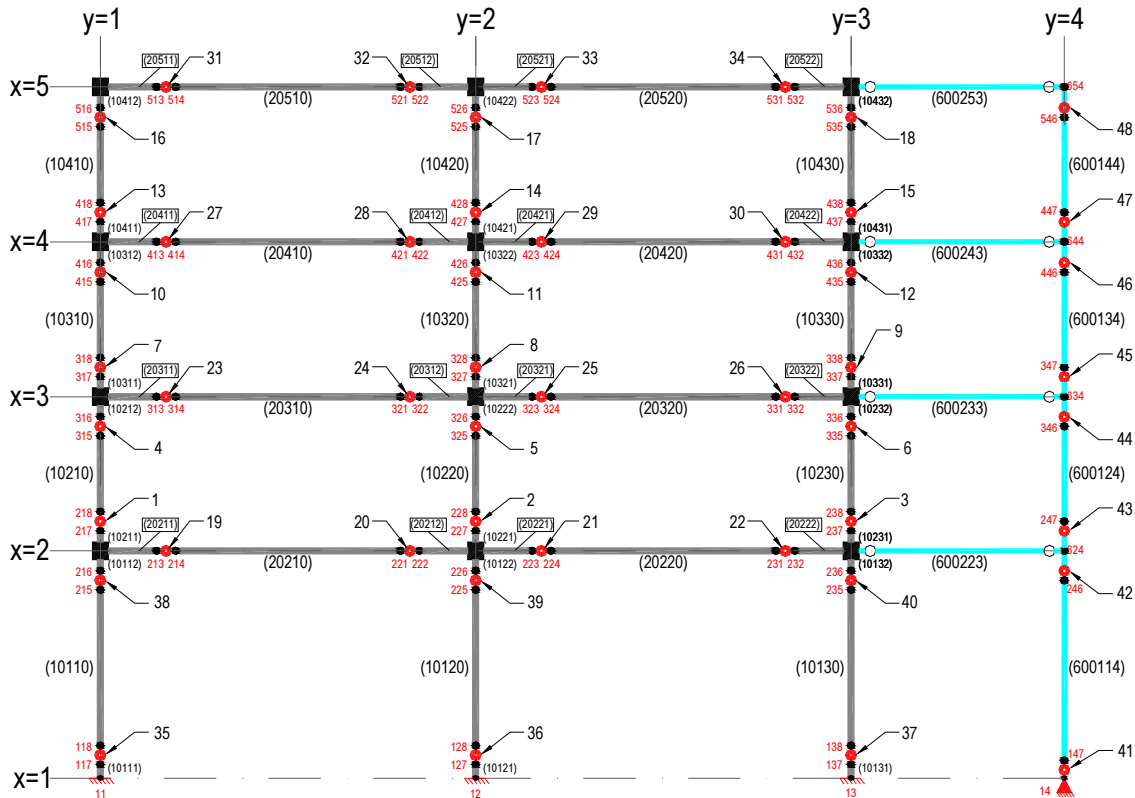


Figure 5.2. Four-story structure model (4PO) to perform pushover analyses.

Pushover analyses consider inelasticity of material and geometric nonlinearities. Hence, usage of 4PO-model pushover analyses provides useful information for the implementation of the proposed procedure:

- Capacity curve of the structure.
- Strength deterioration effects on critical elements for the general stability of the structure.
- Identification of crucial regions expected to develop considerable inelastic deformations.

Consequently, recalling the original *IMK* hysteretic model discussed in section 4.3 (Figure 5.3(a)), three main zones are defined: the elastic stiffness (*i*), strain-hardening stiffness (*ii*), and the post-capping stiffness (*iii*) (i.e., softening branch of the system subsequent to the maximum

resistance  $M_c$ ) regions. Updating of the backbone curve can be likewise divided into the same three regions, considering individually the numerical parameters that control each sector. Additionally, pushover capacity curves calculated from the 4PO-model can also be regionalized into three similar sectors as presented in Figure 5.3(b).

As a result, it is possible to relate the results from pushover analyses with the numerically fitted backbone curve of the global experimental substructure response (Phase I) for a given cycle. The relationship can be seen in Figure 5.3(b), where a capacity curve obtained from the 4PO-model and its associated idealized backbone curve are plotted. This implies that capacity curves can be used to evaluate parameter values that provide a target hysteretic response for a given cycle of vibration.

Pushover curves using the *IMK* model will be able to represent the expected monotonic strength and stiffness deterioration effects, which are inactive on the numerical subdomain due to the implementation of high values on the hysteretic energy dissipation capacity factors ( $\gamma_{s,c,k,a}$ ), as explained in subsection 4.4.1.

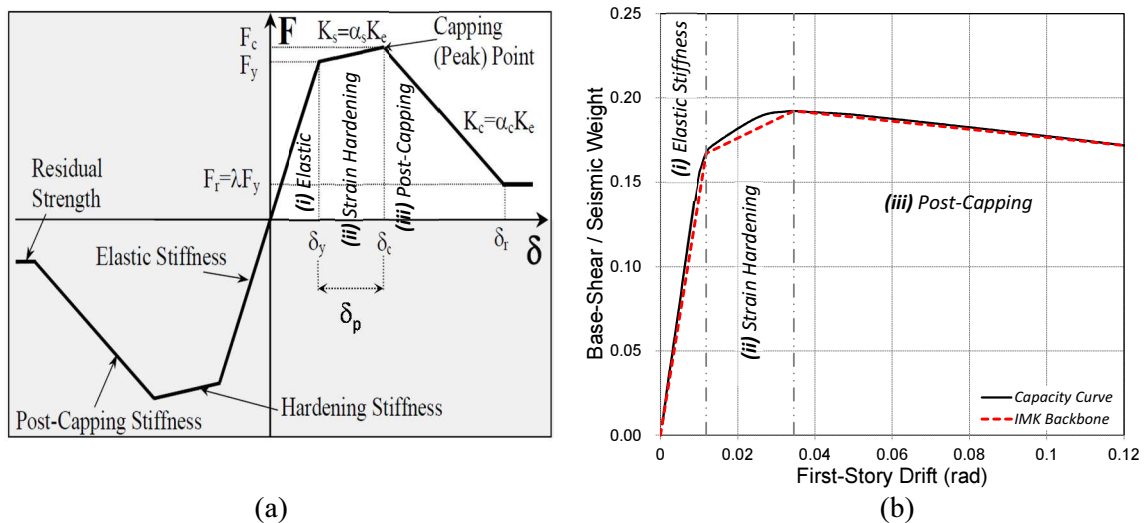


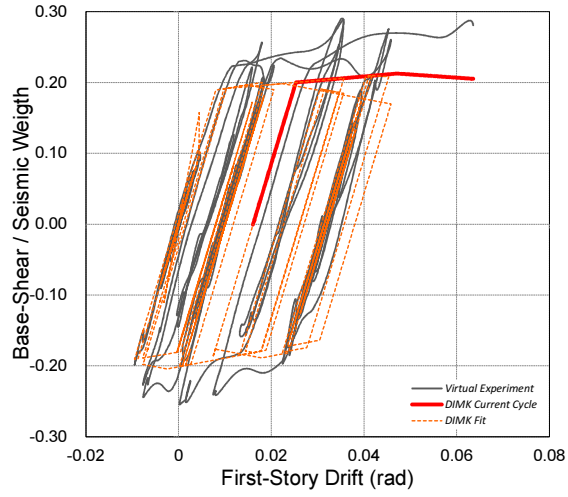
Figure 5.3. Capacity curve-IMK model backbone analogy, (a) IMK model, (b) capacity curve vs. IMK model backbone.



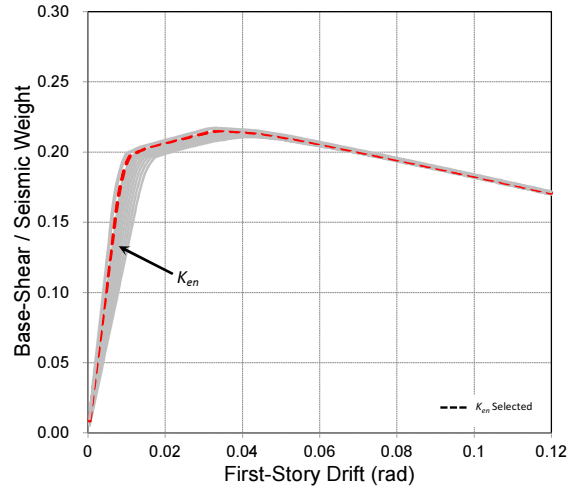
### 5.3. Distribution of damage identified in global domain to local domain

As stated in the preceding sections the adopted approximation to obtain the local component parameters consists of selecting the most adequate array of numerical values through the calculation of capacity curves. The 4PO-model is used specifically for this purpose. Therefore, the parameters of the rotational springs on the 4PO-model are varied one at a time to estimate the most adequate set of values for every updating event. It should be noted that the identification order of the set of parameters follows the *IMK* backbone; it is  $K_{en}$ ;  $F_{yn}$ ;  $\alpha_{sn}$ ;  $\delta_{pn}$  and  $\alpha_{cn}$  (Figure 5.3(a)).

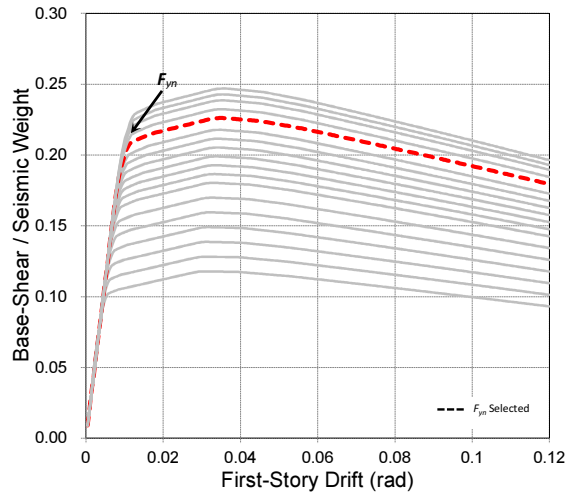
The general procedure to obtain the array of parameters is illustrated using a portion of a hysteretic response that is obtained from a hybrid simulation with substructuring. This hybrid simulation is conducted with the four-story SMRF studied on this research (Figure 5.4(a)). A continuous gray line plotted in Figure 5.4(a) shows the first-story / base shear hysteretic response history from the beginning of the test up to the selected simulation stage. The *DIMK* fitting is superimposed on the same Figure 5.4(a) with a dashed orange line. Likewise, in continuous bold red line, a backbone identified at the current simulation stage (cycle) is highlighted (Figure 5.4(a)). For explanation purposes, it is assumed that the current analysis stage requires an updating event.



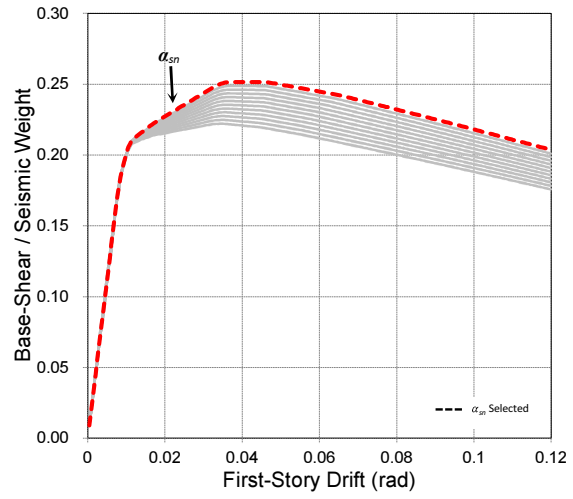
(a)



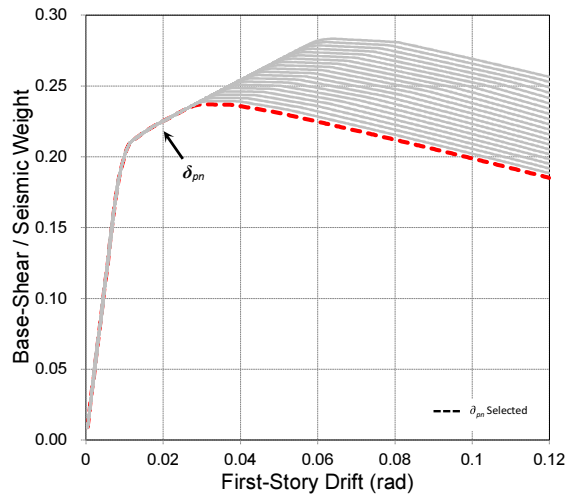
(b)



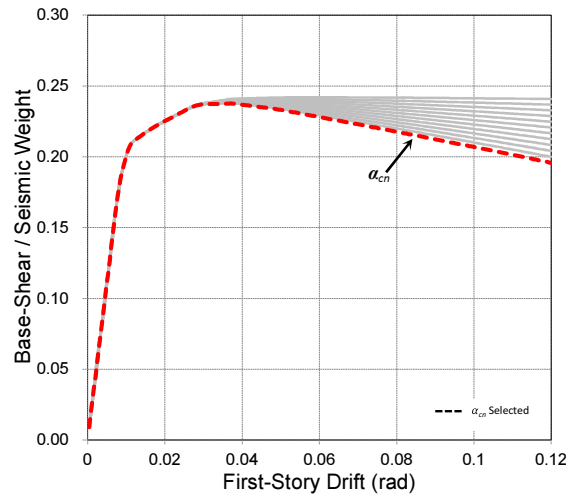
(c)



(d)



(e)



(f)

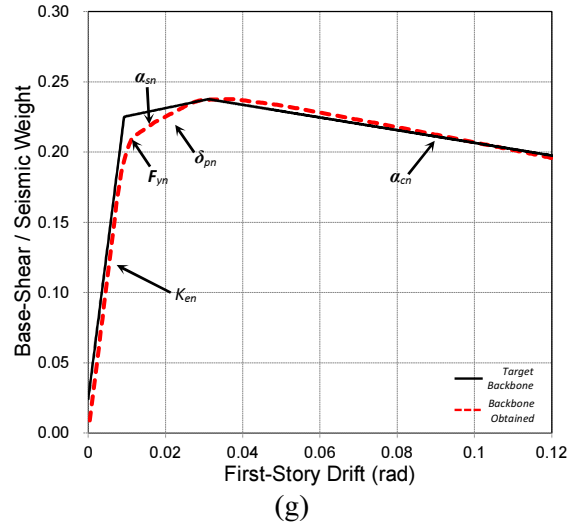


Figure 5.4. Example of parameter selection, (a) *DIMK* selected backbone fit, (b)  $K_{en}$ , (c)  $F_{yin}$ , (d)  $\alpha_{sn}$ , (e)  $\delta_{pn}$ , (f)  $\alpha_{cn}$  selection, and (g) final calibrated backbone-capacity curve.

Capacity curves are then calculated utilizing a triangular loading pattern, based on varying parameter values within a predefined range of values for each variable. The first iteration starts with the smallest value for a given parameter. A search is conducted until the parameter value that produces a capacity curve with a minimum deviation from the target one is found.

For instance, in the case of the elastic slope, a deviation from the sought factor is estimated as the ratio of the identified value from the experimental subdomain (Phase I) to the elastic slope of a capacity curve. This deviation ratio is firstly calculated for the first capacity curve related to the smallest factor in the range of search. The ratio is subsequently calculated for the following capacity curves generated up to the one that reports the optimum, i.e., evaluation ratio.

This approach leads to families of curves such as the ones illustrated in (Figure 5.4(b) to (f)). When the currently calculated capacity curve reaches a minimum deviation for a specific parameter as described (i.e., local minimum), its value is considered to be the most adequate and the search of values and consequently, the generation of more capacity curves, is discontinued. The set of parameters is obtained following the *IMK* backbone construction.

Capacity curves to obtain  $K_{en}$  are calculated first. In this case,  $K_{en}$  is the only parameter fitted during the calculation of the capacity curves while the rest of the parameters are kept constant. From the calculated capacity curves, the one that offers the minimum deviation to  $K_{en}$  utilizing the described evaluation ratios with respect to the one identified on the first-story fitted backbone is selected (see the dashed red bold line in Figure 5.4(b)). Next, keeping the calculated value of  $K_{en}$  and the rest of the parameters constant, a new group of capacity curves are calculated varying only  $F_{yn}$  (Figure 5.4(c)). Later, keeping calculated values of  $K_{en}$  and  $F_{yn}$  and the other backbone parameters constant, a parcel of curves changing only  $\alpha_{sn}$  is constructed (Figure 5.4(d)). The same procedure is used to select the appropriate capacity curve and identify the rotation capacity (Figure 5.4(e)) and post-capping slope factors (Figure 5.4(f)) i.e., keeping the previously calculated and remaining factors constant while the parameter of interest is varied. The backbone-capacity curve calibrated through the application of the previously selected array of parameters into the rotational springs of the numerical 4PO-model is obtained and plotted on Figure 5.4(g).

### **5.3.1. Distribution of damage in the numerical substructure**

Table 5.1 presents the *IMK* parameters subject to recalibration and their associated ranges of values utilized on the updating approach as a result of previous sensitivity studies performed in this research. An important consideration when using information derived from pushover analyses to update hybrid tests is related to the elastic slope values obtained from the same specimen, utilizing different approximations. In other words, static and hybrid tests will not reproduce the same result due to the distinct type of loading input. It should be clarified that a triangular loading pattern is applied to the pushover analyses utilized to identify the variation of elastic slopes, and all along the implementation of the updating approach.

Table 5.1. IMK parameters to update and ranges of search.

<i>IMK PARAMETER</i>	$[0.50-1.50] K_{en}$	$[0.50-1.50] F_{yn-gral}$	$[0.50-1.50] F_{yn-part}$	$[0.50-3.00] \alpha_{sn}$	$[0.50-3.00] \delta_{pn}$	$[0.50-5.00] \alpha_{cn}$
----------------------	----------------------	---------------------------	---------------------------	---------------------------	---------------------------	---------------------------

In order to find a correlation between the two approximations and also limits for the range of calculation of capacity curves during the parameter identification, preliminary analyses were conducted. These analyses consisted first on estimating the evolution of elastic slope ( $K_{en}$ ) values observed on a hysteretic history response of a fully numerical hybrid simulation of the studied four-story SMRF structure. The benchmark case without initial errors was employed to perform the simulation and conduct these observations. It should be noted that this approach considers story stiffness values. Initial parameter values can be calibrated based on component tests or research conducted on similar components as previously discussed on section 4.4.

The structure experiences deterioration during the simulation, leading to softening of the elastic initial slope as the system degrades. Hence for the benchmark case, considering the evolution of elastic stiffness values observed for the first story response (i.e., experimental part) during a hybrid simulation under the chain of scaled ground motions (see section 2.2), slope values of 23.6 kips-in for the median, 20.0 kips-in minimum, and 26.6 kips-in maximum were obtained. This includes all the elastic slope values associated with every loading cycle of the hybrid simulation. This denotes that for this structure and loading input, the system experiences ranges of variation of  $85\% \leq K_{en} \leq 113\%$  along the full simulation within the base case. In order to cover the most likely range of values, the intervals shown on Table 5.1 were used. Regarding  $F_{yn}$ , it was estimated that even though the residual strength factors for every individual rotational spring in the numerical part are set to zero, a combined strength ratio (i.e., springs plus elastic elements in

the experimental portion) of 50% of the global initial value is a conservative lower limit. This boundary is based on observations of outputs of multiple simulations carried out during the implementation of the approach. Ranges for  $\alpha_{sn}$ ,  $\delta_{pn}$ ,  $\alpha_{cn}$  were similarly established based on the same observations. In the case of  $\delta_{pn}$ , smaller values than those presented in Table 5.1 are not likely to be developed by the SMRF, given that ductile behavior is expected in the work hardening zone for this type of system. Additionally, values of  $\delta_{pn}$  close to zero may lead to numerical instability of the simulation. Work hardening and post-capping slopes,  $\alpha_{sn}$  and  $\alpha_{cn}$ , were expected to develop during the simulation. Ratios of 50% of the initial parameter value demonstrated to cover the lower limits of updated values observed during the implementation of the procedure. Besides, it should be recalled that highly nonlinear responses are dominated by parameters on the strain-hardening and post-capping regions. The maximum parameter-range values presented are based on identification of the highest demands observed from multiple simulations performed during the implementation of the procedure.

Even though the maximum limit value in a given parameter range might at first glance seem high (e.g., 5 times the initial estimated value for  $\alpha_{cn}$ ), it is justified by the fact that parameters related to the strain-hardening and post-capping regions, are only updated on rotational springs that have experienced at least one inelastic incursion. The inelastic response is developed exclusively on the rotational springs, due to the concentrated plasticity method approach utilized on this research. Hence, since beam and column members remain elastic and are coupled with the rotational hinges, high values on the latter may be required to reproduce the inelastic response of the system on early stages of nonlinearity when only few zero-length elements are considered. It also should be noted that the search ranges presented are not necessarily covered on every updated event; the search for parameter finalizes when the most adequate parameter is found regardless of

the number of capacity curves generated.

In Chapter 4, Phase I was introduced utilizing an experimental component response (SDOF system). In that condition the updated information was obtained directly from the component response and a numerical fit was applied to obtain the parameters characterizing the hysteretic model utilized, without the need of any transformation or further data manipulation. Nevertheless in the proposed NUA, several additional considerations and intermediate actions are involved to obtain and then communicate recalibrated information. This is due to the fact that the global information characterized from the experimental response (i.e., first-story drift) must be distributed to local numerical components of the analytical part of the hybrid simulation.

As shown in Figure 5.2, the full four-story frame (4PO-model) contains 40 rotational springs, meanwhile the numerical hybrid part has 34 plastic hinges (Figure 5.5), sharing the same numbering pattern to facilitate mapping. Thus, nine *IMK* model parameters can be recalculated for every plastic hinge ( $K_{en}$ , as well as positive and negative  $M_{yn}$ ,  $\theta_{pn}$ ,  $\alpha_{sn}$  and  $\alpha_{cn}$ ), leading to a total amount of 360 individual factors participating on the recalibration of the full structure (4PO-model). On the other hand, when it comes to the hybrid numerical subdomain, the same nine parameters can be recalibrated on the 34 rotational springs in the model (306 factors). Information on the temporal evolution of parameter values during the simulation is stored for both hybrid numerical and 4PO-models. Two master lists allocating the information for the corresponding 360 and 306 parameters are created at the beginning of the simulation. Both lists are used on the 4PO-model and hybrid numerical portion respectively and are initially populated with unitary values.

During the test, yielding of plastic hinges in both numerical and experimental substructures is constantly verified in order to cumulatively list the springs that have experienced at least one inelastic excursion. Once a given spring exceeds an initially assumed yielding strength value

(theoretical value based on available data), it is listed as “yielded” and preserved on a file for subsequent updates.

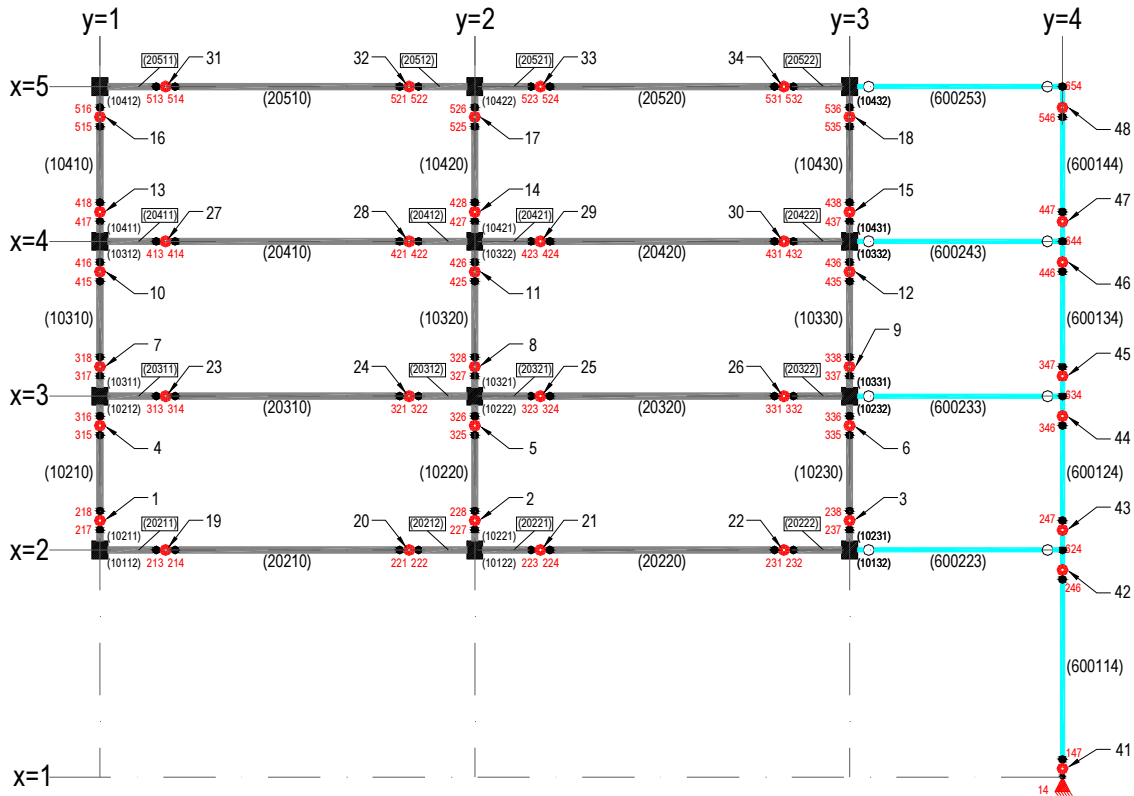


Figure 5.5. Numerical sub-domain model.

In order to use pushover information in hybrid tests carried out on MDOF systems, a transformation is needed. As explained static and hybrid tests would not report the same results. The approach taken in this study is to establish a correlation between both models. The departure point is to consider as pivot the median value of the elastic stiffnesses (23.6 kips-in). This value was estimated from the identified stiffness values for every loading cycle along a fully numerical hybrid simulation of the benchmark case. Since the nonlinear response is dominated by the rotational springs, they are not considered in this calibration procedure directed to match the elastic region of both models, to preserve their nonlinear characteristics along the simulation. Thus, the



correlation is achieved through calibration of the flexural stiffness ( $EI$ ) of only beams and columns (elastic members) of the 4PO-model, to reproduce the calculated dynamic elastic stiffness values of the hybrid test. A set of stiffness values calculated on the 4PO-model, resulting from applying different factors ( $fact_{els}$ ) to the flexural stiffness of the elastic elements ( $E_{al\_ORIG}$ ) was obtained. This modified EI values ( $E_{al\_MOD}$ ) are responsible to produce variations on the elastic stiffness of the 4PO-model. Then, these modified stiffnesses of the 4PO-model (static) are normalized to the pivot median value (23.6 kips-in) to obtain the expected counterpart elastic stiffnesses on the hybrid test (dynamic).

The outcome of this calibration procedure is a second order polynomial equation that relates both hybrid and static approximations. Figure 5.6. shows the correlation between stiffness values. Target hybrid simulation stiffness (dynamic) values are represented on the horizontal axis, whereas the vertical axis shows its correlation to static analysis affected by the  $fact_{els}$  coefficients. Also the fitted equation implemented and the coefficient of determination (i.e.,  $R^2$ ), are shown. For instance a value of 80% of the original elastic stiffness value, estimated from the hybrid simulation (dynamic), correlates with a value of  $fact_{els}=0.86$  that must be applied to the flexural stiffness ( $E_{al\_MOD}$ ) in the pushover analyses in order to match the dynamic and static elastic stiffnesses.

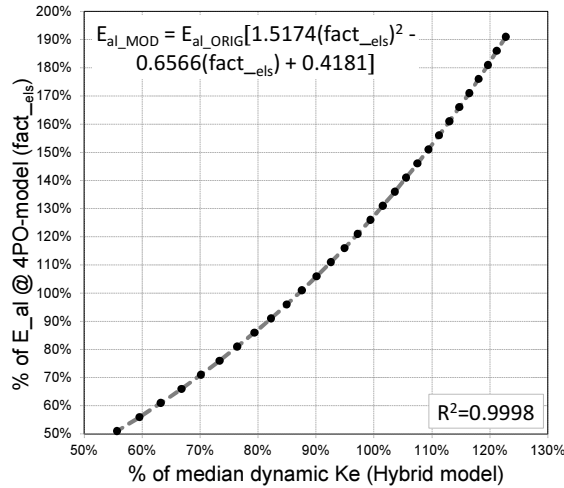


Figure 5.6. Correlation between dynamic (hybrid) and static (4PO-model pushover) stiffnesses.

Considering the initial data allocation (master lists) and transformation of elastic stiffness considerations ( $K_e$  static to  $K_e$  dynamic) when an updating event is targeted, Phase I identifies the main parameters on the experimental substructure needed to update the numerical substructure. Next, the process to find the adequate parameters on the local domain to replicate the experimental response via development of families of capacity curves is triggered. As stated before, the sequence to build the array of recalibrated parameters follows the *IMK* backbone. First,  $K_e$  and  $F_{yn-general}$  (strength value applied equally in all numerical components) are updated in all plastic hinges (40 in 4PO-model and 34 in numerical substructure). Second, making use of the information on hinges that have yielded, a new family of curves is built to fine-tune the correlation of  $F_{yn}$  between experimental and numerical portions. This time  $F_{yn}$  is varied only on the yielded hinges on the calculation of the capacity curves. The value obtained is written in both main lists at locations assigned to the appropriate hinges that have yielded, leading to a general value of  $F_{yn}$  for all hinges ( $F_{yn-general}$ ) and a fine-tuned value ( $F_{yn-particular}$ ) for the yielded springs on the same lists. Third, capacity curves are created varying  $\alpha_{sn}$  on those hinges that have yielded, placing the obtained values on their corresponding positions in the master lists. The same procedure is carried out to

obtain and allocate the values of  $\delta_{pn}$  and  $\alpha_{cn}$  of the yielded rotational springs in the master lists. The master lists are preserved and updated based on the recalibration events during the simulation. Thus, the lists evolve with the history of deterioration of the specimen and are modified every time an updating event takes place. Moreover, the same procedure is applied for both positive and negative quadrants.

The optimized local parameters useful to represent the global degradation condition of the experimental subportion are then fed into the numerical substructure using the *setParameter* command in the OpenSees platform (McKenna, et al., 2000).

## **5.4. Implementation of numerical updating to collapse using shake table ground motions**

A case study is presented herein to illustrate the application of the proposed NUA. In this example, it is assumed that *no* errors in the estimation of initial numerical modeling parameters are present. Therefore, the verification is aimed at demonstrating that the proposed approach is capable of reproducing the base case response during the analysis, while keeping the cyclic deterioration parameters ( $\gamma_{s,c,k,a}$ ) inactive.

The selected substructured model (1.5 stories as virtual experimental substructure) is subjected to the aforementioned chain of earthquakes during a fully numerical hybrid simulation. The accuracy of the proposed approach is evaluated with respect to the hybrid simulation numerical benchmark case that is able to replicate the response history from the shaking table test (section 2.5). It is assumed that the benchmark case contains the *IMK* model hinge parameters with a high degree of fidelity.

First-story drift ratio response histories are plotted in Figure 5.7. A back-to-back

comparison of three fully numerical hybrid simulation scenarios is shown: 1) simulation with correct estimation of parameters and degradation parameters active (benchmark case) in red line; 2) simulation with no calibration errors and deterioration parameters inactive in light gray and; 3) response obtained through the implementation of the proposed NUA shown in black line.

As can be observed from Figure 5.7, when parameters are kept inactive, the structure experiences premature collapse compared to the base case. Also during the *MCE* ground motion the structure starts deviating in drift, up to a difference of 13% on residuals on the free vibration stage previous to the *CLE* record. This is due to the absence of the participation of  $(\gamma_{s,c,k,a})$  parameters, leading to a “strong” system and no cyclic deterioration. On the other hand, the simulation with numerical updating applied is able to follow closely the base case first-story drift response. During the free vibration stage following to the *CLE* ground motion, a difference in residual drift of 2% with respect to the base case can be observed.

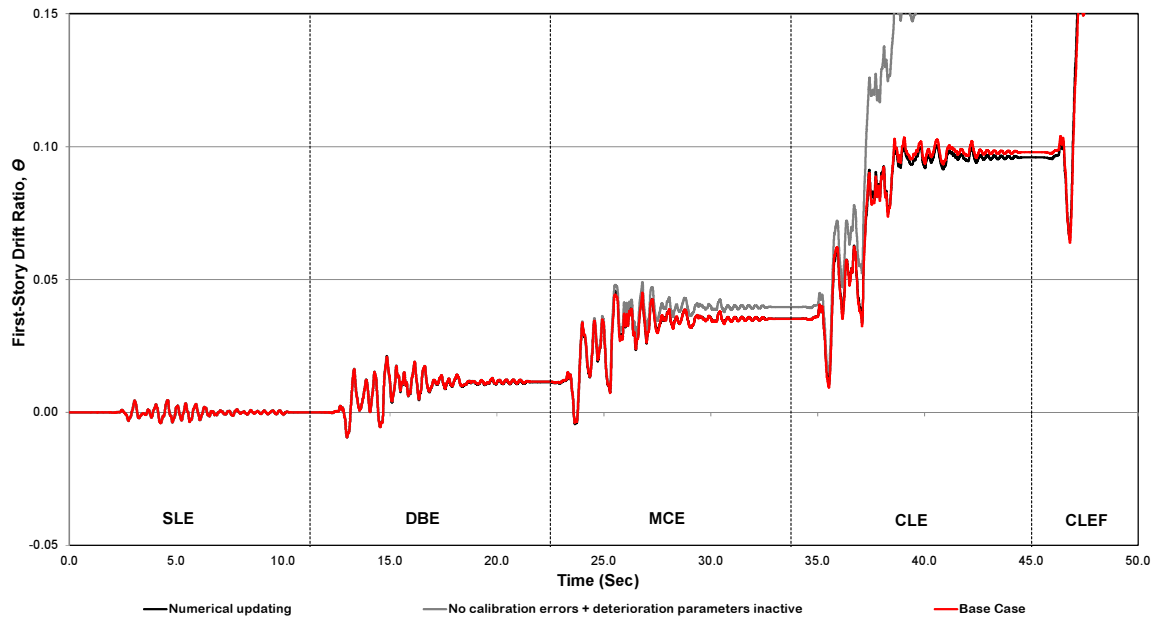
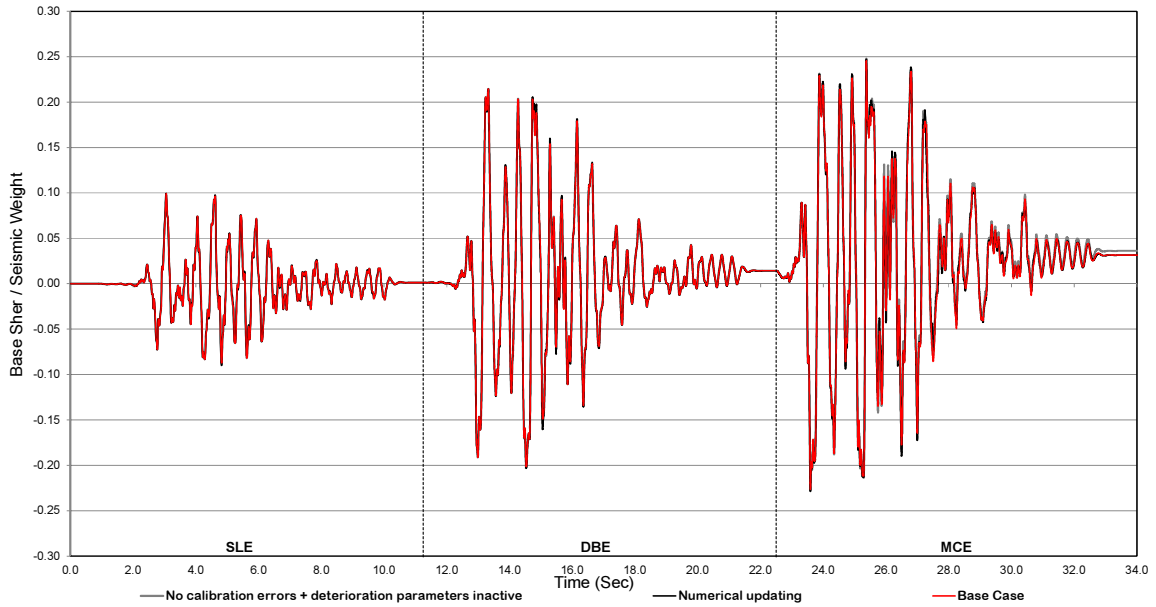


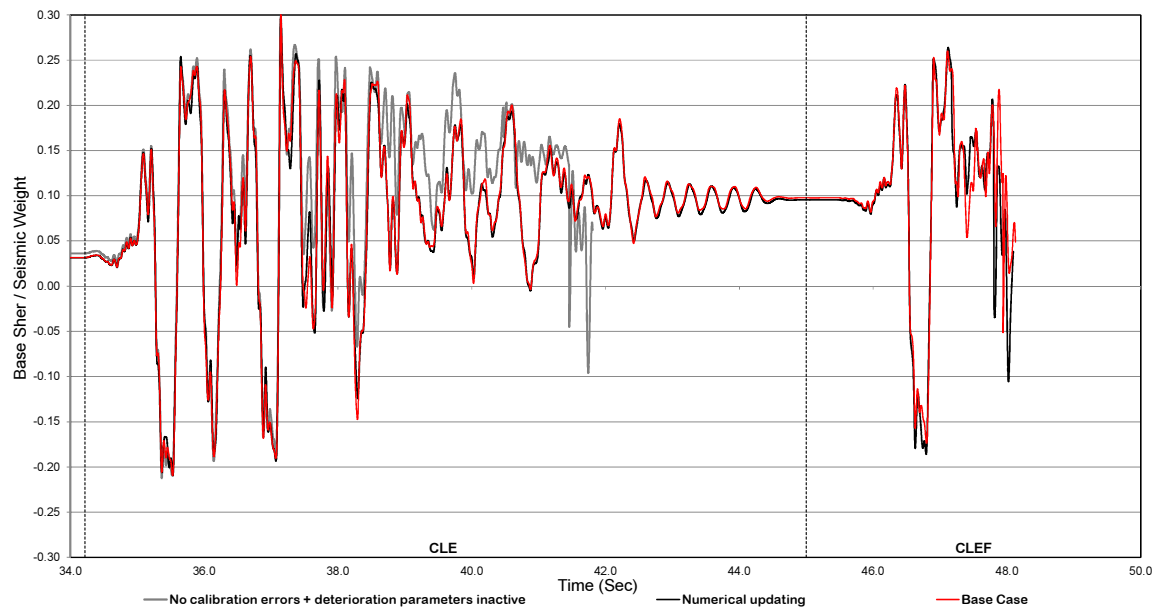
Figure 5.7. First-story drift of a four-story structure hybrid simulation through collapse.

Information on base shear normalized by the seismic weight can also be obtained from the

simulation. Figure 5.8 presents results from the same three described scenarios to show the history of base shear during the simulation time. It is observed that at early stages of nonlinearity (up to *MCE*) the three models depict a close behavior in force, given that low inelastic levels are achieved. During *CLE* ground motion, large differences in force begin to develop in the model with inactive parameters with respect to the base case, leading to collapse around 42 seconds of simulation time. Conversely, the model with updating shows forces that are close to the base case all along the simulation, capturing the collapse time reasonably well. These simulations demonstrated that the updating approach is capable of reproducing the degradation effect of the cyclic deterioration parameters that are calibrated once the full history is available. In this sense, the proposed approach as a first step, avoids the need for cyclic deterioration parameters during the proposed updating approach.



(a)

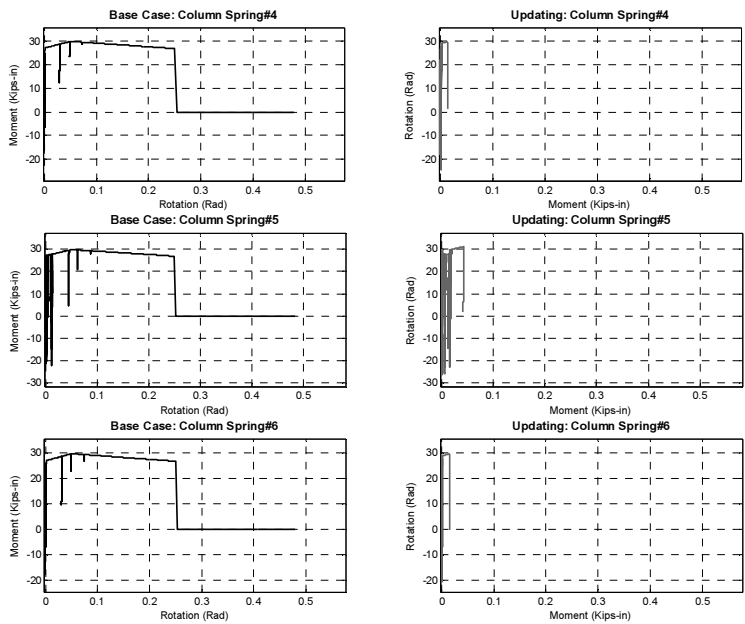
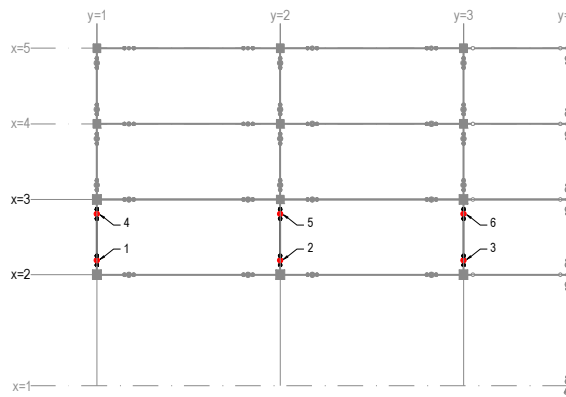
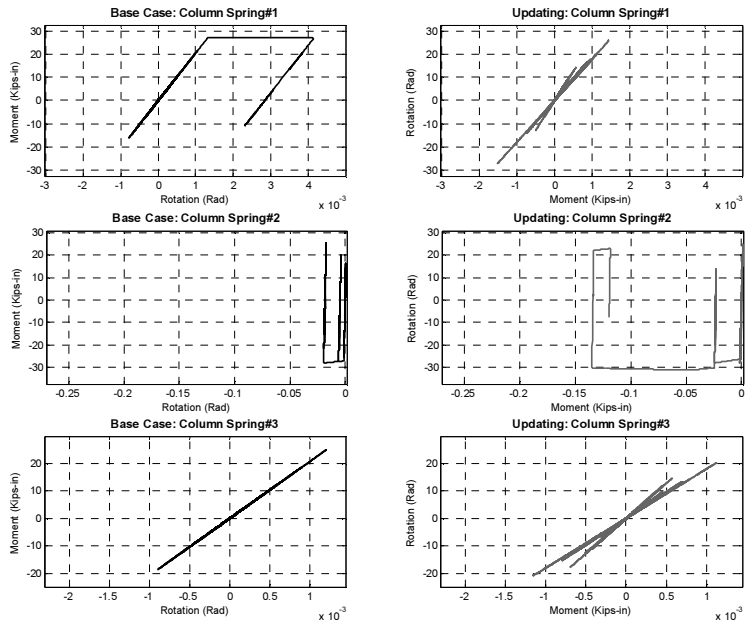


(b)

Figure 5.8. Base shear/seismic weight of a four-story structure hybrid simulation through collapse, (a) *SLE*, *DBE* and *MCE*, (b) *CLE* and *CLEF* limit states.

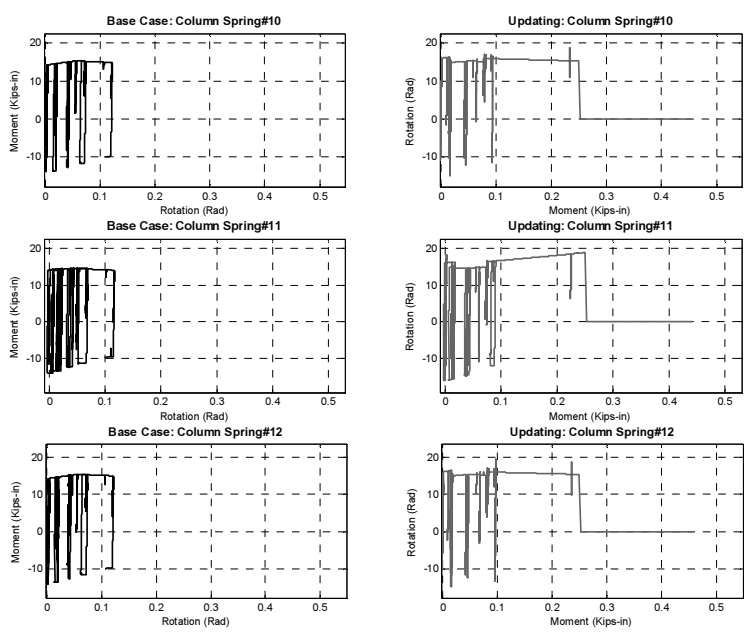
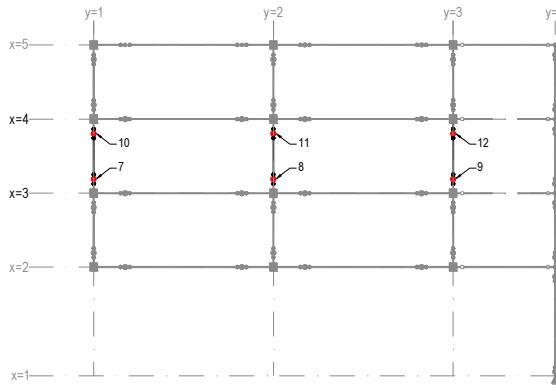
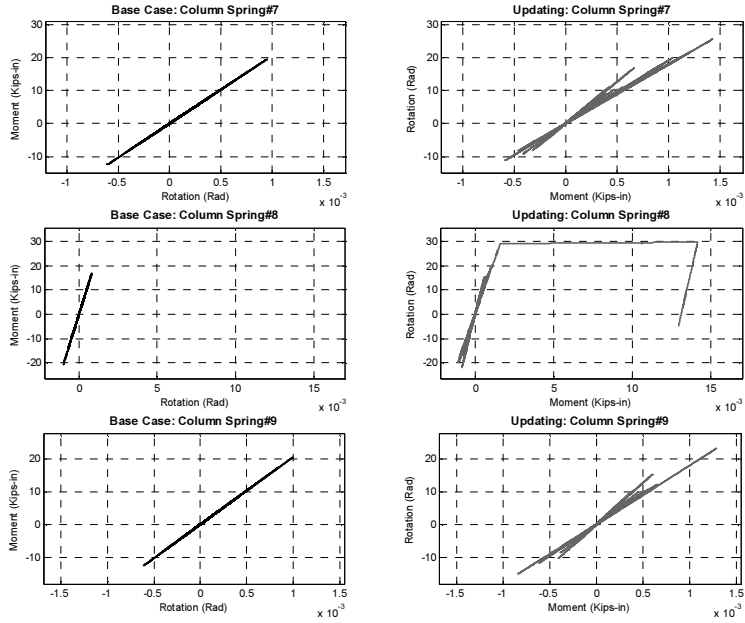
Differences found on the hysteretic behavior of the plastic hinges of the model are additional outcomes from the simulation, showing the recalibration done by the NUA. Nevertheless, it is important to clarify that the procedure builds a set of recalibrated local components to update the numerical part based on the experimental response. The hysteretic

behavior of the individual components can develop several combinations, distinct from the benchmark case to the updated simulation, to reproduce the global behavior of the system. This is demonstrated in Figure 5.9, where the 34 hinges involved on the numerical subdomain for the benchmark case and for the updated analysis on the left and right hand side, are respectively plotted. Observing springs 3, 7, 9, 13, 14, 15 (columns), 33 and 34 (beams) it can be seen how the elastic stiffness is updated from the initial value during the simulation. In this batch of springs the response is always in the elastic range, but it is updated to build a solution to the inactive degradation parameters ( $\gamma_{s,c,k,a}$ ). Another set of springs, 1, 2, 8, 10, 11, 12, 16 (columns) and 23 (beam) highlights the fact that some of the hinges experience higher demands, reaching higher levels of inelasticity than in the base case. The opposite case is seen on springs 4, 5, 6 and 18 (columns) where hinges that reached higher levels of inelasticity on the base case, experience lesser demands on the updated case. Finally, the rest of the hinges (17, 19-22 and 24-32) present smaller differences between both cases. These remaining springs are located on elements that develop high levels of inelasticity in both cases, controlling an important part of the overall inelastic response of the system.

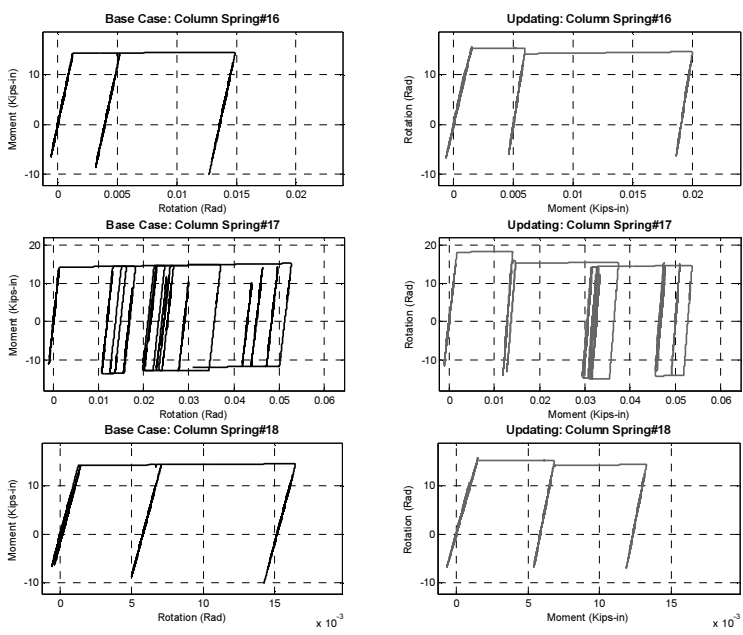
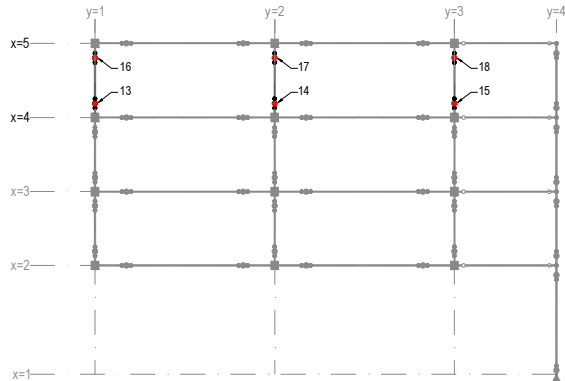
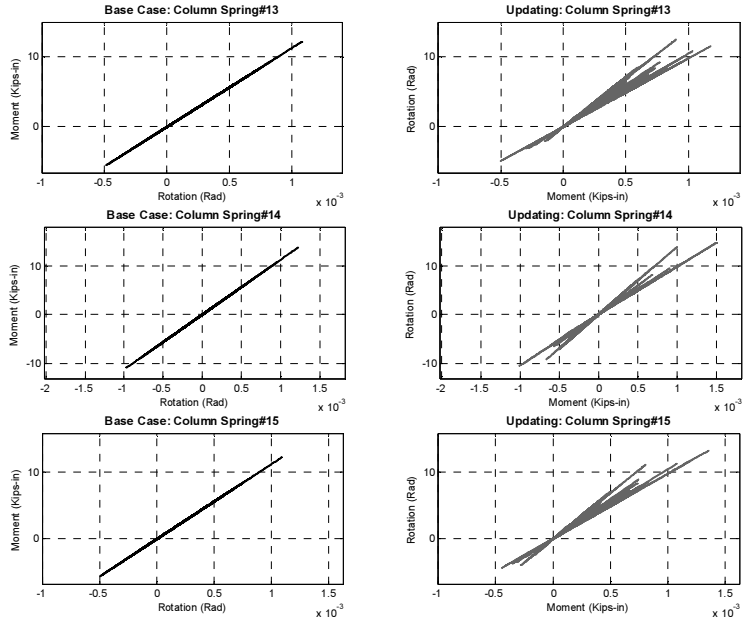


(a)

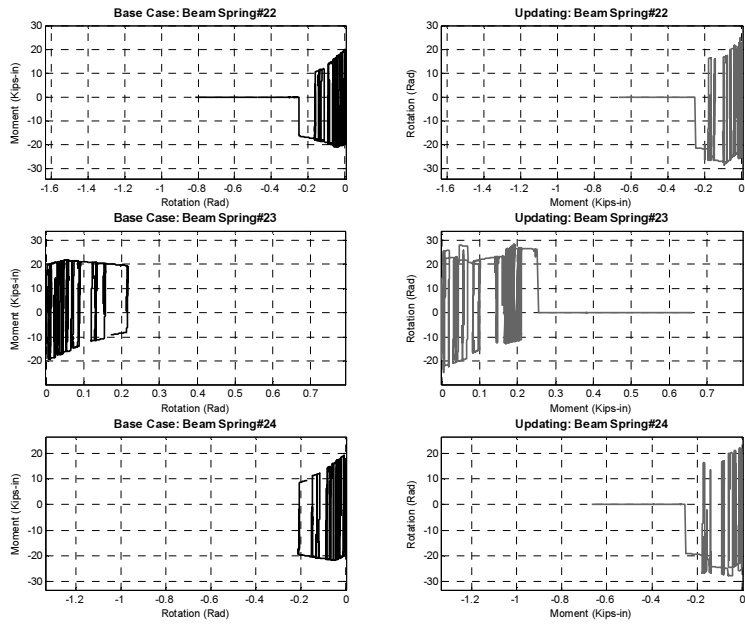
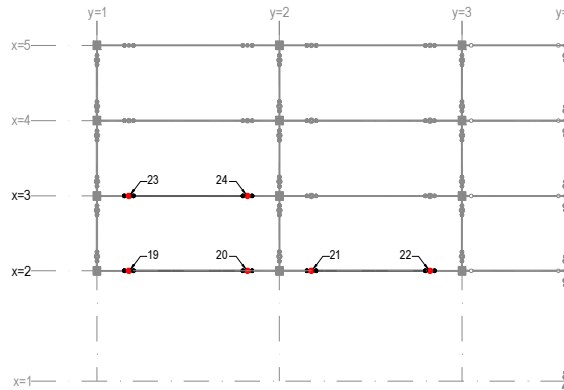
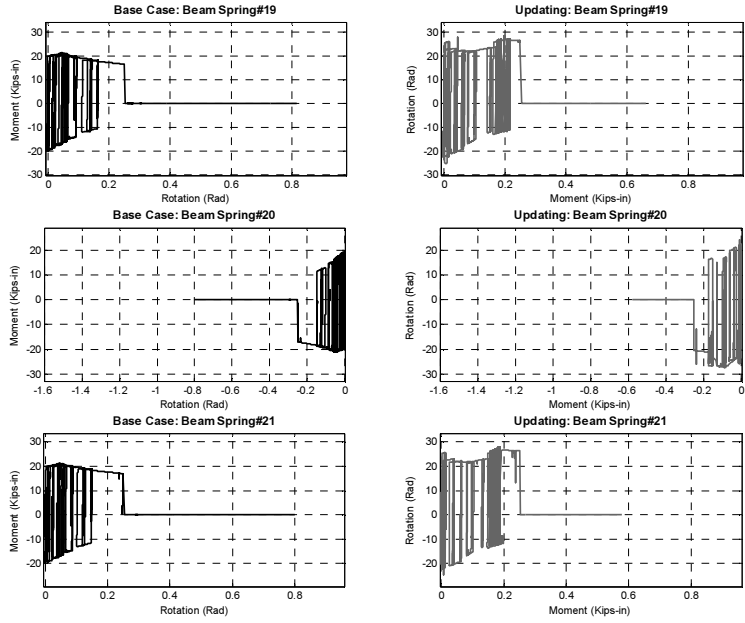




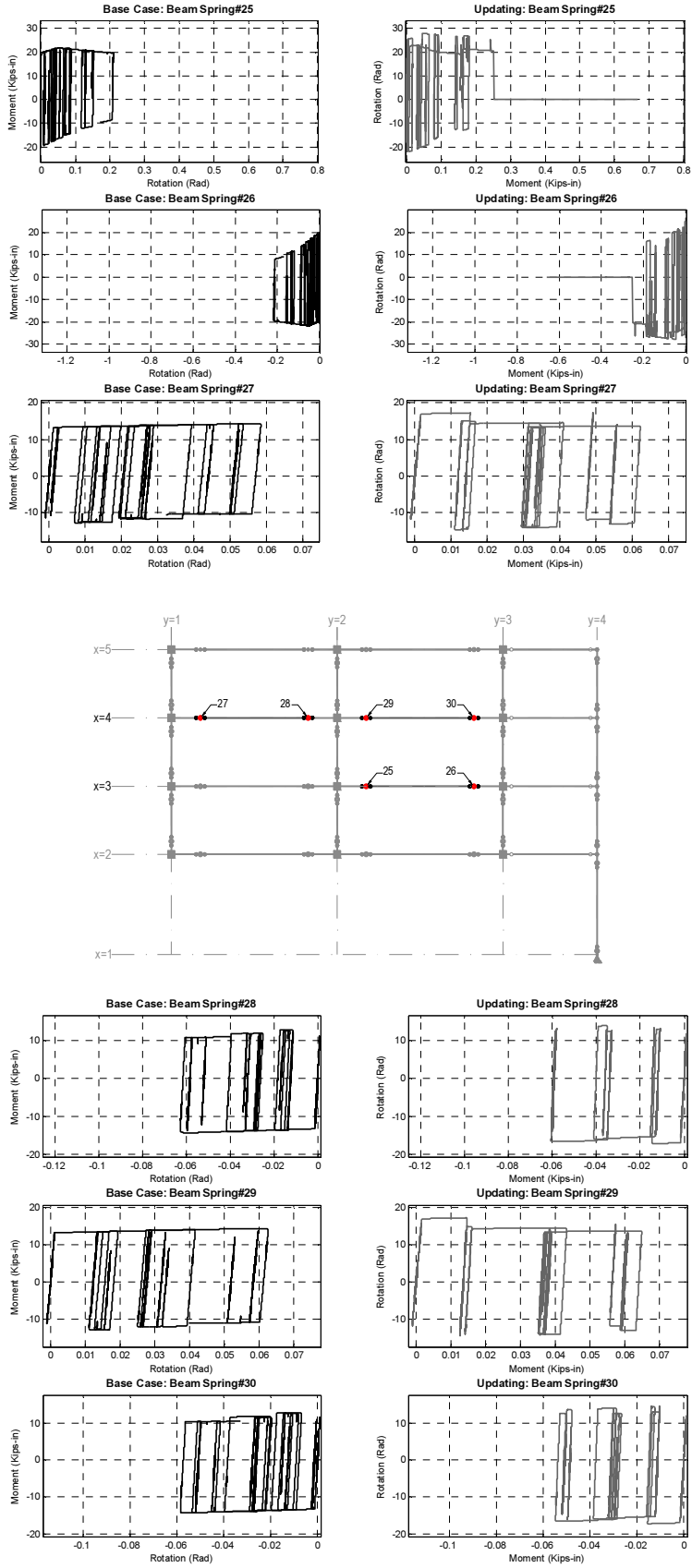
(b)



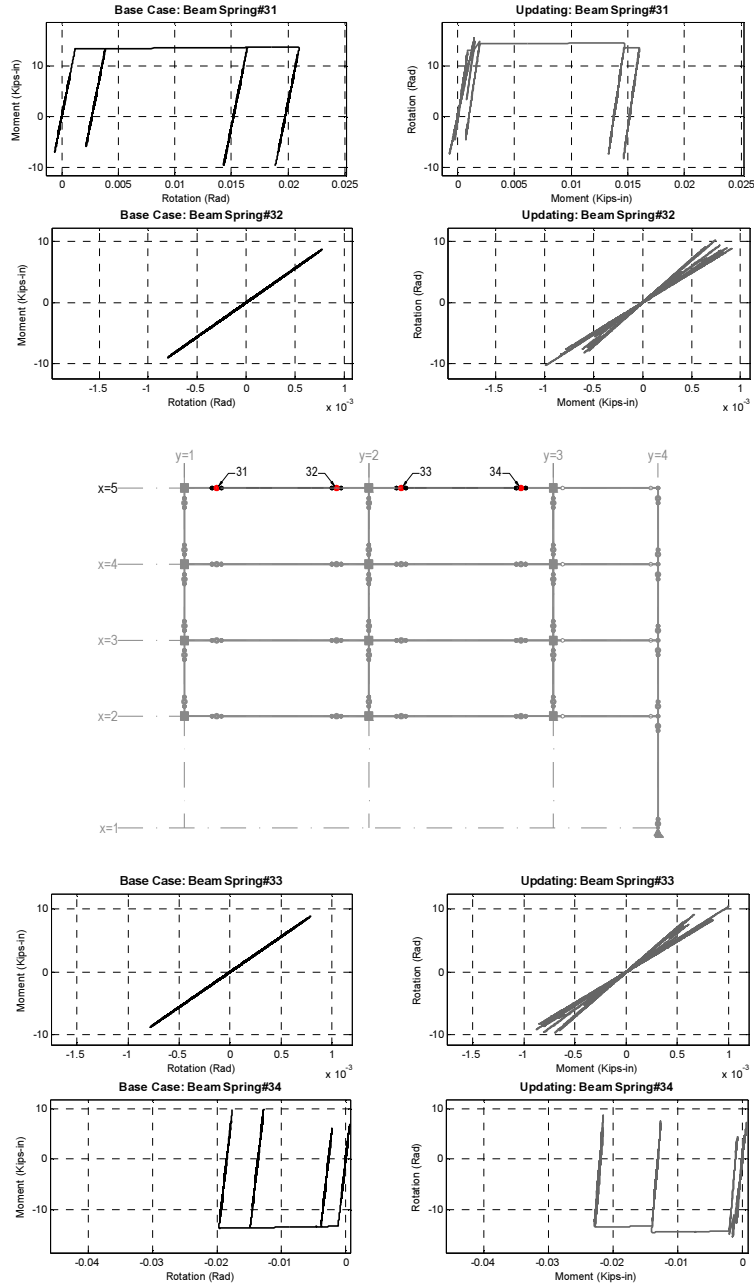
(c)



(d)



(e)



(f)

Figure 5.9. Moment-Rotation time history of springs contained on the numerical subdomain of a four-story structure, (a) springs 1-6, (b) springs 7-12, (c) springs 13-18, (d) springs 19-24, (e) springs 25-30 and, (f) springs 31-34.

Another case study previously reported by Negrete, et. al. (2014) in which it is assumed that errors in the estimation of initial numerical modeling parameters are present, is displayed next. Calibration errors are implemented in the numerical substructure for a HS through collapse for the

four-story SMRF previously described. The error ratios (i.e., estimated of erroneous model parameters normalized by actual or correct values) were obtained using a random number generator. The following deviations in initial parameter values for all the plastic hinges on the numerical model are considered for the case study:

- Elastic stiffness  $K_e$ : + 36.0%.
- Yield moment  $M_y$ : + 28.0%.
- Rotation capacity previous to capping limit  $\theta_p$ : - 13.0%.
- Softening post-capping slope  $\alpha_c$ : + 30.0%.

The accuracy of the proposed approach is again evaluated with respect to the numerical benchmark case. First-story drift ratio response histories of the fully numerical hybrid simulation are shown in Figure 5.10 for three cases: 1) simulation with correct estimation of parameters (benchmark case) is shown in red; 2) simulation with calibration errors and no updating is shown in gray line and; 3) the response obtained through the implementation of the proposed NUA is shown in black line.

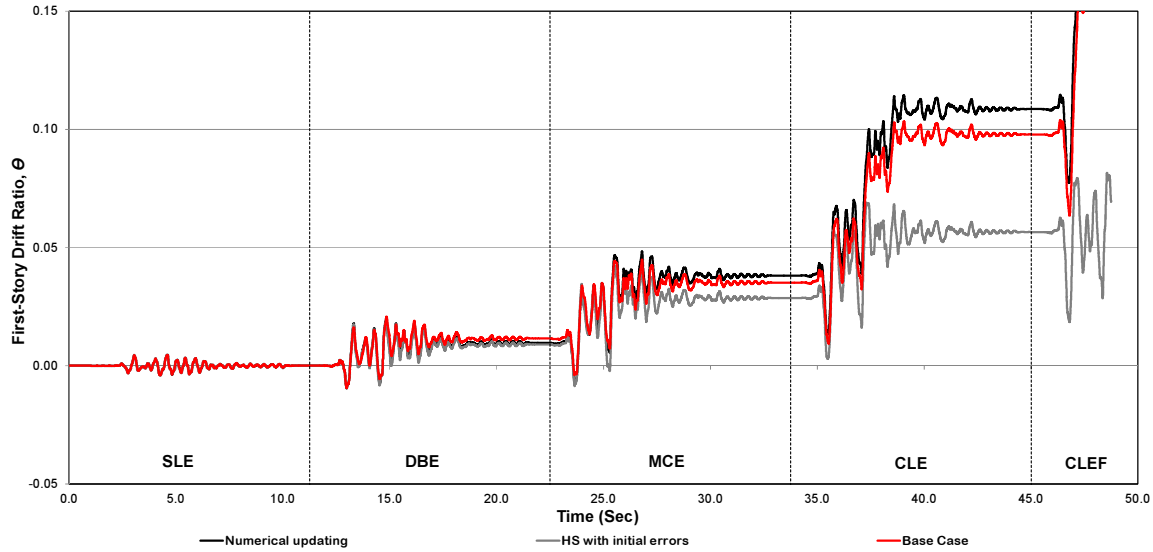


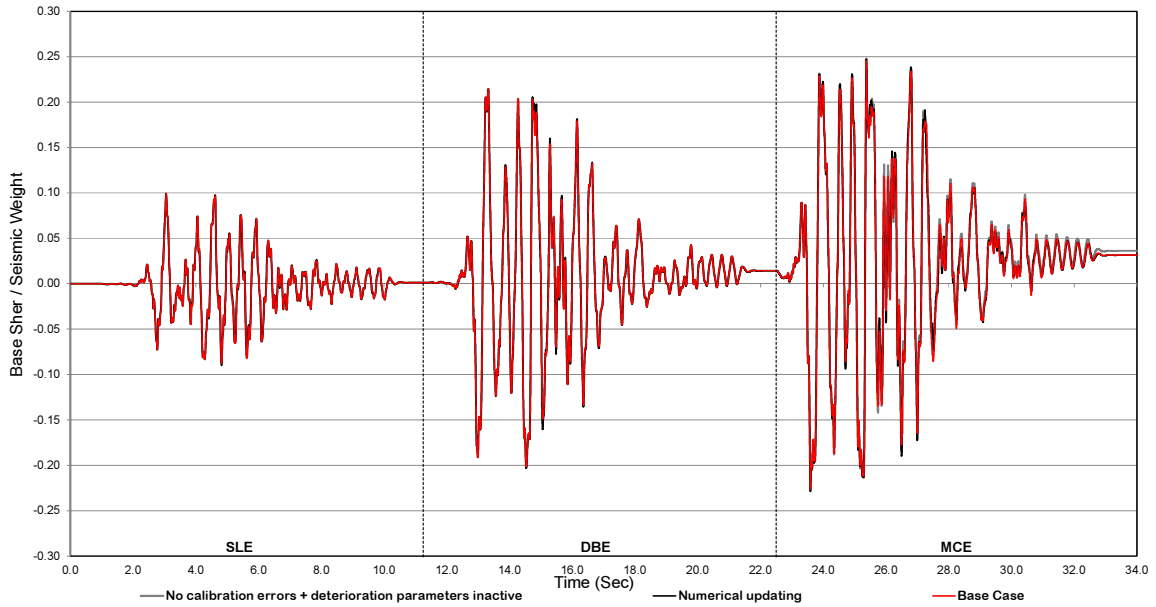
Figure 5.10. Base shear/seismic weight, four-story structure hybrid simulation through collapse study case 2.

When calibration errors are present, it is not possible to capture collapse because the structural model reaches the end of the simulation without experiencing numerical instability. The implication is that if the test were run in a physical laboratory with calibration errors present in the numerical substructure, the hybrid simulation would not be able to capture the actual response of the structure to collapse. In addition, differences in temporal residual drifts between the benchmark case and the test with initial calibration errors reflect the error propagation on the global response of the system. For instance, during the free vibration response after *CLE* its relative error is close to 42% with respect to the base case.

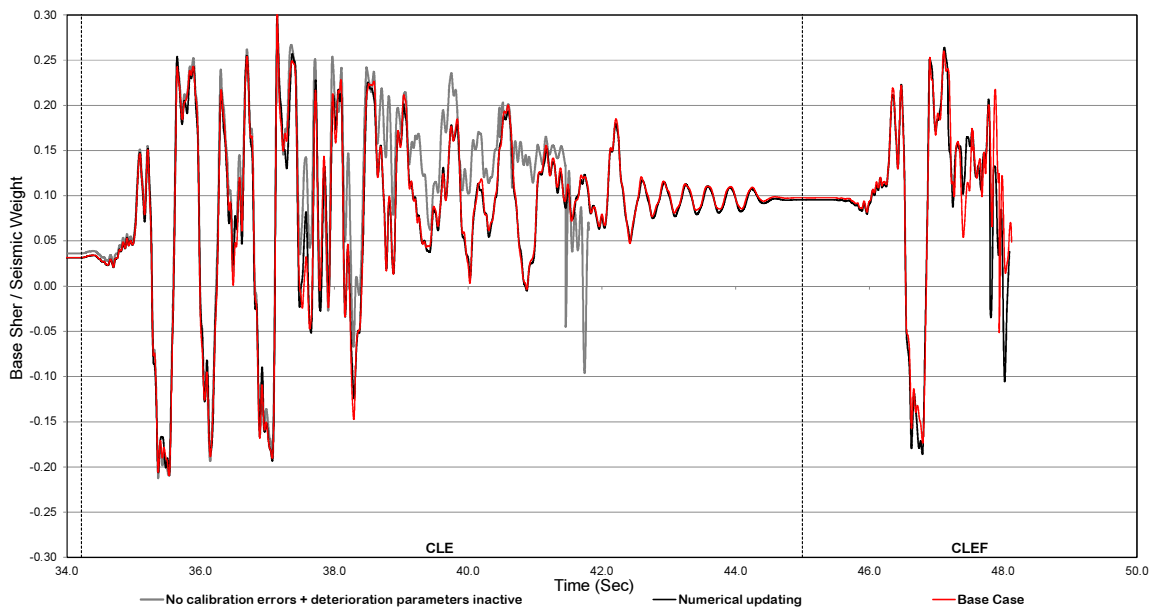
Nevertheless, when numerical updating is implemented, lower discrepancies in residual drift ratios are obtained. For example, during the free vibration response after *CLE* the relative error diminishes to 11%. The time at which numerical instability occurs in the response and the general behavior close to collapse can be more reliably captured. Thus, the proposed approach demonstrates to be capable of reducing errors in the overall response history, especially when the structure transitions to the inelastic range and up to the limit state of collapse.

An evaluation of the base shear response history for all three cases is presented in Figure 5.11. Similar to the case of first-story drift ratio, an error reduction in the estimation of the temporary residual can also be observed on the free vibration response after *CLE*. Without updating, a relative error of 43% is present, whereas the application of the proposed NUA reduces the relative error to 12%. It can also be observed that near the end of the history, the structural model with calibration errors exhibits relatively large values of base shear, which is consistent with a numerically stable dynamic response.





(a)

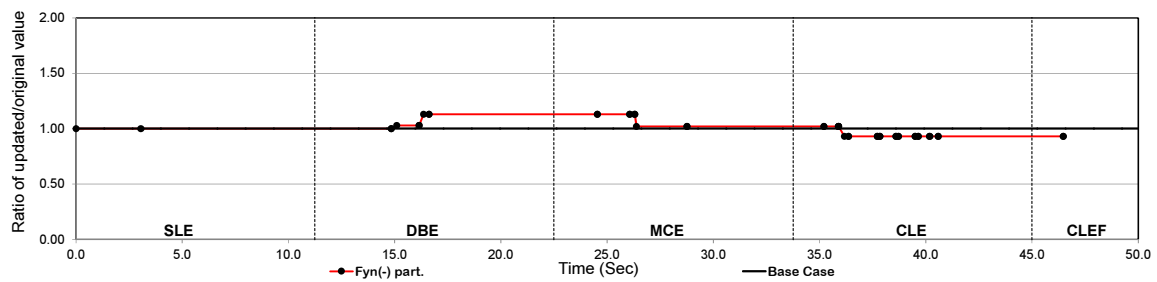
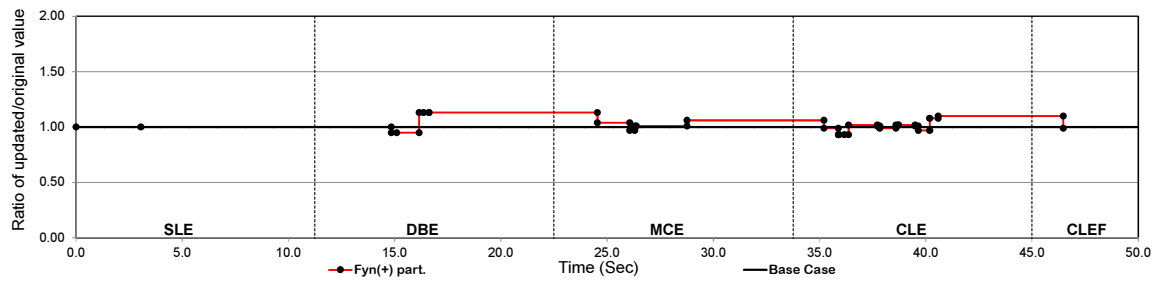
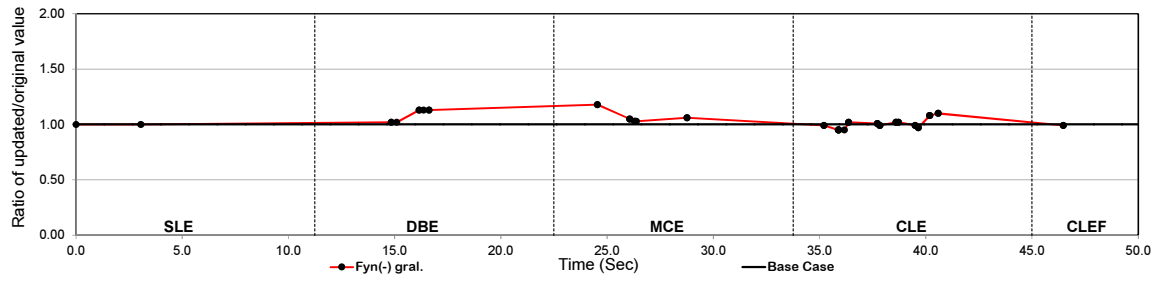
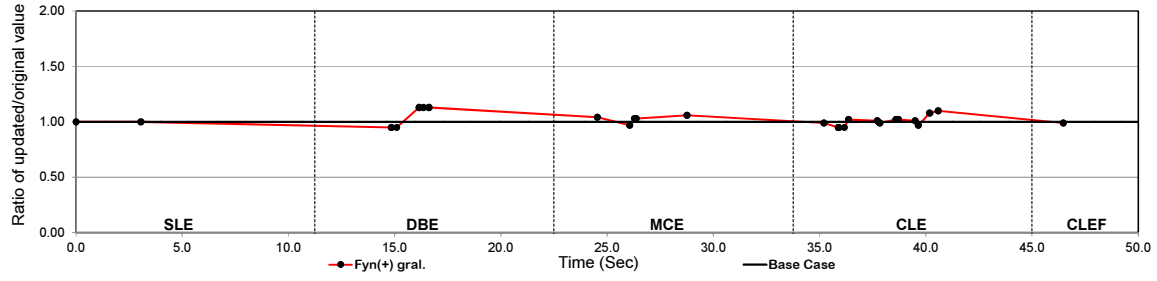
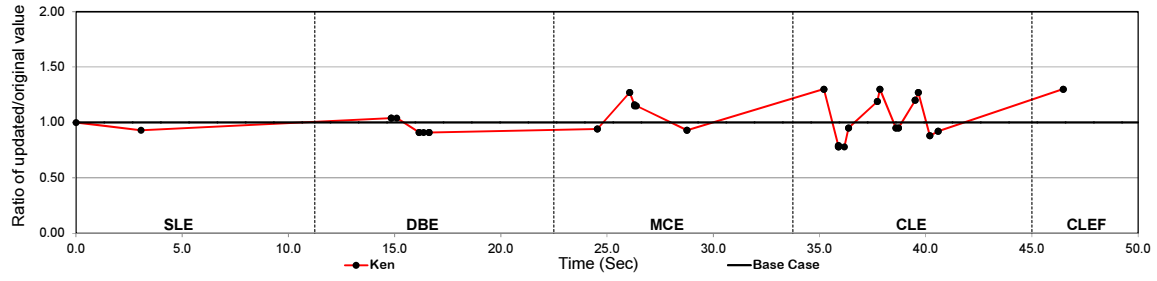


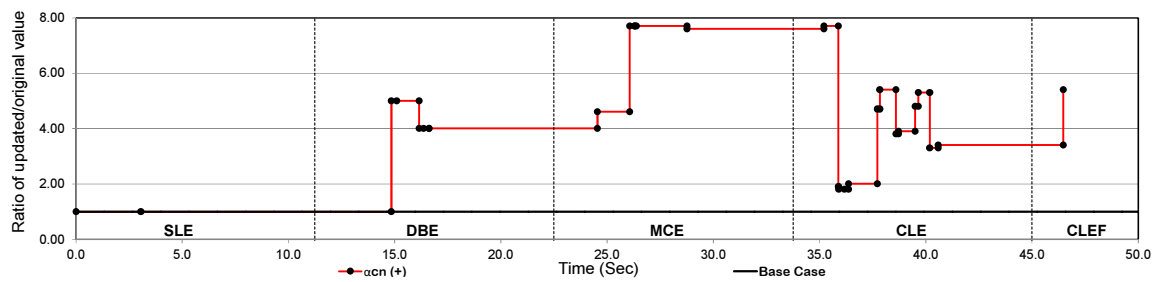
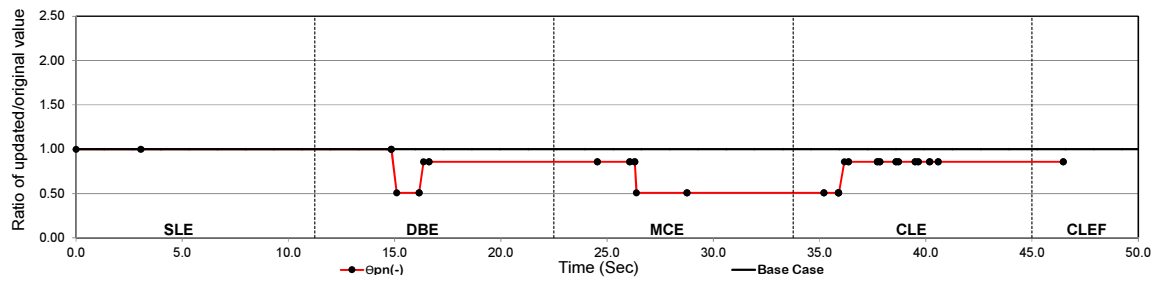
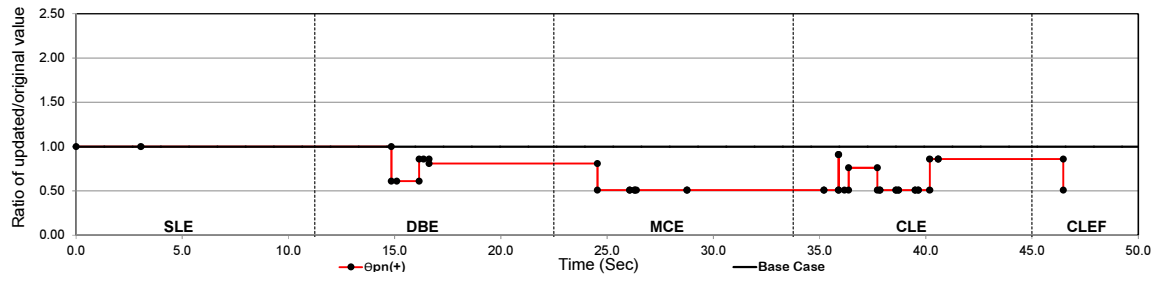
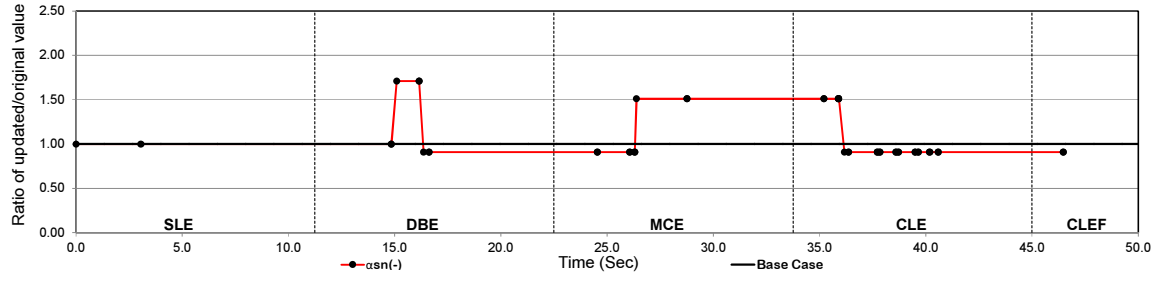
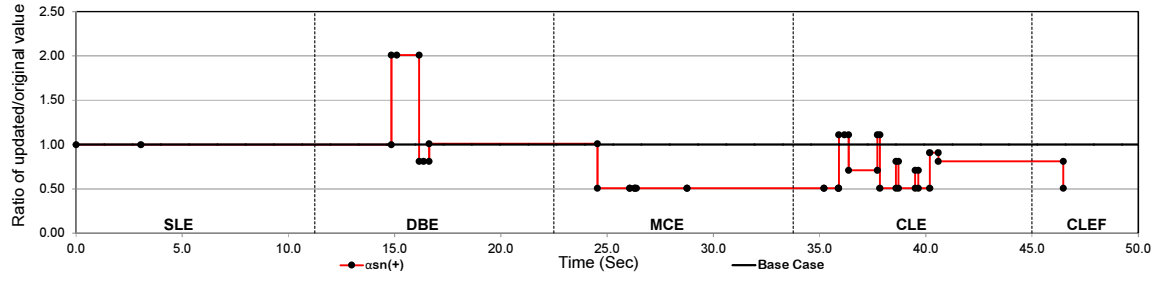
(b)

Figure 5.11. Base shear/seismic weight of a four-story structure hybrid simulation through collapse, (a) *SLE*, *DBE* and *MCE*, (b) *CLE* and *CLEF* limit states (study case 2).

To evaluate the behavioral changes induced by the updating process on the springs during the simulation, the updated values for the selected parameters versus time are plotted in Figure 5.12. As can be seen, the factors vary depending upon the demands induced by the random nature of the input. Also, major recalibration takes place during the strong motion phase of the induced

earthquakes. It is also observed that as expected, the parameters that have lesser variation during the simulation and in this sense, less influence on the response are the ones related to the basic strength of the system, given that the inelastic response is controlled by the parameters related to the regions of the backbone posterior to the elastic range.





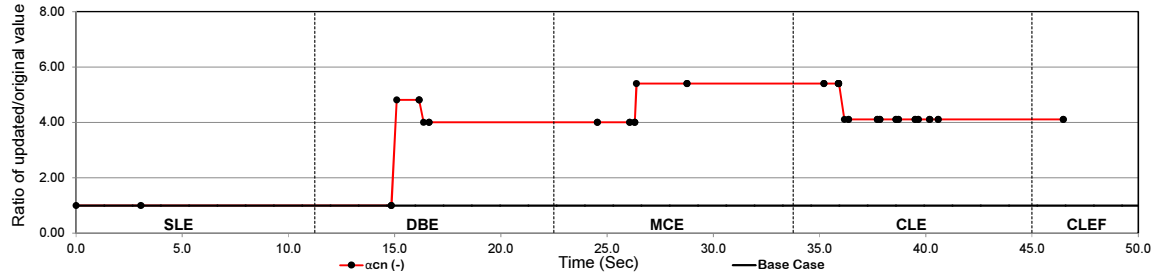


Figure 5.12. Temporal evolution of updated parameters of the numerical subdomain of a four-story structure hybrid simulation through collapse (study case 2).

## 5.5 Summary and conclusions

Phase II of the proposed NUA is discussed. The goal of Phase II is to complete an updating event for a selected vibration cycle through the determination and recalibration of the local component parameters that contribute to the global damage history of the structural system.

Challenges on the optimization of the parameters to update due to the complexity of the selected MDOF structure are present. An additional numerical model consisting of the full SMRF was built and employed (4PO-model) to conduct an identification of the parameters of the local components of the numerical structure subjected to recalibration. The 4PO-model was utilized on the development of families of curves for every single parameter of the *IMK* model involved on the calibration process. Definition of ranges to perform the parameter search was established. The result of the identification process is a solution containing a set of parameters that translates relevant global parameters obtained from Phase I into individual local component parameters on the numerical subdomain. This outcome locally represents the acquired global information from the experimental substructure.

Two case studies are presented. First a verification example with no induced initial errors and inactive deterioration parameters. The procedure showed to be capable of reproducing the degradation effect of the cyclic deterioration parameters. Later, a second case with induced errors

on the initial numerical parameters is presented. These error ratios were obtained through a random number generator and are included in the initial calibration of the *IMK* model factors. The accuracy of the approach is evaluated with respect to the benchmark case. A considerable deviation reduction on the residual drift ratios along the simulation history was obtained. For instance, for the *CLEF* level, a reduction from 42% to 11% of error with respect to the benchmark case was obtained. Besides, the procedure was able to correct the non-collapse behavior of the case with errors, inducing collapse on the updated simulation. Good agreement was also found on the base shear response history where errors are also minimized, for instance a reduction from 43% to 12% after *CLE* ground motion.

## **CHAPTER 6**

### **EPISTEMIC UNCERTAINTY REDUCTION IN HYBRID SIMULATION THROUGH ON-LINE UPDATING**

#### **6.1. Objectives and goals**

Preceding chapters have discussed the development and implementation of a numerical updating approach, which can be incorporated into the conventional hybrid simulation (HS) methodology as an add-on module. One of the objectives of the proposed approach is to reduce the epistemic uncertainty existent on the estimation of the component parameters of the analytical portion of hybrid testing (HT). As a result, the ability to simulate and predict collapse through HT is expected to improve.

The strategy to evaluate the capabilities of the technique is to build a set of study cases with initial calibration errors on the parameters of the local components. Afterward, individual fully numerical HS are performed introducing errors in initial numerical modeling parameters with and without the application of the updating procedure. Then a comparison of results on a case-by-case basis is conducted. The engineering demand parameters to be used in this evaluation are first-story drifts, base shear forces normalized by the seismic weight, and first floor accelerations relative to ground.

#### **6.2. Epistemic uncertainty reduction for ground motion intensity levels**

A method to determine the level of applicability of the NUA consists on inducing random generated errors to the initial component parameters of the numerical portion of the HS, and

compare results generated with and without the NUA. Recalling section 5.3, the set of parameters to be updated and consequently subjected to these induced random errors are: the initial elastic stiffness  $K_e$ , yield moment  $F_y$ , plastic rotation capacity  $\delta_p$  and post-capping rotation slope  $\alpha_c$ .

A random number generator function available in Matlab® is utilized to build bins of error-induced cases. The applied function (i.e., *randn*) returns an  $n$ -by- $n$  matrix containing pseudorandom values drawn from the standard normal distribution. The user provides the mean and the standard deviation to generate the matrices, as described in Equation 6.1.

$$r = \tilde{x} + \sigma_x * randn(i, j) \quad (6.1)$$

where  $r$  is the matrix containing the random generated values,  $\tilde{x}$  and  $\sigma_x$  are respectively the mean value and the standard deviation defined by the user and,  $(i, j)$  is the desired size of the returning matrix. In our case the matrix returns error factors for the component parameters to be affected:  $[factK_e, factF_y, fact\theta_p, fact\theta_{pc}]$ .

These random generated deviation factors are applied equally to all the components of the numerical portion of HS to simulate initial calibration errors. HS with the induced random errors in the numerical part are performed to be compared with the simulations with identical initial conditions applying the NUA. Coefficients of variation (COV) of 10% over the mean, and a mean of 1.00 (i.e., 100% of the original component parameter value) are considered in the design of the error-induced cases. Twenty cases for COV of 10% are investigated.

As previously defined in section 2.2, the 1:8 scaled four story SMRF utilized on this dissertation is subjected to a chain of five consecutive ground motions, increasingly scaled from the Canoga Park record. The scaled ground motions are associated with various intensity levels



(i.e., service *SLE*, design *DBE*, maximum considered *MCE*, collapse *CLE* and imminent collapse *CLEF*). Furthermore, the HS without induced errors on the numerical components is used as the benchmark case.

### 6.2.1 Simulations with random errors related to a COV of 10%

Twenty cases utilizing the described random generator function (Equation 6.1) are built considering a COV of 10% for all parameter values. These random generated deviation factors are equally applied to all the components of the numerical portion of HS to simulate initial calibration errors. Figure 6.1 presents the set of generated values (four for each simulation) for the twenty cases. Random factors range from 71% to 124% of the mean parameter values.

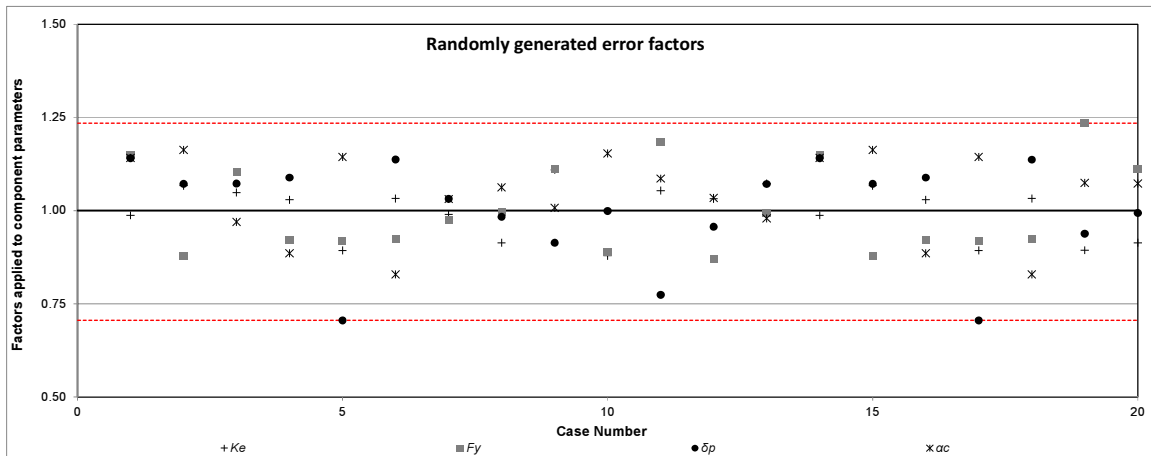


Figure 6.1. Randomly generated error factors considering a COV of 10% over the mean.

First-story drift time histories are shown considering the cases with initial errors (Figure 6.2(a)) and with the application of the numerical procedure (Figure 6.2(b)). Twenty HS first-story drift results are presented in gray lines meanwhile the benchmark case is plotted in bold red line. The first observation from Figure 6.2(a) is that four (i.e., cases 5, 11, 18 and 20) out the twenty simulations do not experience collapse (i.e., 20%). Contrarily, from Figure 6.2(b) it can be

observed that the procedure is able to correct the influence of the initial calibration errors especially on the high nonlinear range, improving to a 100% of collapsing cases. The improvement of the 20% non-collapsing cases might imply the difference between a failed experiment and a completed simulation on a testing laboratory.

Table 6.1 presents the random generated error factors applied to the numerical component parameters of the four non-collapsing cases. As can be seen, the factors that control the response during the elastic and slightly inelastic stages (i.e.,  $K_e$  and  $F_y$ ) are close to 1.00. From the combination of these parameters it can be pointed out that when induced errors are smaller than the mean values, an overestimation of the drifts is observed, contrarily when the combination of parameters report values above the mean the estimated drifts are lower than the benchmark case, leading to a “stiffer” and “stronger” system.

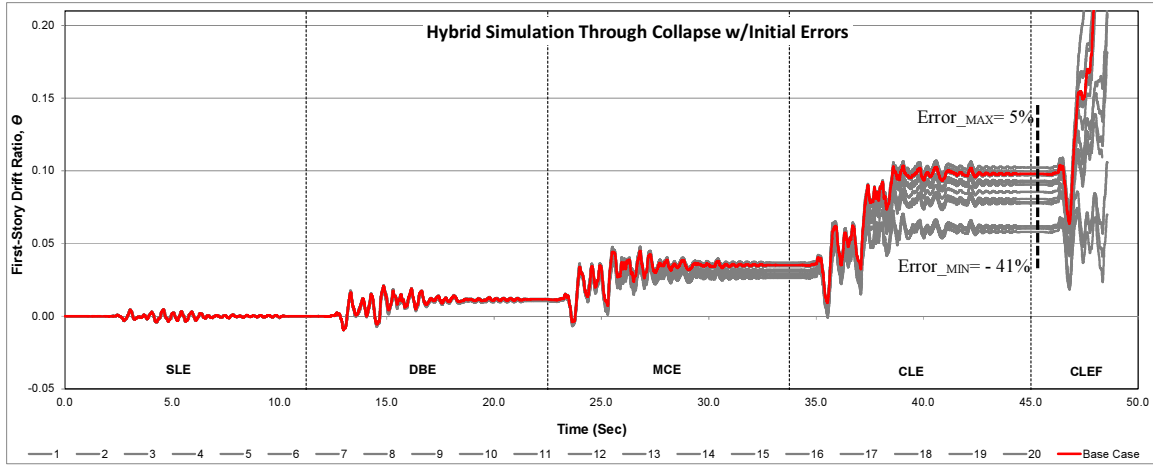
On the other hand, the parameters associated with the post-capping slope ( $\theta_{pc}$ ) and the deformation when the post-capping slope is initiated ( $\theta_p$ ) control the inelastic response of the system. At the same time according to the definition of strain-hardening slope, it is influenced by the value of  $\theta_p$  utilized on its estimation. Thus, the strain-hardening slope is affected by the latter factor ( $\theta_p$ ). The error factors utilized for  $\theta_p$  and  $\theta_{pc}$  are spread from 71% to 116% of the original “correct values”. Additionally, as observed from Figure 6.2(a), the deviation with respect to the benchmark case for these four cases increases as the inelastic demands increase (i.e., during and after *MCE* ground motion), where  $\theta_p$  and  $\theta_{pc}$  have a greater influence on the nonlinear response.

Table 6.1. Random generated error factors applied to the numerical component parameters of non-collapsing cases.

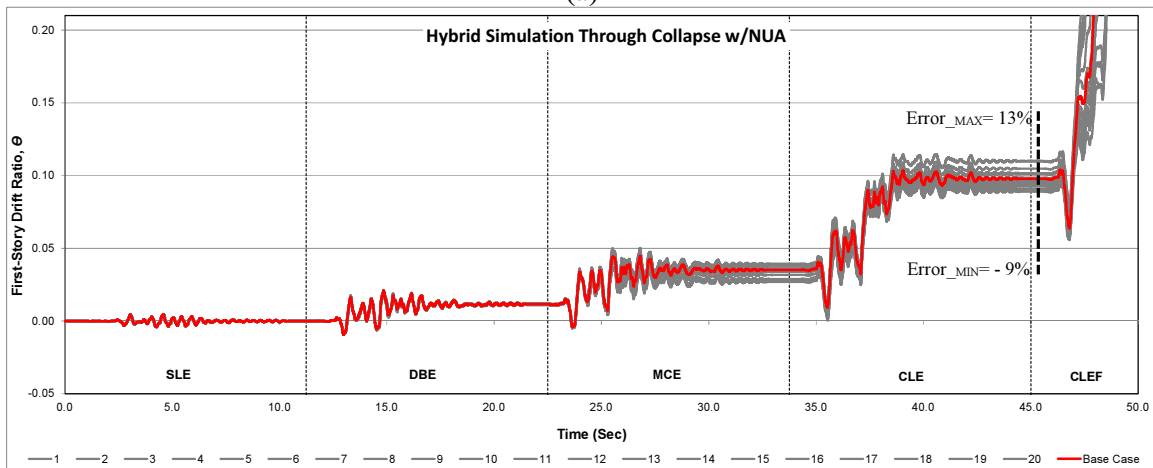
<b>CASE NUMBER</b>	<b><i>factKe</i></b>	<b><i>factFy</i></b>	<b><i>fact <math>\theta_p</math></i></b>	<b><i>fact <math>\theta_{pc}</math></i></b>
5	0.89	0.92	0.71	1.14
11	1.05	1.18	0.77	1.09
18	1.03	0.92	1.14	0.83
20	0.92	1.03	0.73	1.16

Comparing the global results for the twenty cases for the free vibration stage located between *CLE* and *CLEF*, for the set of HS with induced errors (Figure 6.2(a)), deviations from -41% to 5% over the benchmark case are reported. Meanwhile, for the outputs when the NUA is utilized (Figure 6.2(b)), the deviations are minimized to an interval of -9% to 13% over the base case. It can also be seen that for low levels of inelasticity (i.e., *SLE* and *DBE*) both output bins, with errors and with updating, are close to the benchmark results. In the case of the induced errors (Figure 6.2(a)) this implies that errors are not significant enough to change the behavior of the system at low levels of inelasticity.

When the updating approach is employed (Figure 6.2(b)), the methodology is capable of substituting the strength and stiffness deterioration effects in the *IMK* model via recalibration of the component parameters. The deterioration modes in the *IMK* model are governed by hysteretic energy dissipation factors, calibrated once the complete history is available. On the NUA, deterioration modes are kept inactive given that not enough information exists at the start of the simulation, and their effects are replaced by the recalibration process during the analysis.



(a)



(b)

Figure 6.2. First-story drift for 20 cases, (a) with induced initial parameter component errors (ICCE), (b) with the application of the proposed NUA.

Table 6.2 presents the temporary first-story residual drifts estimated for the 20 HS with and without the application of the NUA. These values are associated with the free vibration stages located between *MCE* and *CLE* (34 seconds of simulation) and after *CLE* (45 seconds of analysis). Additionally, deviation percentages over the benchmark case are calculated. Estimated deviation ratios for the results derived from the application of the NUA are written in blue when the procedure improved the error-induced outputs, and in red when the deviations were increased by the updating procedure.

Four cases are selected to examine the performance of the NUA (i.e., 5, 6, 7 and 11)

highlighted in yellow on Table 6.2. Case 5 and 11 (Figure 6.3 and Figure 6.4) represent a condition where the error-induced HS reports non-collapsing cases with large drift deviations over the base case (i.e., -39% and -38% respectively). Later, case 6 (Figure 6.5) presents a HS where the estimated drifts on both error-induced and updated results yields values relatively close to one another. Finally, case 7 (Figure 6.6) reports results of a simulation where the NUA increases the interstory drifts on the high nonlinear stage of the analysis with respect to the error-induced HS.

Table 6.2. First-story temporary drift residuals for 20 cases.

CASE NUMBER	FIRST-STORY TEMPORARY DRIFT RATIOS							
	34 sec (after MCE)				45 sec (after CLE)			
	INIT. ERROR	Deviation to base	NUA	Deviation to base	INIT. ERROR	Deviation to base	NUA	Deviation to base
1	0.037	4%	0.039	12%	0.086	-13%	0.096	-2%
2	0.028	-20%	0.028	-21%	0.091	-7%	0.096	-1%
3	0.037	5%	0.039	11%	0.093	-5%	0.098	0%
4	0.031	-11%	0.034	-4%	0.097	-1%	0.091	-7%
5	0.028	-20%	0.029	-18%	0.060	-38%	0.095	-3%
6	0.032	-10%	0.035	-2%	0.102	5%	0.094	-4%
7	0.035	-2%	0.036	1%	0.097	0%	0.110	13%
8	0.036	1%	0.038	8%	0.097	-1%	0.089	-9%
9	0.035	-1%	0.038	9%	0.081	-18%	0.094	-4%
10	0.030	-16%	0.032	-10%	0.092	-6%	0.099	1%
11	0.031	-11%	0.039	10%	0.058	-41%	0.090	-8%
12	0.026	-25%	0.027	-24%	0.078	-21%	0.101	3%
13	0.034	-2%	0.036	3%	0.093	-5%	0.098	0%
14	0.037	4%	0.039	12%	0.100	2%	0.093	-5%
15	0.028	-20%	0.028	-21%	0.086	-13%	0.098	0%
16	0.031	-11%	0.034	-3%	0.091	-8%	0.105	7%
17	0.028	-20%	0.029	-18%	0.097	-1%	0.095	-3%
18	0.032	-10%	0.035	-2%	0.060	-38%	0.094	-4%
19	0.032	-9%	0.036	1%	0.102	5%	0.110	12%
20	0.035	0%	0.034	-3%	0.062	-37%	0.102	4%

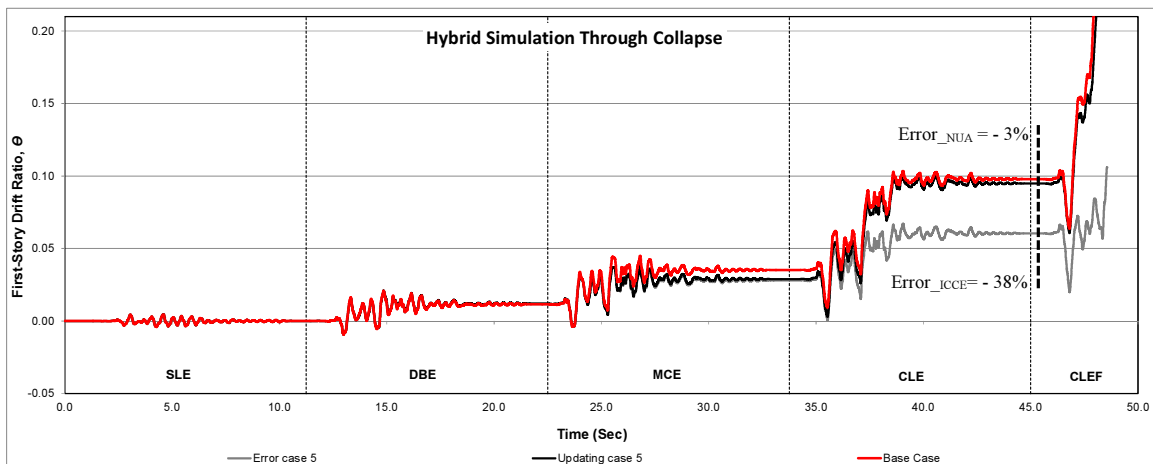


Figure 6.3. First-story drift for case 5, with ICCE and with the application of the proposed NUA.

Figure 6.3 depicts the first-story drift time histories for case 5. The results for the induced error HS are plotted with gray line. The black line represents the outputs of the HS when the NUA is applied, while the benchmark case is traced in red bold line. As can be observed, the case with errors reaches the end of the simulation without experiencing collapse with a large interstory drift deviation value (38% over the base case). The application of the NUA is able to minimize the error in temporary interstory drifts by 35% and to lead the structure to follow closely the benchmark case up to collapse.

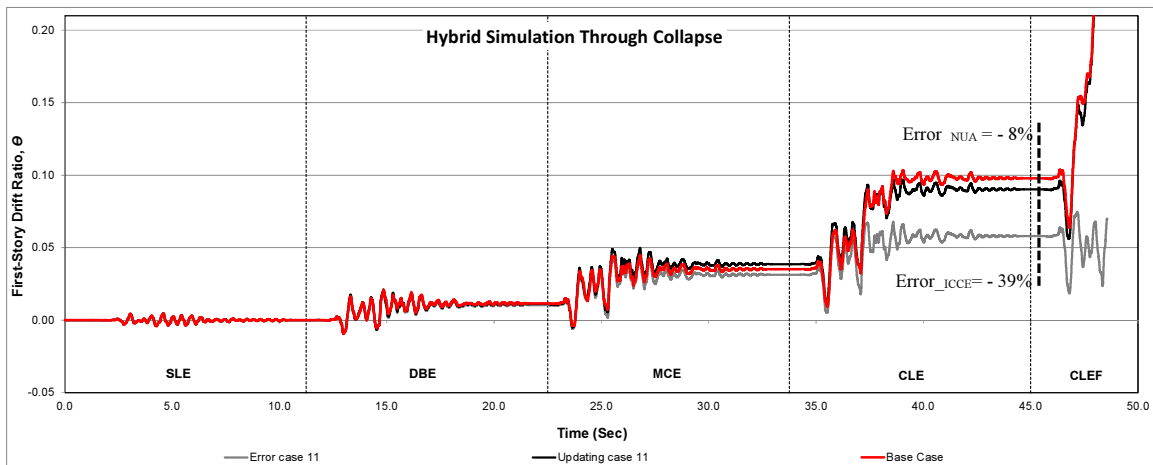


Figure 6.4. First-story drift for case 11, with ICCE and with the application of the proposed NUA.

Similar results are obtained for case 11, where a non-collapsing simulation is attained with the error-induced parameters. As can be noted in Figure 6.4, a large deviation in interstory drift is estimated for the high nonlinear stage of the HS. Deviations are minimized from -39% to -8% with respect to the base case for the free vibration stage after *CLE* ground motion.

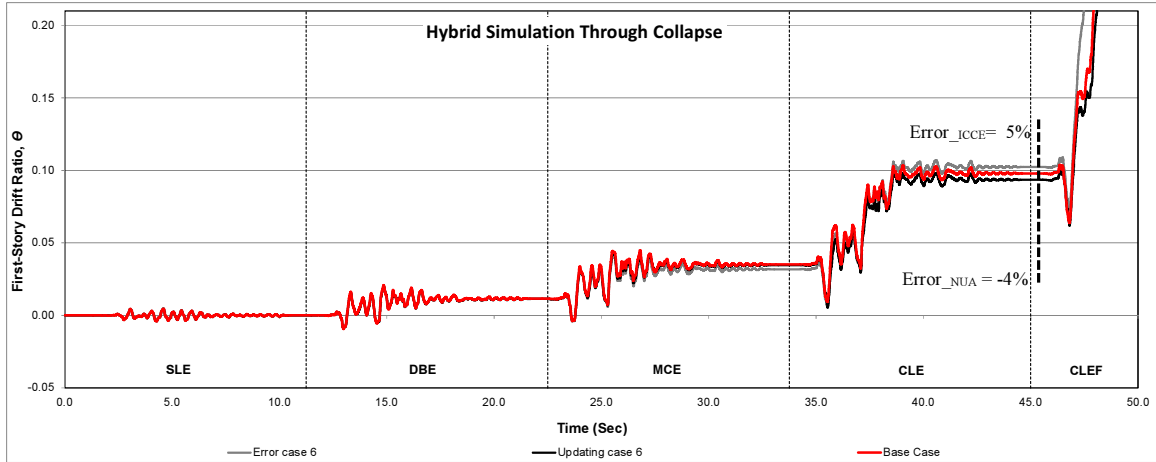


Figure 6.5. First-story drift for case 6, with ICCE and with the application of the proposed NUA.

The estimated deviations for case 6 first-story drifts with error-induced parameters and with the application of the NUA are -4% and 5% respectively, compared to the base case (Figure 6.5). Hence, the application of the NUA is able to reproduce the effect of the deterioration parameters deactivated on the proposed approach, reporting similar accuracy in this particular simulation. This result provides added confidence on the application of the NUA when potential initial errors do not affect substantively the outputs of HS.

Nevertheless, from first-story drift ratio histories plotted in Figure 6.6 (case 7), it can be observed that the outputs for the case with induced errors reports no deviation from the benchmark case. Conversely, for this particular case, the application of the NUA overestimates the drifts on the high nonlinear stages, increasing the deviation up to 12% with respect to the base case. Even that for case 7 an increment in drifts is reported, the simulation is completed without numerical instability or premature collapse of the system.

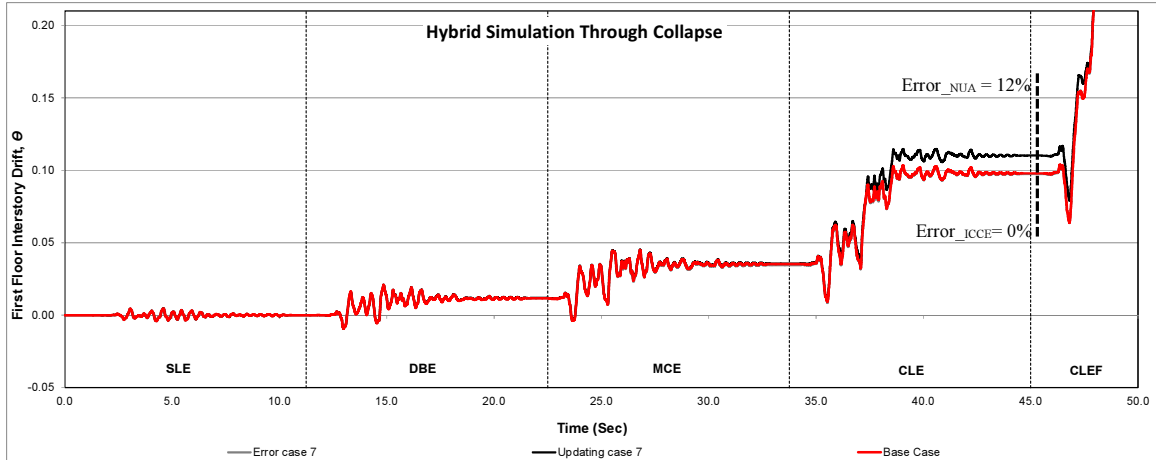


Figure 6.6. First-story drift for case 7, with ICCE and with the application of the proposed NUA.

This behavior can be explained by the influence of higher mode effects. Similar behavior is found for five additional simulations (i.e., 10, 12, 16, 19 and 20) presenting values of interstory drift on the high non-linear range over the benchmark case (i.e., 1%, 3%, 7%, 12% and 4% respectively) when the NUA is used. The difference relies on the fact that the NUA recalibrates the parameters of the numerical components as the data is generated, conducting a parameter selection based on hysteretic information acquired during the analysis. This may add difficulty to the identification of the main parameters due to the “wavy” shape of the hysteretic information acquired during the simulation (see Figure 6.7(a)). A selected time window extracted from the hysteretic information highlighted on a black square presented in Figure 6.7(a) is divided into first-story drift (Figure 6.7(b)) and base shear normalized by the seismic weight (Figure 6.7(c)) time histories. Recalling the target periods of the benchmark structure are: 0.47sec, 0.14sec and 0.07sec respectively for first, second, and third mode of vibration. Thus, Figures 6.7(b) and (c) illustrates two analysis stages where a period of 0.13sec is identified, corresponding to the “wavy” shape of experimental hysteresis from Figure 6.7(a), for that selected analysis time. This identified period correspond to the second mode of vibration.

Another fact is that a sideways response is obtained. For instance, from Figure 6.7(a) it is



observed that for early stages of the simulation, positive loading side shows parameter information that can be used during the updating, differently from the negative side that does not show clear post-capping portions. Thus, negative loading path produces significantly less information. In some instances when the nonlinear demand increases at a specific simulation time, the NUA might not be capable of react adequately, owe to the fact that enough information to update has not been so far generated (see Figure 6.6, 38 seconds of analysis time).

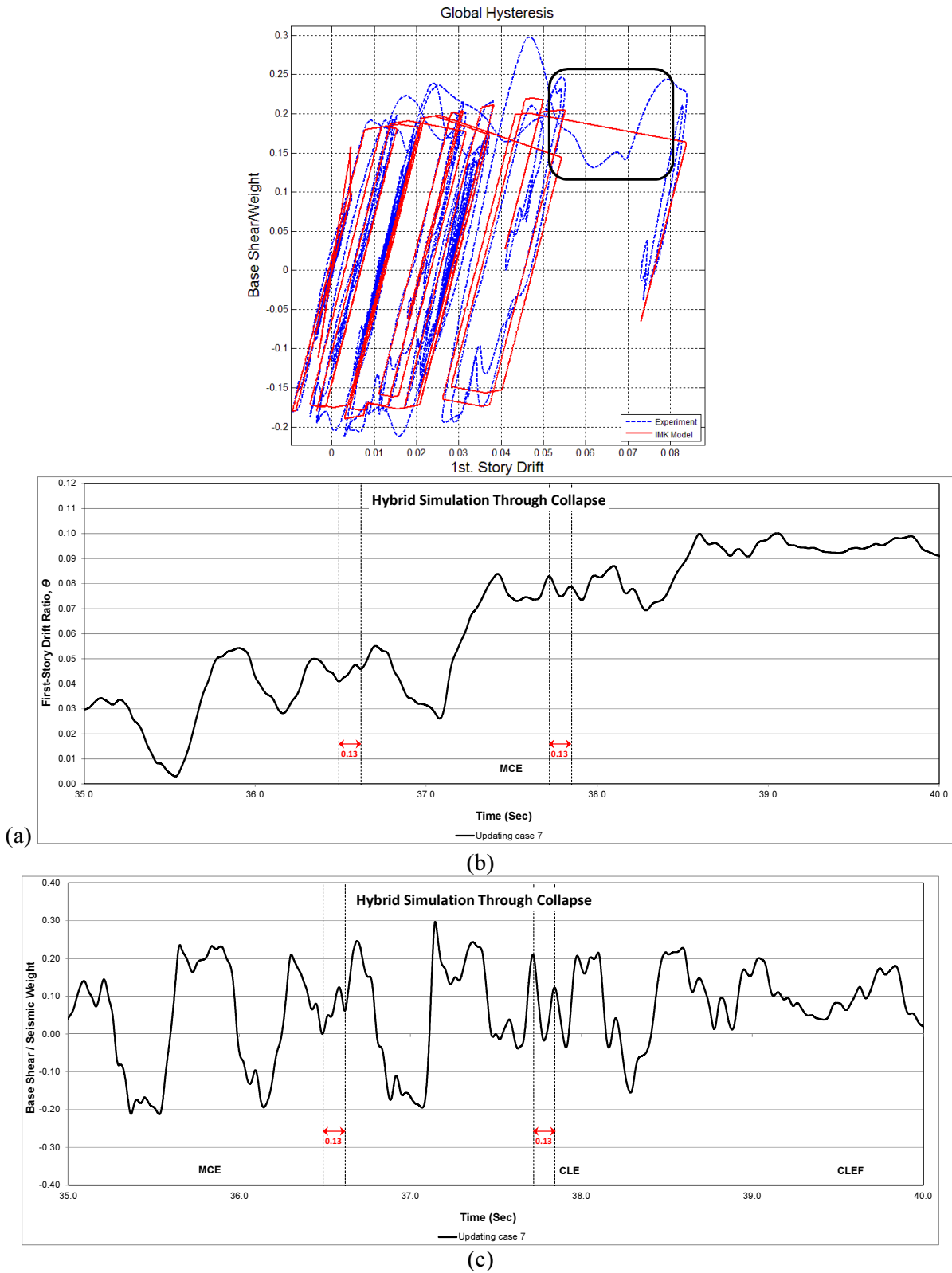
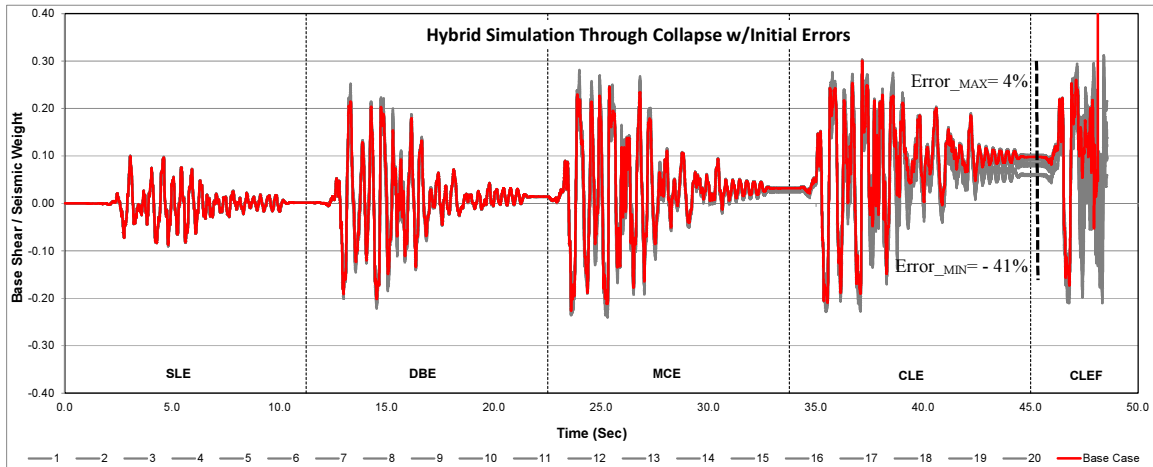
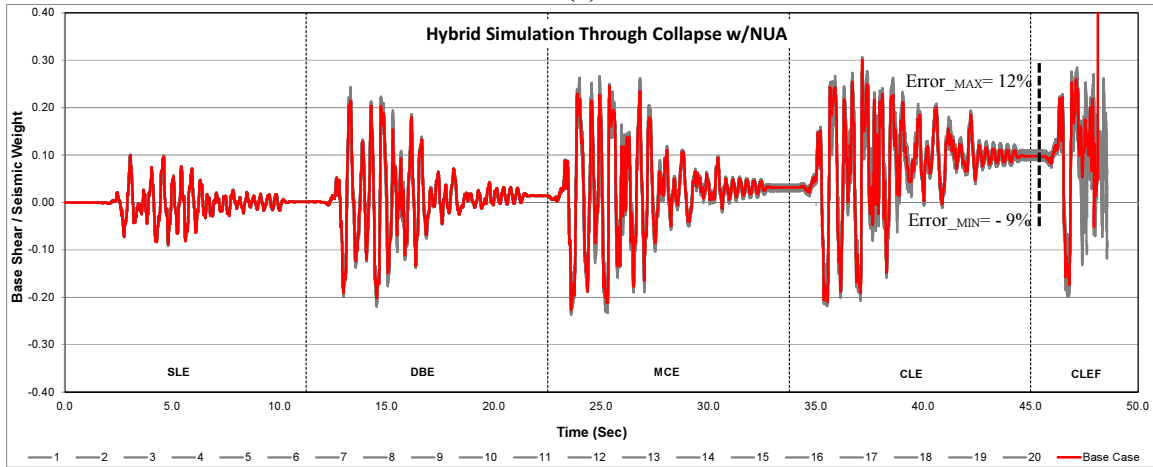


Figure 6.7. Identification of second mode effect for case 7 with NUA, (a) first-story drift - base shear/seismic weight hysteresis diagram, (b) first-story drift ratio, (c) base shear / seismic weight.

Base shear force normalized by the seismic weight of the SMRF is presented on Figure 6.8. Similar to the case of interstory drift, results for the twenty generated cases are plotted with gray lines while the benchmark case is represented with continuous red bold line. During *MCE* and *CLE* ground motions, force demands beyond the benchmark case on the positive and negative sides are present, as can be observed from Figure 6.8(a). During the free vibration stage after *CLE*, deviations of -41% to 4% are estimated for the error-induced cases. This divergence is minimized up to -9% to 12% over the benchmark case through the application of the NUA (Figure 6.8(b)). Besides, at the end of the simulation, it is noted on the set of error-induced cases (Figure 6.8(a)) that more intense forces are reported versus the HS with the application of the NUA (Figure 6.8(b)). When structures collapse they lose their ability to withstand forces, meaning that on the set of induced errors some of the simulations did not collapse and are standing and resisting forces at the end of the simulation.



(a)



(b)

Figure 6.8. Normalized base shear for 20 cases, (a) with ICCE, (b) with NUA.

Case 5 base shear time history is presented in Figure 6.9. It is observed at the end of the simulation high shear forces withstood by the structure. This implies that the structure has not collapsed. Besides, a high deviation from the base case is observed on the free vibration stage after *CLE* (-39%). The collapse behavior is corrected by the NUA, additionally minimizing the deviation to -3% to the base case.

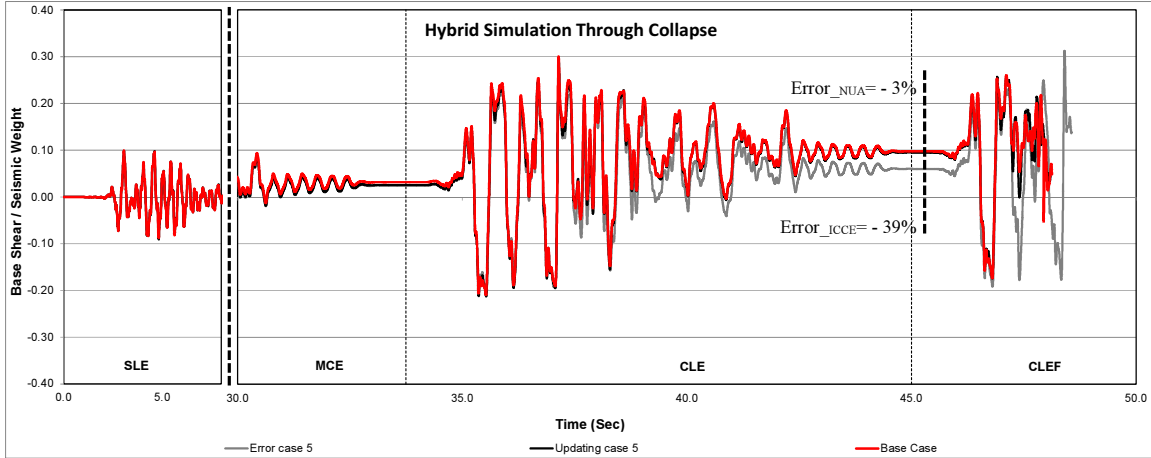


Figure 6.9. Normalized base shear for case 5, with ICCE and with NUA.

Similarly, Figure 6.10 demonstrates an improvement on shear force consistent with the behavior reported for interstory drift for case 11. The deviation from the base case is minimized from -41% to 7% for the free vibration located after *CLE*.

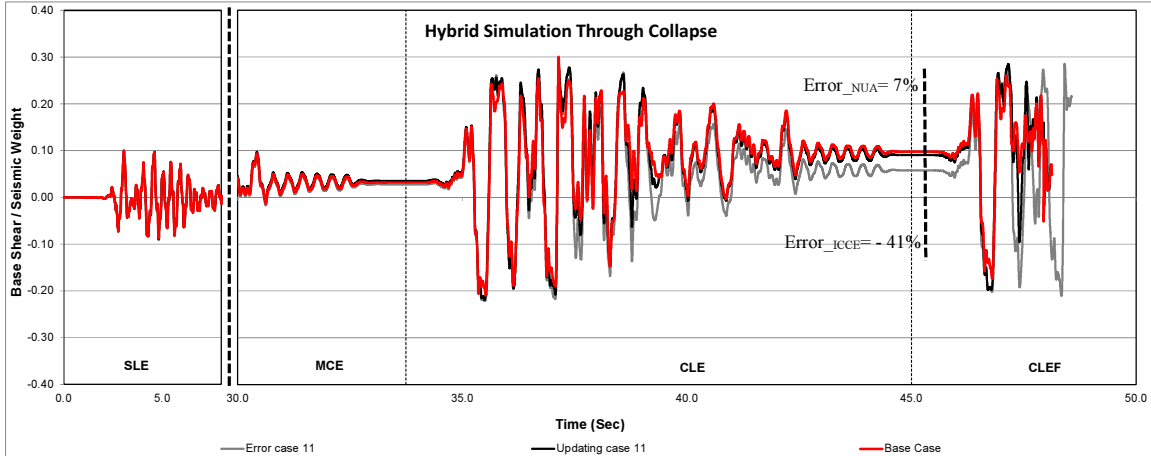


Figure 6.10. Normalized base shear for case 11, with ICCE and with NUA.

Base shear time histories for study case 6, represented in Figure 6.11 show a slight improvement on the deviation (i.e., 3%) compared to the base case. It is observed that the application of the NUA reports similar results to the base case and to the error-induced HS.

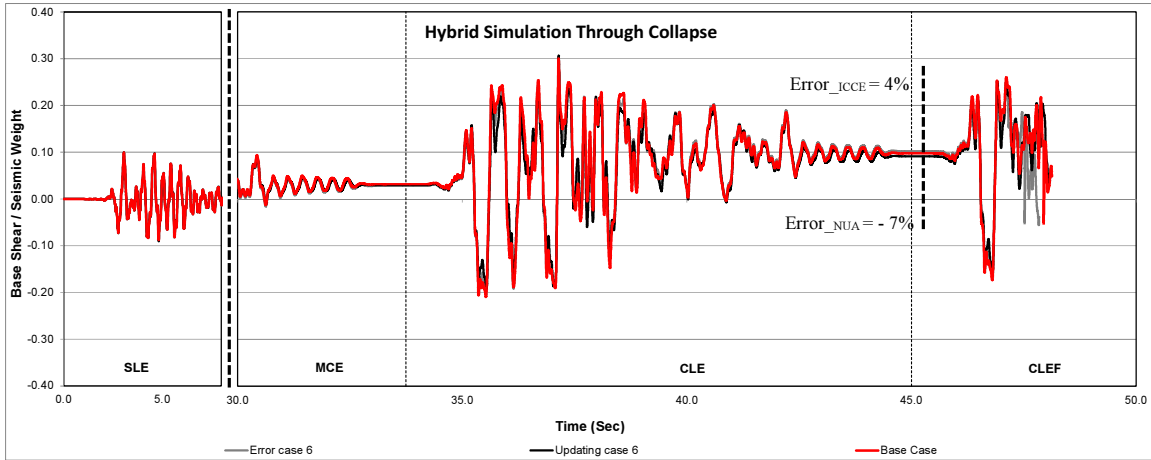


Figure 6.11. Normalized base shear for case 6, with ICCE and with NUA.

Regarding study case 7, from Figure 6.12 it can be observed that the application of the NUA increases the deviation of the force with respect to the base case from 1% to 12%. Similar to the first-story drift for the same case 7, it is caused by the estimation of updating parameters fitted from experimental hysteretic information containing higher mode effects and limited data on the negative loading path from the early history of the analysis.

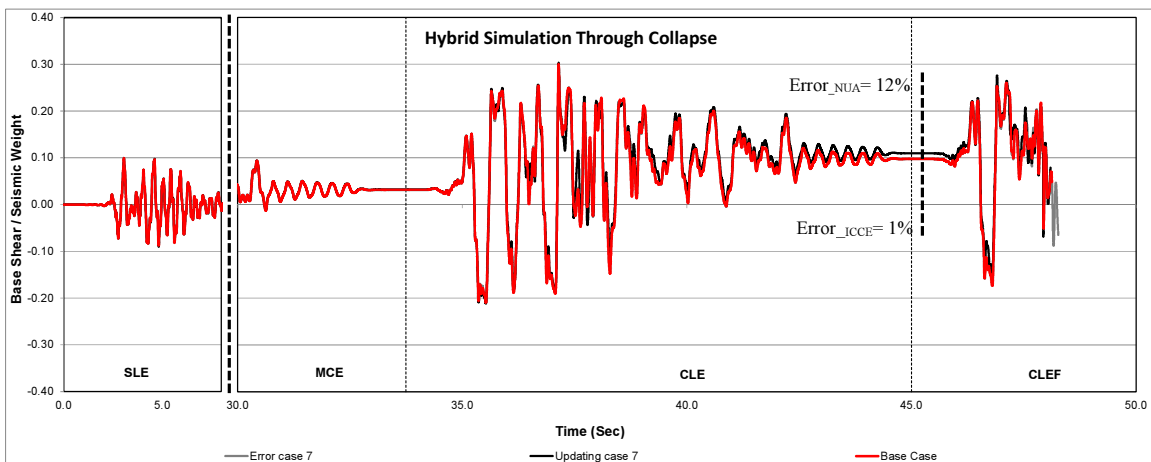


Figure 6.12. Normalized base shear for case 7, with ICCE and with NUA.

With respect to first-floor accelerations, results for the twenty cases with and without the application of the NUA are plotted in Figure 6.13. Outputs correspond to a window of analysis

time from 36 to 39 seconds related to the *CLE* ground motion stage. As can be observed particularly close to 37.50 seconds of analysis, a slight minimization of the deviation on the acceleration is achieved. Nevertheless, besides these minimum differences, the acceleration responses are virtually equal. Given this fact, first-floor relative accelerations would not be considered on later discussions of the performance of the NUA.

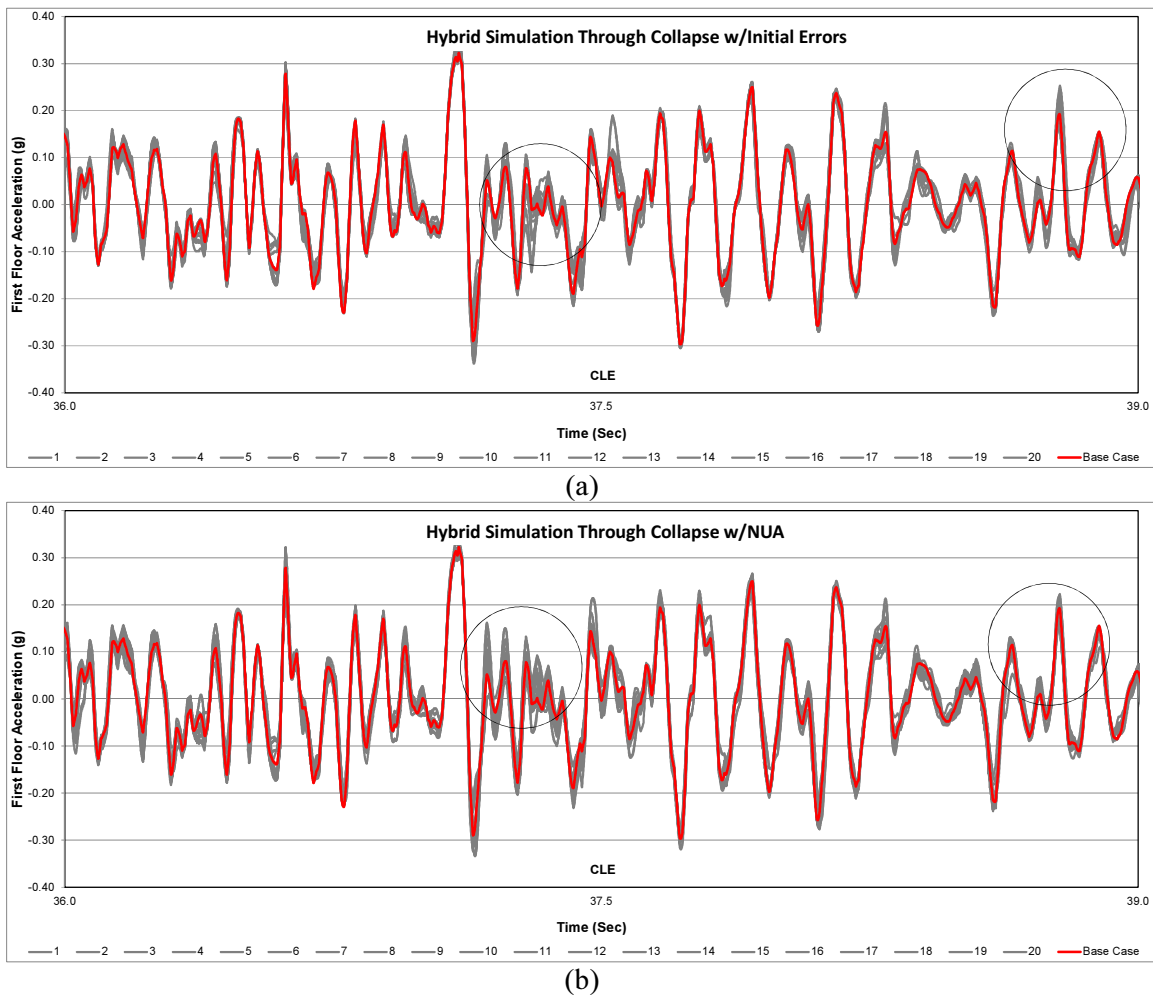


Figure 6.13. First floor acceleration for 20 cases, (a) with ICCE and, (b) with NUA.

Based on the presented results it can be concluded that for a COV of 10% over the mean, the proposed NUA is capable of correcting the epistemic error-induced to the component parameters of the numerical portion of HS. In most of the cases studies in this dissertation, the

NUA helped minimize the deviations of first-story drift ratios and base shear time histories. Another important contribution is the correction of non-collapsing cases. The observed drawback is an underestimation of the resistance of the system at high non-linear stages in a few study cases, leading to attain increased displacements compared to the benchmark case.

### **6.3. Final remarks on the applicability of the NUA**

The applicability of the proposed NUA was examined for a dispersion of 10% of the standard deviation over the mean (i.e., 71% to 124% of the mean component parameter values) of the numerical portion of HS.

Recalling Table 1.2 where statistical information about yield and capping strength to effective yield strength is presented, the reported dispersion is approximately 12% and 3% respectively, and the differences with respect to the mean values range from 6% to 9%. Besides, Table 1.3 showed respectively dispersions of 24%, and 25% for pre-capping rotation ( $\theta_p$ ) and post-capping rotation ( $\theta_{pc}$ ) of steel components with RBS connections. The latter considers sections equal and deeper to 21", which may increase the dispersion due to the spread of sizes and geometric properties.

The spread of error factors obtained covers the highest dispersion presented in Table 1.2 and Table 1.3, for the yielding and capping strength, pre-capping rotation, and post-capping rotation. The latter two parameters govern most of the behavior of the system on high nonlinear stages close to collapse.

### **6.4. Summary and conclusions**

The proposed NUA is based on recalibrating the numerical portion of HS during the analysis based on key information acquired from the experimental part has been detailed on the



preceding chapters of this dissertation. The present chapter quantified the accuracy of the procedure via 20 simulations with induced randomly generated initial parameter component errors.

Random error factors were equally applied to the parameters of the numerical components of the analytical part of the HS. The parameters considered were: initial elastic stiffness  $K_e$ , yield moment  $F_y$ , plastic rotation capacity  $\delta_p$  and post-capping rotation slope  $a_c$ .

Thus, a bin of twenty error-induced cases for a standard deviation of the mean of 10% were generated. The most important findings from examining the generated HS are:

- Results from the bin showed that NUA is capable of diminishing the influence of initial calibration errors, correcting 20% of non-collapsing simulations to a 100% of cases experiencing collapse.
- First-story drift was minimized from [ $error_{min} = -41\%$  to  $error_{max} = 5\%$ ] to [ $error_{min} = -9\%$  to  $error_{max} = 13\%$ ] whereas base shear diminished from [ $error_{min} = -41\%$  to  $error_{max} = 4\%$ ] to [ $error_{min} = -9\%$  to  $error_{max} = 12\%$ ].

Four study cases were particularly examined, two presented significant improvement (i.e., 5 and 11), whereas a third case (i.e., 6) where the induced errors were not enough to significantly deviate the response from the base case, the NUA was able to reproduce the deterioration of the system via recalibration of the component parameters; on a fourth case (i.e., 7), the NUA increased the deviation to the benchmark case. The major conclusions are:

- The application of the NUA on cases 5 and 11 corrected the non-collapsing trend of the error-induced case and minimized the deviation of first-story drift ratios by a 35% and 31%, while shear forces improved by 36% and 34% respectively. These latter values were calculated for the free vibration stage after *CLE*.
- The importance of case 6 relies on the fact that the results with error-induced parameters

showed a low deviation with respect to the base case, and through the application of the NUA. Moreover, good agreement on the results with respect the base case were obtained, augmenting the confidence on the effectiveness of the procedure. A slight improvement of 1% for first-story drifts and 3% for shear forces on the first floor was attained.

- NUA in case 7 increased the deviation from 0% to 12% for first-story drifts and 1% to 12% for shear forces on the first story. Nevertheless, the increase on deviations did not induced numerical stability, reaching collapse at similar timing as the error-induced case.

The COV of 10% over the mean utilized on the design of the 20 study cases, covers the likely deviation estimation of parameters reported on the literature for the type of structural system and steel shapes employed of the models studied on this dissertation.

## CHAPTER 7

### SUMMARY AND CONCLUSIONS

#### 7.1. Summary

Hybrid testing (HT) combines the experimental advantages of shaking table tests and the economy of quasi-static tests, emerging as a *safe*, efficient and cost-effective alternative to test large-scale complex multi-degree-of-freedom structures. The testing technique consists on dividing the structural system in experimental and numerical portions, interacting all along the simulation.

The present dissertation accounts for the reduction of epistemic uncertainty existing on the estimation of numerical component parameters of HT. The presence of this uncertainty on the calibration of component parameters calls into question the reliability of our numerical models. Consequently, the implementation during the analysis of a recalibration technique for the numerical components of the analytical part of HT is expected to improve our ability to predict collapse. Aleatory uncertainty due to record-to-record variability is not accounted for. Experimental errors are not considered since the setup utilized is a numerically modeled virtual laboratory.

The proposed numerical updating approach (NUA) consists of two primary phases: I) global (first-story drift / base shear) hysteretic information is acquired from the virtual experiment or experimental substructure during an analysis, II) this calibrated global response is used to find the parameters of component models to distribute damage from global to local domain of the

structural system under study.

The objective of Phase I is to translate experimental global information into global parameters related to a hysteretic model with deterioration capabilities. A set of rules was designed to identify during the analysis, relevant parameters of the Ibarra-Medina-Krawinkler hysteretic model (Ibarra, et al., 2005) in order to capture the response to collapse of the virtual experimental substructure.

Utilizing the measured and characterized response of the experimental portion (Phase I) according to the hysteretic model, updating of the component parameters (Phase II) of the numerical subdomain of the structural system is conducted during the analysis. The goal of Phase II is to update the local parameters that contribute to the global damage history of the system, completing a numerical updating event initiated on a selected vibration cycle (Phase I) to be applied to the following cycle in the same loading direction.

Twenty study cases (i.e., fully numerical HS) were performed with the inclusion of random calibration errors with and without the proposed NUA. Comparative results obtained for engineering demand parameters (i.e., first-story drift, base shear / seismic weight and first-floor accelerations) were examined. The implementation of the NUA demonstrated that the procedure is capable of minimizing the influence of the epistemic uncertainty on the estimation of numerical component parameters of the analytical part of HT, and hence, improve the accuracy of simulations to collapse.

## **7.2. Conclusions**

The most salient contributions of this research are listed next:

- 1) The proposed NUA is relies upon the development and implementation of an on-line

recalibration procedure of the numerical subdomain of HT, based on the acquired information of the experimental portion *during the analysis*. The NUA was successfully implemented as an add-on module without affecting the established hybrid testing architecture.

- 2) The NUA improves our ability to simulate and predict collapse through hybrid testing with substructuring techniques. This is achieved via minimization of the epistemic uncertainty on the initial calibration of component parameters. Twenty case studies were generated utilizing a random number generator considering a COV of 10% over the mean (i.e., initial calibration error values ranging from 71% to 124% of the mean parameter values). 20% of the study cases presented a non-collapse behavior at the end of the simulation. The NUA was able to diminish the influence of initial calibration errors, leading the systems to collapse on adequate timing. Additionally, the proposed NUA demonstrated to improve the accuracy of the results through the response history up to the limit state of collapse.

Deviations of residual drifts with respect to the base case were minimized. For instance, first-story residual drifts for the set of twenty cases, calculated on the free vibration stage after *CLE* diminished from [ $error_{min} = -41\%$  to  $error_{max} = 5\%$ ] to [ $error_{min} = -9\%$  to  $error_{max} = 13\%$ ], whereas base shear deviation was reduced from [ $error_{min} = -41\%$  to  $error_{max} = 4\%$ ] to [ $error_{min} = -9\%$  to  $error_{max} = 12\%$ ] when the NUA was utilized. Hence, the global response of the system was represented more accurately by capturing deformation and strength demands up to the limit state of collapse.

- 3) An important achievement was the development and implementation of a chain of in-house Matlab® coding utilized to control the evaluation of updating events, dynamic numerical fitting on Phase I, management of generation of capacity curves via OpenSees models,

parameter identification on the generated curves (Phase II), administration of listings of parameters to update and control of pausing of OpenSees during updating events. At this stage, the coding is adapted to work with OpenSees, OpenFresco, and the *IMK* model, but it could be extended to other software and numerical models. Furthermore, the designed routines are developed with basic Matlab® commands that could become easily familiar to future users. And as part of a funded project, they can be publicly available for its implementation in future research.

- 4) The NUA was developed through a virtual experimental laboratory. This allowed performing multiple simulations in a practical manner without the need for physical specimens and laboratory equipment. At the same time, the approach allowed to efficiently conduct repetitive explorations of the behavior of the system on stages of high nonlinearity, close and up to collapse.
- 5) A parameter correlation approximation approach was developed and implemented to associate first-level (experimental) global responses to local-level hysteretic updated information, considering the level of demands that vary along complex MDOF structures. This correlation is aimed at distributing the detected response on the global domain to the local domain, a key task on the NUA.
- 6) The functionality of the *setParameter* command in OpenSees was corrected to work with bilin models, and new executable files were compiled directly from the OpenSees source code. This modification avoided the need of reverting the simulation to the beginning of the analysis.
- 7) The selection of an adequate analysis step resolved the challenges (e.g., convergence issues) of utilizing a piecewise linear hysteretic model versus smooth curvilinear models,

taking advantage of the relative small number of parameters to update on the *IMK* hysteretic model.

### **7.3. Limitations**

Some limitations on the proposed NUA are lined up next:

- 1) The performance of the NUA in a laboratory facility utilizing a physical specimen could not be investigated. Nevertheless the NUA was compared to the benchmark case obtained from a shake table test to validate the results of its application on fully simulated HT. Besides, results of hybrid testing conducted with the same substructuring option and numerical models without updating were available to validate the outputs of the NUA.
- 2) The NUA developed is based on a scaled four-story MDOF two dimensional frame-type structure. Thus, limitations on its application to larger MDOF or 3D structures may exist. For instance, testing on steel components have been mainly conducted enforcing behavior in one plane. Additionally, parameter identification in capacity curves should be calculated for two directions, and bidirectional moments and torsion should be considered on 3D systems.
- 3) The efficiency of the correlations established to relate global to local responses could be limited by the different demand levels on local components of a larger MDOF system or even become inapplicable for the case of 3D structures.
- 4) Due to the existence of a benchmark study conducted on a shake table test of a scaled four-story SMRF designed to act as a system of elastic members and plastic hinges, a concentrated plasticity approach was utilized. Structures with distributed plasticity are out of the scope of this research and the results obtained on this investigation may not be

extrapolated.

- 5) The simulation time added by the NUA to the regular calculations and transfer of information during HT. This may be an issue on a real facility utilizing a physical specimen and laboratory equipment due to the delay time the actuators need to be awaiting for the next commanded displacement to be applied to the specimen.

#### **7.4. Future work**

The presence of epistemic uncertainty on the estimation of numerical component parameters in HS influences the reliability of numerical models. In order to reduce the epistemic uncertainty, numerical recalibration approaches like the one presented in this research are needed. Recommendations for future investigation on this topic are presented next:

- a) Implementation of the NUA on a laboratory facility employing a physical specimen under real testing conditions.
- b) More research needs to be conducted utilizing alternative MDOF structures and different loading inputs to generalize the proposed NUA. This may lead to the need for refining the correlations between the experimental response and the numerical portions of the system, especially those located far from the interaction with the boundary between experimental and numerical substructures.
- c) Extension of the NUA to different hysteretic models (e.g., smooth curvilinear models) and different approximations such like fiber models to make its application more general.
- d) Implementation of a “real time virtual library” containing existing and up-to-date information from previous component experimental tests. This information could be used in conjunction with HT results to provide a more accurate recalibration numerical model



parameters.

- e) The method could be investigated for its application to distributed hybrid testing utilizing multiple experimental substructures, managing more than one source of experimental information.
- f) The application of the method could also be extended to 3D structural systems subjected to different loading inputs. For instance bridge structures subjected to seismic and additionally different type of loading conditions (e.g., traffic, winds) could be investigated.

## LIST OF REFERENCES

- Ahmadizadeh, M., 2007. *Real-time seismic hybrid simulation procedures for reliable structural performance testing*. Buffalo, NY.: PhD. Dissertation, State University of New York at Buffalo.
- AISC, 2010. *Prequalified connections for special and intermediate steel moment frames for seismic applications*, Chicago, IL.: AISC.
- Benjamin, J. & Cornell, C., 1970. *Probability, statistics and decision for civil engineers*. 1st ed. United States: Mc Graw Hill.
- Chen, C., Avramova, N., Sanchez, F. & Pong, W., 2013. *Analysis and evaluation of "Smart" hybrid simulation with parameter adaptation*. Taipei, Taiwan, 5th International Conference on Advances in Experimental Structural Engineering.
- Chi, B. a. U. C.-M., 2002. Cyclic response and design recommendations of reduced beam section moment connections with deep columns. *Journal of Structural Engineering*, pp. 464-473.
- Clark, P., Frank, K., Krawinkler, H. & Shaw, R., 1997. *Protocol for Fabrication, Inspection, Testing, and Documentation of Beam-Column Connection Tests and Other Experimental Specimens*, SAC Joint Venture, Sacramento, CA.: Report No. SAC/BD-97/02.
- Deierlein, G., Hajjar, J. & Kavinde, A., 2001. *Material nonlinear analysis of structures: a concentrated plasticity approach*, Minneapolis, Minnesota: University of Minnesota.
- Eads, L., Miranda, E. & Krawinkler, H. a. L. D., 2012. An efficient method for estimating the collapse risk of structures in seismic regions. *Earthquake Engineering and Structural Dynamics*, 42(1), pp. 25-41.
- Elanwar, H. & Elnashai, A., 2014. On-line model updating in hybrid simulation tests. *Journal of Earthquake Engineering*, 18(3), pp. 350-363.
- Hakuno, M., Shidawara, M. & Hara, T., 1969. Dynamic destructive test of a cantilever beam, controlled by an analog-computer. *Transactions of the Japan Society of Civil Engineers*.
- Hashemi, M., Del Carpio Ramos, M. & Mosqueda, G., 2013. *Substructuring techniques for hybrid simulation of complex structural systems through collapse*. Taipei, Taiwan, 5th International Conference on Advances in Experimental Structural Engineering.
- Hashemi, M. J., 2013. *Collapse Simulation of Multi-Story Buildings Through Hybrid Testing with Substructuring Techniques*. Buffalo, NY, USA.: PhD. Dissertation..

- Hashemi, M., Masroor, A. & Mosqueda, G., 2013. Implementation of online model updating in hybrid simulation. *Earthquake Engineering and Structural Dynamics*, 43(3), pp. 395-412.
- Ibarra, L. a. K. H., 2005. *Global collapse of frame structures under seismic excitations*, Stanford, Ca.: The John A. Blume Earthquake Engineering Center.
- Ibarra, L. F., Medina, R. A. & Krawinkler, H., 2005. Hysteretic Model that Incorporate Strength and Stiffness Deterioration. *Earthquake Engineering and Structural Dynamics*, pp. 34:1489-1511.
- Jeyasehar, C., Kumar, K., Muthumani, K. & Lakshmanan, N., 2009. Seismic performance evaluation methodologies for civil engineering structures. *Indian Journal of Engineering and Material Sciences*, Issue 16, pp. 220-228.
- Karakostas, S. a. M. E., 2000. Evaluation of the ductility features in steel structures with softening moment-rotation behaviour based on a nonconvex optimization formulation. *Engineering Computations*, 17(5), pp. 573-592.
- Krawinkler, H., 1996. Cyclic loading histories for seismic experimentation on structural components. *Earthquake Spectra, The Professional Journal of the Earthquake Engineering Research Institute*, 12(1), pp. 1-12.
- Kuhlmann, U., 1989. Definition of flange slenderness limits on the basis of rotation capacity values. *Journal of Constructional Steel Research*, Volumen 14, pp. 21-40.
- Kwon, O. & Kammula, V., 2013. Model updating method for substructure pseudo-dynamic hybrid simulation. *Earthquake Engineering and Structural Dynamics*, 42(13), pp. 1971-1984.
- Lignos, D., 2008. *Sidesway Collapse of Deteriorating Structural Systems Under Seismic Excitations..* Stanford, Ca. USA.: PhD. Dissertation..
- Lignos, D., 2012. [http://opensees.berkeley.edu/wiki/index.php/Modified\\_Ibarra-Medina-Krawinkler\\_Deterioration\\_Model\\_with\\_Bilinear\\_Hysteretic\\_Response\\_%28Bilin\\_Material%29](http://opensees.berkeley.edu/wiki/index.php/Modified_Ibarra-Medina-Krawinkler_Deterioration_Model_with_Bilinear_Hysteretic_Response_%28Bilin_Material%29). [Online] [Accessed January 2013].
- Lignos, D. & Krawinkler, H., 2011. Deterioration modeling of steel components in support of collapse prediction of steel moment frames under earthquake loading. *Journal of Structural Engineering*, 137(November), pp. 1291-1302.
- Lignos, D., Krawinkler, H. & Whittaker, A., 2008. *Shaking table collapse tests of two scale models of a 4-story moment resisting steel frame*. Beijing, China, 14WCEE.

- Magonette, G., 2001. Development and application of large-scale continuous pseudodynamic testing techniques. *Dynamic Testing of Structures: Papers of a Theme, Philosophical Transactions of the Royal Society: Mathematical, Physical and Engineering Sciences*.
- Mahin, S. & Shing, P., 1985. Pseudodynamic method for seismic testing. *Journal of Structural Engineering*, 111(7), pp. 1482-1503.
- Mahin, S., Shing, P., Thewalt, C. & Hanson, R., 1989. Pseudodynamic test method-current status and future directions. *Journal of Structural Engineering*, 115(August), pp. 2113-2128.
- McKenna, F., Fenves, G. & Scott, M., 2000. *Open system for earthquake engineering simulation*, Berkeley, Ca.: University of California at Berkeley.
- Moncarz, P. a. K. H., 1981. *Theory and application of experimental model analysis in earthquake engineering*, Stanford, California: John A. Blume Earthquake Engineering Center.
- Mosqueda, G., 2010. *Hybrid simulation of complex structural systems*. Buffalo, NY: Webinar SUNY Buffalo.
- Mosqueda, G., Stojadinovic, B. & Mahin, S., 2005. *Implementation and accuracy of continuous hybrid simulation with geographically distributed substructures*, s.l.: Earthquake Engineering Research Center, University of California, Berkeley, 183.
- Mueller, A., 2014. *Real-time hybrid simulation with online model updating*. Kalamazoo, MI: Master's thesis.
- Negrete, M. et al., 2014. *Numerical updating on collapse simulation of a four-story building through hybrid testing*. Anchorage, AK., Tenth U.S. National Conference on Earthquake Engineering.
- PEER, 2010. *Guidelines for performance-based design of tall buildings*, Berkeley, California: Pacific Earthquake Engineering Research Center.
- Phillips, B. & Spencer, B. J., 2012. *Model-based framework for real-time dynamic structural performance evaluation*, Urbana, IL: NSEL Report Series.
- Rahnama, M. & Krawinkler, H., 1993. *Effects of soft soil and hysteresis model on seismic demands*, Stanford, California: John A. Blume Earthquake Engineering Center.
- Saouma, V. & Sivaselvan, M., 2008. *Hybrid Simulation, Theory, Implementation and Applications*. s.l.:Taylor and Francis Group.
- Schellenberg, A., Huang, Y. & Mahin, S., 2008. *Structural FE software coupling through the experimental software framework, OpenFresco*. Beijing, China, The 14th World Conference on Earthquake Engineering.

- Schellenberg, A., Kim, H. & Mahin, S. A., 2010. <https://nees.org/resources/openfresco>. [Online].
- Scott, M. & Haukaas, T., 2008. Software framework for parameter updating and finite-element sensitivity analysis. *Journal of computing in Civil Engineering*, 22(5), pp. 281-291.
- Shing, P., Nakashima, M. & Bursi, O., 1996. Application of pseudodynamic test method to structural research.. *Earthquake Spectra.*, 12(1), pp. 29-56.
- Song, W. & Dyke, S., 2014. Real-time dynamic model updating of a Hysteretic Structural System. *Journal of Structural Engineering*, 140(3).
- Stratan, A., 2014. *Desing for seismic and climate changes..* Timisoara: Politehnica University of Timisoara.
- Takanashi, K. & Nakashima, M., 1987. Japanese activities on on-line testing.. *Journal of Engineering Mechanics.*, pp. 1014-1032.
- Takanashi, K. et al., 1975. Nonlinear earthquake response analysis of structures by a computer-actuator on-line system. *Bulletin of Earthquake Resistant Structure Research Centre.*
- Thewalt, C. & Mahin, S., 1987. *Hybrid solution techniques for generalized pseudodynamic testing*, Berkeley, Ca.: Earthquake Engineering Research Center.
- TheWalt, C. & Mahin, S., 1991. The pseudodynamic test method: numerical aspects. In: *Experimental and numerical methods in Earthquake Engineering*. Dordrecht, The Netherlands: Kluwer Academic Publishers, pp. 47-62.
- Uang, C. M., Yu, Q. S. & Gilton, C. S., 2000. *Effects of Loading History on Cyclic Performance of Steel RBS Moment Connections*. Auckland, New Zealand, A. A. Balkema, 2000.
- Wang, T. & Wu, B., 2013. *Real-time hybrid testing with constrained Unscented Kalman Filter*. Taipei, Taiwan, 5th. International Conference on Advances in Experimental Structural Engineering.
- Yamada, Y. & Iemura, H., 1992. *Substructured hybrid loading tests of steel box-section columns of inelastic earthquake response of frame structures*. Balkema, Rotterdam, 10th European Conference on Earthquake Engineering.
- Yang, T., Mosqueda, G. & Stojadinovic, B., 2008. *Evaluating the Quality of Hybrid Simulation Test Using an Energy-Based Approach*. Beijing, China, s.n.